Title

Combining Functional and Structural Connectivity: A Preliminary Model for Healthy Volunteers and the Network Dynamics of Patients with Disorders of Consciousness

Author

Dell'Italia, John

Publication Date

2019

Peer reviewed|Thesis/dissertation

UNIVERSITY OF CALIFORNIA
Los Angeles

Combining Functional and Structural Connectivity: A Preliminary Model for Healthy Volunteers and the Network Dynamics of Patients with Disorders of Consciousness

A dissertation submitted in partial satisfaction
of the requirements for the degree
Doctor of Philosophy in Psychology

by

John Dell'Italia

2019

ABSTRACT OF THE DISSERTATION

Combining Functional and Structural Connectivity:
A Preliminary Model for Healthy Volunteers and
the Network Dynamics of Patients with Disorders of Consciousness

by

John Dell'Italia
Doctor of Philosophy in Psychology
University of California, Los Angeles, 2019
Professor Martin M. Monti, Co-Chair
Professor Keith Holyoak, Co-Chair

In this thesis, I identified and addressed four problems of network analyses: 1) arbitrary enforcing of network density, 2) network measures are not independent of each-other with three studies, 3) failure to account for structural information in shaping functional networks, and 4) network dynamics – estimating network change over time. The first chapter introduces the problems and describes current methods within neuroimaging that attempt to address each problem. The second chapter introduces exponential random graph models (ERGM), which is a framework capable of addressing all four problems. The third chapter demonstrates the interaction of problem #2 and problem #3 on the estimation of functional in patients with disorders of consciousness (DOC) and Human Connectome Project (HCP) participants while allowing each patient and HCP to have both their functional and structural connectivity naturally vary (i.e., problem #1). The fourth and fifth chapters focused on the importance of network dynamics for DOC (i.e., problem #4). The fourth chapter describes the use of structural connectivity to investigate the network dynamics of formation and dissolution of connectivity associated with recovery of consciousness over complex behavior in patients with DOC. The fifth chapter describes the use of functional connectivity combined with structural connectivity metrics in a single model to investigate network dynamics in a smaller cohort of 12 patients with DOC. The sixth chapter describes general discussions

about the final three chapters and possible future work.

The dissertation of John Dell'Italia is approved.

Mark Stephen Handcock

Chris Hakwan Lau

Keith Holyoak, Committee Co-Chair

Martin M. Monti, Committee Co-Chair

University of California, Los Angeles

2019

To the formation of friendships and
the perseverance to keep those important in your life,
while dissolving the toxic connections in your life.
Dynamic connectivity is the key to happiness!

TABLE OF CONTENTS

LIST OF FIGURES

LIST OF TABLES

VITA

2001–2005	Computer programmer for United States Air Force
2009	A. A. (Psychology), Morris County Community College–New Jersey.
2010–2012	Research Assistant, Psychology Department, Rutgers University. Barry Komisaruk.
2011–2012	Research Assistant, Psychology Department, Rutgers University.
2012	B.A. (Psychology) and B.A. (Philosophy), Rutgers University–The State University of New Jersey.
2012–2013	Distinguished University Fellowship, Psychology, UCLA.
2013–2014	Neuroimaging Training Program Fellow, National Institute of Health
2014	M.A. (Psychology), UCLA, Los Angeles, California.
2014–2017	National Science Foundation Graduate Research Program Fellow, National Science Foundation
2014–present	Teaching Assistant, Psychology, UCLA.

PUBLICATIONS

Dell'Italia, J., Johnson, M. A., Vespa, P. M. & Monti, M. M. (2018). Exponential Random Graph Models in Disorders of Consciousness: Network analysis in disorders of consciousness: four problems and one proposed solution (Exponential Random Graph Models.) *Frontiers*

CHAPTER 1

Introduction

In the past 15 years, in vivo studies of the healthy and diseased brain have increasingly focused on approaches aimed at assessing the spontaneous functional architecture of the brain, conceived as a network of interacting regions (Raichle et al., 2001). Network analyses have been successfully employed in many fields, including sociology (Freeman, 1978), computer sciences (McQuillan, 1977), public health (Luke and Harris, 2007), epidemiology (Lucek and Ott, 1997) and transportation (Guimera et al., 2005), among others, to capture salient aspects of each phenomenon. Indeed, while different fields often employ different approaches to assessing network properties, they all share the common goal of characterizing important aspects of complex network function into a limited number of metrics, which can, jointly, capture both what is unique and what is shared across systems. Network approaches have also been extensively employed towards understanding specific aspects of cognition (e.g., Cao et al., 2014), development (Fransson et al., 2010) and aging (Micheloyannis et al., 2009) , and, perhaps most frequently, the pathological brain (e.g., Alzheimer's disease; Sanz-Arigita et al., 2010, Parkinson disease; Wu et al., 2009, severe brain injury; Pandit et al., 2013). This approach has also found fruitful application in the study of human consciousness (e.g., Monti et al., 2013; Chennu et al., 2014; Crone et al., 2018). Indeed, many of the proposals of how human consciousness arises from neural function often make reference to aspects of brain activity as a network of interacting areas, such as the reverberation and spread of neural activity across fronto-parietal association regions (Baars, 2002; Baars et al., 2003), the presence of synchronized long-range activity in specific frequency bands (e.g., Engel and Singer, 2001; Tallon-Baudry, 2009) and specific neural circuits (e.g., cortico-thalamic loops; Dehaene and Changeux, 2005), the dynamic competition between assemblies of cells (Crick

and Koch, 2003), or to the degree to which a network possesses certain topological characteristics (e.g., integration and differentiation; Tononi, 2008). These network approaches are of key interest to discern patients with disorders of consciousness (DOC). DOC are a set of conditions in which patients survive a severe (traumatic or non-traumatic) brain injury, but fail to fully recover the two cardinal aspects of consciousness: awareness and wakefulness (Laureys, 2005). DOC includes coma (i.e., lacks both cardinal elements of consciousness), vegetative state (VS; or unresponsive awareness syndrome; i.e., wakefulness in the absence of any behavioral sign of awareness of the self or the environment; Monti et al., 2010), and minimally conscious state *minus* (MCS-; i.e., wakefulness with intermittent but reproducible signs of low-level non-reflexive behaviors, such as orientation to noxious stimuli; Bruno et al., 2011b), minimally conscious state *plus* (MCS+; i.e., wakefulness with intermittent but reproducible signs of high-level non-reflexive behaviors, such as response to command, intelligible verbalization, or gestural or verbal yes/no responses; Bruno et al., 2011b), and an ermerging from minimally conscious state (EMCS), which involves additional return of cognitive functions (e.g., return of functional communication or tool use Aubinet et al., 2018).

In the context of consciousness, these network level descriptions often lead to two types of hypotheses: specific regional connectivity and network topology. On the one hand, researchers use hypotheses based on specific regional connectivity to test patterns of connectivity based on an objective property of a node (e.g., lobe of the brain, resting state network or putative anatomical/functional region). For example, the reverberation and spread of neural activity within fronto-parietal regions reflects specific connectivity patterns between frontal and parietal regions (Baars, 2002; Baars et al., 2003). On the other hand, network topology can be used to investigate the amount of integration and/or differentiation (Tononi, 2008) via path based measures and clustering coefficient (Monti et al., 2013). These hypotheses are tested as if they are independent of each of other (i.e., either across various studies or using separate statistical tests), however, this independence does not hold because the interactions of the generative processes that generate the observed network structure that is measured by outcome metrics (e.g., degree, clustering coefficient and modularity).

There are four putative generative processes (i.e., sociality, selective mixing, triadic clo-

sure and clustering) in network analysis (Handcock et al., 2007; Goodreau et al., 2009; Krivitsky et al., 2009), but there are multiple outcome metrics that are used to measure each generative process. First, sociality is the propensity of a node to generate edges (Goodreau et al., 2009), and it can be measured using degree (i.e., a node's number of edges; Rubinov and Sporns, 2010). This process is specific to the node itself, while other processes involve multiple nodes (i.e,, selective mixing, triadic closure and clustering).

Second, selective mixing is the propensity to form an edge between two nodes (dyad-level process; Goodreau et al., 2009) based on an observed attribute of the nodes (e.g., lobe of the brain, resting state network or putative anatomical/functional region), and it can be measured by specific counts of edges based on nodal attributes, but in other fields, it is measured by homophily (i.e., edges between nodes within category) or heterophily (i.e, edges between nodes between categories) based on an exogenous attribute (Goodreau et al., 2009; McPherson et al., 2001). For example, if a node is part of default-mode network, the likelihood of an edge changes depending on the membership of the other node in that dyad (e.g., default-mode, fronto-parietal or somato-motor networks). The winthin network connectivity (e.g., default-mode to default-mode network) is homophily and the between network (e.g., default-mode to fronto-parietal network) is heterophily.

Third, triadic closure is the propensity to form an edge based on the relationship between three nodes (triad-level process; Goodreau et al., 2009), and it is measured with transitivity or clustering coefficient (Rubinov and Sporns, 2010). For example, if there are three nodes (A, B and C), and node A has an edge with node B and node B has an edge with node C, the likelihood of an edge between node A and C will be higher. Finally, clustering is a process that involves multiple nodes that form a group that increases the likelihood of edges between them (Handcock et al., 2007; Krivitsky et al., 2009). For example, if there is a eight node network (A, B, C, D, E, F, G and H), and nodes (A, B, C and D) form one cluster and nodes (E, F, G and H) form a second cluster, the nodes within each cluster are more likely to have edges within each cluster than between the two clusters.

Each outcome metric does not capture the unique aspects of each generative process (i.e., there is not a one-to-one relationship between generative processes and outcome metrics, but

a one-to-many relationship; Goodreau et al., 2009). Thus, each outcome metric quantifies certain aspects of networks, but it does not isolate the generative process that is responsible; however, the interpretations of these outcome metrics are linked to a single generative processes. For example, clustering coefficient can be described as the level of segregated neural processing (i.e, the amount of specialized processing that occurs due to groups of nodes; Rubinov and Sporns, 2010) within a network, but only if triadic closure was responsible for generating the values produced by clustering coefficient, because triadic closure is a process that results from triads of nodes influencing each other's edge formation. The change in values for clustering coefficient, however, could be due to other generative processes. For example, if sociality is highly influential in the generation of a given graph, each node will be more likely to have more edges and this will lead to more triangles to form; thus, this will increase the clustering coefficient metric and not a result of triadic closure.

In what follows, we propose that it is best to have both seed based and graph theoretic questions in a single model. In the neuroimaging literature, there are a number of limitations of current approaches which have hindered the ability to use a single model for combining seed based and graph theoretic approaches, but there are models that have been developed by other fields (Holland and Leinhardt, 1981; Hunter, 2007; Hunter et al., 2008; Goodreau et al., 2009; Handcock et al., 2017).

1.1 Four problems in current network analysis approaches

Current graph theory methods as employed in neuroimaging (Bullmore and Sporns, 2012; Rubinov and Sporns, 2010) suffer from a number of important shortcomings which are particularly relevant in the domain of DOC. (We note that the following discussion is in the context of network analysis as currently implemented for neuroimaging data, and is not meant to imply that other fields have not found solutions to them. In fact, as we will argue below, we are advocating for importing into the field of neuroimaging methods that have successfully been applied in other domains.)

1.1.1 Problem #1: Arbitrary enforcing of network density

Conventional graph theoretic approaches in neuroimaging require sparse networks. That is to say, they require networks (i.e., connectivity matrices) to have some connections (i.e., edges) with non-zero values (typically integer, in binary networks, or fractional, in weighted networks) and some with zero values – as opposed, for example, to fully connected networks in which all edges have non-zero values (i.e., each node is connected to all other nodes with non-zero edges). Yet, since brain networks are typically derived from pairwise correlations across time-series of regions of interest, the starting point for network analysis is typically a fully connected network (in fact, a complex network, which is both fully connected and has positive and negative edges; Rubinov and Sporns, 2011). It is thus common procedure to make the connectivity matrices sparse by fixing their density (i.e., the proportion of non-zero edges to the total number of possible edges), which is done by retaining the strongest d connections and setting all remaining ones to zero. The resulting network is thus sparse, with density $\frac{d}{N(N-1)/2}$, where N is the number of nodes in the network. On the one hand, this procedure ensures that any uncovered difference across networks (e.g., patients vs volunteers; time-point A vs time-point B) reflects some systematic aspect of their topological characteristics and not, more trivially, the fact that they have different densities. On the other hand, however, because of the lack of a principled approach to perform this procedure, it is currently typical to iteratively re-calculate network characteristics at several density levels, from a lower bound meant to ensure that networks are estimable (such that the average nodal degree is no smaller than $2 \times \log(N)$; Watts and Strogatz, 1998) to an upper bound such that the mean small-world characteristic of networks is no smaller than 1 or 1.5 (e.g., Monti et al., 2013). While conventional, the idea of enforcing graphs to have the same density across groups, time-points, or conditions is in itself problematic, because it is not hard to imagine that some graphs might be naturally denser than others (see Nielsen et al., 2013). This is particularly relevant in the context of the typical comparisons of interest in DOC such as patients versus healthy volunteers, patients in a Vegetative State versus patients in a Minimally Conscious State (versus patients in a Locked-in Syndrome), or within-patient changes over time (e.g., acute-to-chronic designs). Of course, similar problems are

encountered in many other contexts (e.g., adolescents versus older adults) and might even apply to normal, within-group, variability in the healthy brain. Mandating equal density across graphs might obscure important differences across conditions of interest, bias results, and lead to spurious findings.

One solution to the problem of network iterative thresholding is to analyze complex networks (i.e., fully connected and signed matrices; Rubinov and Sporns, 2011; Fornito et al., 2013, 2016). Yet, despite this problem having been well documented, as shown in a recent review focused on the use of graph-theoretic approaches in the clinical context, less than 7% of 106 published papers (up to April 2016) employed complex matrices (Hallquist and Hillary, 2018). All remaining studies only considered non-negative and/or sparse matrices. In addition, it is important to note two potentially unwanted limitations of using complex matrices. First, the use of complex matrices assumes that the probability of connectivity between two regions is spatially stationary, but it is in fact well known to be inversely related to distance at both the neuronal and region levels (see Hellwig, 2000; Averbeck and Seo, 2008; Braitenberg and Schüz, 1998). Second, the use of complex matrices affects the formulation of some metrics (e.g., modularity; Rubinov and Sporns, 2011; Fornito et al., 2013) because positive and negative edges are treated as separate sparse networks, an issue that is further complicated by the frequent use of mean-centering preprocessing strategies which are known to shift the distribution of positive and negative edges (Murphy et al., 2009; Saad et al., 2012). Furthermore, the formulation and interpretation of other metrics (e.g., path based metrics such as characteristic path length/local efficiency, betweenness centrality, etc.; Fornito et al., 2013; Wang et al., 2017), are also affected since the weights represent both the strength and probability of the connections (i.e., density). Thus, analyzing fully connected signed graphs does avoid the thresholding issue but at the cost of clouding the interpretation of metrics such as density and path-based graph statistics.

1.1.2 Problem #2: Network measures are not independent of each-other

A standard network analysis, as currently implemented in the field, typically assesses a number of different topological measures in parallel, such as characteristic path length, average clustering, efficiency, and small-world characteristic, among others (c.f., Rubinov and Sporns, 2011). Many of these characteristics, however, are not independent of each other. In fact, they are often interrelated and can greatly influence each other (van Wijk et al., 2010; Braun et al., 2012; Zalesky et al., 2012). Consider two metrics often employed in graph theoretic analysis of brain data: clustering coefficient and density. Density, as explained above, is a measure of the number of existing edges within a network (i.e., connection with non-zero value), divided by the total number of possible edges. These two network characteristics are strongly interrelated: It has been shown that there is a clear relationship between a networks density and its clustering coefficient (Zalesky et al., 2012). Similarly, dependencies between many other network measures frequently employed in the neuroimaging literature (e.g., degree, clustering coefficient, characteristic path length, and small world index) have also been reported (van Wijk et al., 2010; Braun et al., 2012), highlighting the need to control for these relationships in order to minimize the potential for spurious findings (see Rubinov and Sporns, 2010; van Wijk et al., 2010). Conventionally, this problem is addressed by arbitrarily fixing network density (see Problem #1). This approach, however, suffers from two important shortcomings. First, as explained above, different networks might well have different levels of natural – or stable – density. Second, it is a rather weak control. For example, it only addresses the dependencies of network measures on density, but ignores the many other known correlations among features of networks that are often assessed (cf., van Wijk et al., 2010), which, to date, have gone unaccounted for in virtually all of the extant literature in the field.

1.1.3 Problem #3: Failure to account for structural information in shaping functional networks

In the clinical context of DOC, despite the fact that patients are well known to have heterogeneous underlying pathology, which introduces many concerns for proper diagnosis (Bruno et al., 2011a; Coleman et al., 2009), functional (e.g., Boly et al., 2012; Crone et al., 2018,?; Ku et al., 2011; Lee et al., 2009; Laureys et al., 2000b; Monti et al., 2013; Rosanova et al., 2012) and structural connectivity (Fernández-Espejo et al., 2011, 2012; Newcombe et al., 2010; Wilson, 2010; Tollard et al., 2009; Zheng et al., 2017) are typically investigated separately. This narrow approach is very problematic because it has been shown, in the rodent model (Díaz-Parra et al., 2017) and in healthy humans (Bettinardi et al., 2017; Mess et al., 2015), that structural data can predict the functional connectivity as estimated by correlations in the fMRI signal, as well as EEG phase coupling in healthy volunteers (Finger et al., 2016). Failing to include both structural and functional data will have a similar effect on the analysis of functional networks as omitting any other graph metric (i.e., problem #2): it will result in improper estimation of the terms in the model and potentially spurious results. This issue is particularly important in the clinical context of DOC given their highly heterogeneous pathology and the fact that this can change over time, which affects longitudinal comparison of brain networks over time.

Diffusion weighted imaging (DWI) and blood oxygenation level dependent (BOLD) can be used in conjunction to estimate connectivity matrices using joint independent component analysis (jICA; Kessler et al., 2014), Connectivity Independent Component Analysis (connICA; Amico and Goñi, 2017) or partial least squares (PLS; Mii et al., 2016). In general, all three methods produce multiple group connectivity matrices based on the covariance of BOLD and DWI data across all participants. Both jICA and connICA produce multiple components that are maximally spatially independent (for a complete explanation of jICA see Calhoun et al., 2006, 2009; Sui et al., 2011, and for a complete explanation of connICA see Amico et al., 2017). PLS produce a linear combination of latent variables that maximally covary with each other based on weighted structural and functional connections (for a

complete explanation of PLS see McIntosh and Lobaugh, 2004; Abdi, 2010; Krishnan et al., 2011; McIntosh and Mii, 2013). These methods incorporate both structural and functional connectivity in the estimation of the connectivity matrices, but they require researchers to choose the number of components (in jICA and connICA) or number of latent variables (in PLS). Changing these parameters influences the results of the connectivity estimation and the standards for these parameters are still being investigated for both jICA and connICA (Hyvrinen and Oja, 2000; Calhoun et al., 2009; Abou-Elseoud et al., 2010; Ray et al., 2013). We thus propose an alternative to these methods that avoids the necessity to estimate the functional and structural connectivity jointly. In the approach we describe below, the structural and functional connectivity matrices are estimated separately, and the former is used as a variable in estimating graph statistics for the latter (see section §2.2 for a complete description).

1.1.4 Problem #4: Network dynamics – Estimating network change over time

Finally, contrary to the assumption underlying conventional network analysis in neuroimaging, connectivity between areas is unlikely to be stationary processes. Rather, brain activity might best be viewed as a malleable and variable process over time (Ioannides, 2007). Yet, even in the few cases where this limitation has been addressed (e.g., Barttfeld et al., 2015), these types of approaches do not quantify dynamic change of connectivity across time (or states). Rather, they just dissect a time-series into multiple static networks and compare them over their respective topological properties. In other words, even these approaches are static in nature and fail to capture the dynamics of network connectivity over time. In the context of DOC, for example, this means that longitudinal analysis of brain data can be employed to reveal differences in topological properties of networks at two different time-points, but do not allow saying anything of the process of interest, which is the dynamics of how one network transitioned into another (e.g., how a network transformed as consciousness was regained over time). These patients with a DOC are typically investigated in a cross-sectional analysis by comparing healthy participants with a static network at a single time point to group of patients with static network at a single time point (e.g., VS to

healthy controls; Boly et al., 2011; Crone et al., 2011, 2015; Fernández-Espejo et al., 2012; Kotchoubey et al., 2013; Sitt et al., 2014; Vanhaudenhuyse et al., 2010; Zhou et al., 2011) or between patient groups (e.g., VS compared to MCS; Casali et al., 2013; Casarotto et al., 2016; Crone et al., 2011, 2015; Comolatti et al., 2018; Demertzi et al., 2015; Fernández-Espejo et al., 2011, 2012; Kotchoubey et al., 2013; Laureys et al., 2000a; Rosanova et al., 2012; Sitt et al., 2014; Vanhaudenhuyse et al., 2010; Zhou et al., 2011). Additionally, there have been some investigations into the parallel restoration of connectivity for a single patient (Laureys et al., 2000a) and for a larger cohort (Crone et al., 2018), but these analyses still investigate the differences between two networks. Together, all of these types of analyses reveal the differences between the network architecture of patients and healthy controls, or between patients with different levels of DOC, but does not investigate the recovery process which involves the reorganization of networks and their topologies. In other words, it will show the differences between the generative processes of each network, not the generative processes to get from one network to another. This underlying generative process is the key for each patient to recover. These processes involve network connectivity forming, networks maintaining connectivity, or networks reducing connectivity. An extension of ERGM, seperable temporal ERGM (STERGM) allows for the modeling of two independent processes: the formation of new connectivity and the dissolution of connectivity (i.e, both maintaining and dissolving connectivity, see §2.1).

In this thesis, we addressed the four problems of network analyses with three studies and a chapter describing the ERGM framework (see §2). The first study (see §3) demonstrated the interaction of problem #2 and problem #3 on the estimation of functional in patients with DOC and HCP participants while allowing each patient and HCP to have both their functional and structural connectivity naturally vary (i.e., problem #1). The second and third study focused on the importance of network dynamics for DOC (i.e., problem #4). The second study (see §4) used structural connectivity to investigate the network dynamics of formation and dissolution of connectivity associated with recovery of consciousness over complex behavior in patients with DOC. The third study (see §5) used functional connectivity combined with structural connectivity metrics in a single model to investigate network

dynamics in a smaller cohort of 12 patients with DOC.

CHAPTER 2

Exponential Random Graph Models

In response to these four shortcomings of current network analysis, we present and demonstrate a novel (in the context of DOC, for other contexts within neuroimaging, cf.: Simpson et al., 2011, 2012, 2013) approach to graph analysis, referred to as Exponential Random Graph Models (ERGM; Holland and Leinhardt, 1981). The core idea underlying ERGM is that instead of considering graphs as fixed entities which can be described in terms of topological properties (e.g., clustering, path length, small world property), it attempts to generate hypotheses about the (unobserved) stochastic processes that gave rise to an observed network (Robins et al., 2007). Contrary to the prevalent approach in neuroimaging, then, the presence/absence of an edge within a network is not considered to be a fixed property of a graph, but rather a random variable generated by a stochastic process. In other words, rather than assuming the observed network as "given" and fix, and describing its topological characteristics (e.g., characteristic path length, clustering coefficient), it tries to characterize the processes that have generated the observed network. One particularly appealing aspect of this approach is that, so long as the total number of nodes (i.e., ROIs) constituting a network remains unchanged, it allows for comparing across networks with different density levels, thereby solving problem #1. The ERGM framework uses the following exponential model:

$$P_\theta(Y = y) = \frac{\exp(\theta^T g(y))}{c(\theta)} \tag{2.1}$$

where θ is a parameter vector that is modeled by g(y) (i.e., any statistic of the graph). The parameter $c(\theta)$ is a normalizing constant representing the parameter estimate for all possible graphs (Hunter et al., 2008). This normalizing constant is not able to be analytically solved due to the combinatorics of the graph structure. We can nonetheless approximate the

unknown population mean using $c(\theta_s)$ (i.e., the sample mean):

$$\begin{aligned} \frac{c(\theta)}{c(\theta_s)} &= E_{\theta_s} \exp(\theta - \theta_s)^T g(y_i) \\ \frac{c(\theta)}{c(\theta_s)} &\approx \frac{1}{M} \sum_{i=1}^{M} \exp(\theta - \theta_s)^T g(y_i) \end{aligned} \tag{2.2}$$

for derivations (see Hunter et al., 2008). These equations allows for an approximation of the population mean using sample mean. A bootstrapping method using Markov Chain Monte Carlo (MCMC) methods is used to sample and estimate the population mean. These methods assume Markovian principles of independent draws and the ability to reach equilibrium. Equilibrium is the state in which any edge that is toggled on or off results in an equally probable graph. The general method is to take the ratio of the probabilities of $Y_{ij} = 1$ (i.e., adding a single edge) and $Y_{ij} = 0$ (i.e., no edge) conditioned on $Y_{ij}^C = y_{ij}^C$ (i.e., all other pair of nodes in the graph).

$$\begin{aligned} \frac{P(Y_{ij} = 1 | Y_{ij}^C = y_{ij}^C)}{P(Y_{ij} = 0 | Y_{ij}^C = y_{ij}^C)} &= \exp \theta^* (s(Y_{ij} = 1) - s(Y_{ij} = 0)) \\ \log \frac{P(Y_{ij} = 1 | Y_{ij}^C = y_{ij}^C)}{P(Y_{ij} = 0 | Y_{ij}^C = y_{ij}^C)} &= \theta^* \Delta(s(Y_{ij})) \\ \text{LPL}(\theta) &= \sum \log[P(Y_{ij} = y_{ij}) | (Y_{ij}^C = y_{ij}^C)] \end{aligned} \tag{2.3}$$

where the LPL(θ) is the log-pseudolikelihood for θ, which is maximized by taking the maximum pseudolikelihood for θ (Hunter et al., 2008). This estimation process is performed for the model with all the parameters (i.e., θ). The estimates give the mean and standard error. These estimates were tested for significance in each functional data set. Due to the MCMC, a t-statistic can be estimated and is reported in the model output along with a p-value.

For interpretation purposes, equation 2.1 can be represented as follows (the full derivations can be found in Hunter et al., 2008):

$$\text{logit}(P_\theta(Y_{ij} = 1 | nactors, Y_{ij}^C)) = \sum_{k=1}^{K} \theta_k \delta_{Z_k(y)} \tag{2.4}$$

where k is the number of network statistics in the model and θ_k is the parameter estimate for each statistic. The $\delta_{Z_k(y)}$ is the change in network statistic if a edge were added between

any node i and j. Thus, the interpretation of the network statistics involve the change in probability of an adding a edge with certain network statistic. The significance of a parameter estimate is one compared to the expected parameter estimate in a null model with the probability of all edges equal to 0.5 (i.e., Erdös and Rényi, 1959).

2.1 Separable Temporal Exponential Random Graph Model

STERGM (Krivitsky and Handcock, 2014) is an extension of the original ERGM. It is used to assess the dynamics of networks as they change over time . The same underlying methods for estimating ERGM is used in STERGM. A model with network statistics is used to estimate the parameter estimates for a network that changes over time. To achieve this, two separate networks are investigated. A formation network is generated conditional on forming edges,

$$P(Y^+ = y^+|Y^t;\theta^+) = \frac{exp(\theta^+ g(y^+, X))}{c(\theta^+, X, Y^+(Y^t))}, y^+ \in Y^+(y^t) \tag{2.5}$$

where a formation network Y^+ is characterized by formation parameters θ^+ (Krivitsky and Handcock, 2014). The formation network statistics are $g(y^+, X)$ and the normalizing constant is $c(\theta^+, X, Y^+(Y^t))$. The second network formed is a dissolution network that is conditional on the edges that dissolve. This network is represented by the same variables labeled with minus instead of a plus,

$$P(Y^- = y^-|Y^t;\theta^-) = \frac{exp(\theta^- g(y^-, X))}{c(\theta^-, X, Y^-(Y^t))}, y^- \in Y^-(y^t) \tag{2.6}$$

where a dissolution network $Y-$ is characterized by dissolution parameters $\theta-$ (Krivitsky and Handcock, 2014). The dissolution network statistics are $g(y-, X)$ and the normalizing constant is $c(\theta-, X, Y-(Y^t))$. These networks can form a new network at time $t+1$ by applying formation and dissolution networks on y^t. This can be expressed as:

$$Y^{t+1} = Y^t \cup (Y^+ - Y^t) - (Y^t Y^-) \tag{2.7}$$

The formation and dissolution networks are independent of each other across the $t+1$ time points (Krivitsky and Handcock, 2014). STERGM has the unique ability to model

networks as they transform over time enabling research questions about the dynamics of a network. The same model in Equation 4.1 was used in both the formation and dissolution models. The quantifications of these networks are similar to ERGM, but these two models slightly change the interpretation of the parameter estimates. In the formation model, a positive parameter estimate indicates a tendency for edges for a network statistic form at time point $t + 1$, and a negative parameter estimate indicates a lack of formation of edges for a particular network statistic at time point $t+1$. The dissolution model has two separate interpretations based on the sign of the parameter estimate. A negative parameter estimates are interpreted as edges are more likely to dissolve and positive parameters indicate edges are more likely to be preserved. Despite these differences in interpretation, all the same procedures were used in STERGM as were used in ERGM (PM, FM, quality control using MCMC diagnostics, and assessing fit using GOF) for both the formation and dissolution models.

2.2 Graph Statistics

All ERGM models we used to analyze the patient data included the same graph statistics. The model used for the first and third studies was specified as follows, where $P_\theta(Y = y)$:

$$= \frac{\begin{array}{c}\exp(\theta_1\text{edges} + \theta_2\text{nodecov(degree)} + \theta_3\text{nodecov(efficency)} + \theta_5\text{nodematch(latent)} \\ + \theta_5\text{nodecov(cluster)} + \theta_6\text{nodemix(rest)} + \theta_7\text{nodematch(lobe)} + \theta_8\text{gwesp(alpha} = \lambda))\end{array}}{c(\theta)} \tag{2.8}$$

Edges refers to the total number of edges for each functional connectivity graph. This term allows control for the density of each graph over and above the types edges accounted for by the rest of the terms in the model.

There are four nodal covariate terms for the diffusion data–three nodal covariates (i.e., degree, efficiency and cluster) and the nodemix (latent) term–and two nodal covariate for the functional connectivity (i.e., nodemix for resting state networks and a nodematch for the cerebral lobes). Degree is the number of edges for each structural node. Efficiency is the local efficiency of each node. Cluster is the clustering coefficient of each node. The

nodecov term estimates the probability of functional connectivity edge as a function of each distribution of the structural terms (i.e., degree, local efficiency and clustering coefficient). A positive coefficient indicates an increase in the probability of a functional connectivity edge as structural term increases in magnitude. On the other hand, a negative coefficient indicates an increase in probability of a functional connectivity edge as the structural term decreases.

As shown in equation 4.1, there are two nodemix terms: latent and resting. The nodemix (latent) is the within and between module connectivity of the structural connectivity. Thus, this mixing term represents the probability of a functional connectivity edge given the modular membership based on the structural connectivity. The number of modules and modular membership of each node is determined by a position latent cluster ERGM (Handcock et al., 2007; Krivitsky and Handcock, 2008). These models have shown to be able to use a latent space model with an a priori determined number of dimensions using the parameter d (3 dimensions). The nodes are arranged in a euclidean system with proximity equating to probability of an edge. The clusters are determined by the parameter G. This parameter sets the number of Gaussian spherical clusters that are introduced in the latent space. The estimation of position latent cluster ERGM is a two step Bayesian estimation, but the exact specification is beyond the scope of this paper (see Handcock et al., 2007).

The nodemix (resting) is our mixing term for determining the inter- and intra-regional connectivity of the resting state networks and sub-cortical regions of the functional data. Multiple parameter estimates were produced for this term. Additionally, these mixing terms used the exogenous node labels for each nodes membership in the seven resting state networks (Yeo et al., 2011) and sub-cortical regions. Each node of the brain network was labeled either: frontoparietal, visual, somato-motor, limbic, dorsal attention, ventral attention, default, subcortex, basal ganglia, cerebellum, and thalamus. Each combination of the inter- and intra-regional connectivity produced a mixing term and parameter estimate. For example, one inter-regional mixing term would be frontoparietal and thalamic connectivity. This parameter estimate would give the probability of an edge existing between the frontoparietal network and thalamus. An example of intra-regional mixing term would be frontoparietal

to frontroparietal. This term would express the probably of an edge within the frontoparietal network. These mixing terms were used to assess the connectivity between the within the resting state networks, between the resting state networks, within the sub-cortical regions, between the sub-cortical regions, and between resting state networks and sub-cortical regions. This term incorporates questions that would be addressed using seed based connectivity analyses. The nodematch for lobe term incorporates another another exogenous nodal labeling of ROIs using their anatomical location within the four cerebral lobes (i.e, frontal, occipital, parietal, and temporal) and final term for the entire subcortex. This was chosen to specifically model the intra-lobe functional connectivity.

The geometrically weighted edged shared partners (GWESP) can be expressed by this equation (Hunter, 2007):

$$\begin{aligned} \theta_t &= log\lambda_t \\ v(y;\theta_t) &= e^{\theta_t} \sum_{i=1}^{n-2} \left[1-(1-e^{-\theta_t})^i\right] EP_i(y) \end{aligned} \tag{2.9}$$

In this equation, v is the GWESP term and θ_t is the log of the decay parameter that was fixed in all the data sets. The $EP_i(y)$ is the edge shared partners term for the entire graph. It accounts for the number of each type of edge shared partner. An edged shared partner is triangle that shares a common base. Edge shared partners is a metric used to quantify the amount of clustering in the form of transitivity in a network. High positive parameter estimates indicate that transitivity is present above and beyond all the other statistics in the model. Transitivity is a higher order relationship present in most graphs which are the local and/or global communication and the amount of local cohesion. Differences in transitivity between patients could be a key change that occurs from injury. This would be a disruption of the clustering found within the patients brain. This type of disruption would hamper local and/or global communication and additionally it would indicate a lack of local cohesion within a network.

The analysis was performed using the ERGM package (Hunter et al., 2008) in R. There are two ERGMs used on the patient data. A FM and used all the terms from equation 4.1. The FM was fit multiple times to get assess the proper λ (the decay parameter) for the

GWESP term. The range of λ began at 0.05 and increase by increments of 0.05 up to 2.0. Each iteration was checked by inspecting the diagnostics of the MCMC. The models that have the best fit for the parameter estimate GWESP were chosen (i.e., $\lambda = 0.45$). A second model, the PM was fit. The structural terms (i.e., the three nodecov and the nodemix for latent) were omitted from this model to demonstrate the effects on the rest of the parameter estimates.

The FM's graph statistics were chosen based on two reasons: the type of functional data being analyzed (i.e., resting state data) and the first three problems outlined above (see section §1.1.1, §1.1.2 and §1.1.3). The nodemix (resting) terms were chosen because this patient's functional connectivity matrices were estimated from the BOLD correlations during the resting state scans. Thus, the intra- and inter- regional connectivity would be best characterized by putative resting state networks. The number of resting networks were chosen based on a data driven approach (i.e., Yeo et al., 2011) that estimates a number of networks based on stability of clusters (for details on the clustering algorithm see Lashkari et al., 2010) estimated from 1000 subjects' functional data. A seven network parcellation was chosen because it minimized the instability (Yeo et al., 2011) and matches what has been previously discussed in the literature (e.g., Buckner, 2010; Cohen et al., 2008; Fox et al., 2006; Vincent et al., 2008). Additionally, the thalamus group was added because of its possible involvement in DOC (e.g., Crone et al., 2014; Laureys et al., 2000b; Vanhaudenhuyse et al., 2010; Zhou et al., 2011) or anesthesia induced loss of consciousness (e.g., Boveroux et al., 2010; Martuzzi et al., 2010; Schrouff et al., 2011; Stamatakis et al., 2010). Finally, the subcortical and cerebellum groups were added to ensure every node fit a grouping label.

The edges term allows for networks with varying density to be modeled and compared (cf., Problem #1, section §1.1.1). The higher order term (i.e., GWESP) describes the local and/or global communication which could be an important aspect in the recovery from brain injury (e.g., Chennu et al., 2014; Crone et al., 2014; Schröter et al., 2012), and because it alleviates the problem of interrelation among graph theoretic measures (cf., Problem #2, section §1.1.2) by accounting for the higher order term's variance and thus avoiding it being improperly allocated to lower order terms (i.e., edges, node mixing, and structural terms). As

shown below, failing to include the higher order term can affect the estimation of parameters in either magnitude or sign. Structural connectivity is important because, as stated in third problem (cf., section §1.1.3), it can be severely affected by TBI, systematically changing over time and/or patient cohorts, and because it is interrelated with functional connectivity. Thus, we chose four terms for the structural connectivity that would capture the number of connections of each node (i.e., degree), a measure of integration (i.e., local efficiency Rubinov and Sporns, 2010), and higher order relationships (i.e., clustering and modularity). The two higher order terms were chosen because they capture two different higher order dynamics: local grouping of nodes (i.e., clustering coefficient Rubinov and Sporns, 2010) and community structure (i.e., modularity; Rubinov and Sporns, 2010).

CHAPTER 3

A Single Model for Structural and Functional Connectivity: Preventing misinterpretations of connectivity differences in patients with TBI

3.1 Methods

We apply the powerful and flexible ERGM approach to estimating network statistics for characterizing (brain) networks to demonstrate that problem #2 and problem #3 cause false positives (FPs) and false negatives (FNs), but in patients they occur at different rates depending on the level of consciousness by behavioral assessment and the stage of TBI (i.e., different rates between acute and chronic patients). To anticipate the key points that will follow, ERGM, which has been successfully employed in other contexts (Goodreau et al., 2009; Holland and Leinhardt, 1981; Hunter, 2007; Hunter et al., 2008), offers a number of substantial advantages which are particularly important in the clinical context of DOC. First, it does not require imposing (and assuming) the same level of density across graphs, thus allowing estimating characteristics of each graph at its natural density level. Second, it allows for controlling the dependencies between network characteristics. In this sense, in contrast to the conventional approach, which can be viewed as a series of univariate regressions (i.e., one per metric) assessing the topological characteristics across groups of graphs (e.g., patient groups and controls versus patients), ERGM is making use of a multiple regression framework (Goodreau et al., 2009), in which all features are considered together, and thus returns the "unique" contribution of each network measure. Third, the multiple regression framework extends to graph theoretic measures characterizing the structural connectivity

of a network, thus accounting and "parceling out" the effect of cross-sectional differences (e.g., Zheng et al., 2017) and longitudinal changes in structural connectivity (e.g., Voss et al., 2006; Thengone et al., 2016) across graphs. Finally, we used 12 patients' functional connectivity to show the effects on false positives FPs and FNs when the structural terms or triadic closure term (i.e., GWESP term) are left out of the model. The same analysis was conducted for 12 age and sex matched HCP participants using their two functional imaging sessions that were one day apart.

3.1.1 Human Connectome Project Participants

The data for this analysis was taken from the Human Connectome Project (HCP; Van Essen et al., 2013), which is a public repository of high quality structural and functional MR data in a large set of healthy volunteers. For the purposes of this study, we selected a subset of the data (N=12) so to match the characteristics (i.e., age and gender) of the the final set of patient population to be used in Study #1. These HCP participants (see Table 3.1 were randomly sampled from the S1200 (n=9) release, the Q3 release (n=1), S500 (n=1) and S900 (n=1) releases to best match the age and gender of the patients at the time of their injury (see Table 3.2 for the patients that were matched and see Table 4.1 for their demographics). These HCP participants only had a single DWI imaging session. We will use that DWI imaging for the structural connectivity for both days of resting state data.

3.1.1.1 HCP Experimental Design

From the HCP dataset, we made use of anatomical (T1-weighted), diffusion (Diffusion Tensor Imaging; DTI), and functional (T2*-weighted) data. T1-weighted images were acquired with a 3D MPRAGE sequence (repetition time [TR] = 2400 ms, echo time [TE] = 2.14 ms, flip angle [FA] = 8 deg). DTI images were acquired with a spin-echo echo planar sequence (TR = 5520 ms, TE = 89.5 ms, FA = 78 deg / 160 deg, 96 directions). Finally, blood oxygenation level dependent (BOLD) functional image were acquired with a gradient-echo echo planar image (TR = 720 ms; TE = 33.1 ms; FA = 52 deg). All the data were downloaded

	Subject	Release	Acquisition	Gender	Age	Full 3T MR	RS fMRI	fMRI TR	fMRI TE	fMRI Slice Thickness	DTI TR	DTI TE	DTI Slice Thickness	DTI.B.values
HCP_001	169545	S1200	Q13	M	22-25	true	100%	720 ms	33.1 ms	2 mm isotropic, 72 slices	5520 ms	89.5 ms	1.25 mm isotropic, 111 slices	1000 2000 3000
HCP_002	193845	S1200	Q13	M	22-25	true	100%	720 ms	33.1 ms	2 mm isotropic, 72 slices	5520 ms	89.5 ms	1.25 mm isotropic, 111 slices	1000 2000 3000
HCP_003	350330	S1200	Q13	F	22-25	true	100%	720 ms	33.1 ms	2 mm isotropic, 72 slices	5520 ms	89.5 ms	1.25 mm isotropic, 111 slices	1000 2000 3000
HCP_004	634748	S1200	Q13	F	22-25	true	100%	720 ms	33.1 ms	2 mm isotropic, 72 slices	5520 ms	89.5 ms	1.25 mm isotropic, 111 slices	1000 2000 3000
HCP_005	694362	S1200	Q13	F	22-25	true	100%	720 ms	33.1 ms	2 mm isotropic, 72 slices	5520 ms	89.5 ms	1.25 mm isotropic, 111 slices	1000 2000 3000
HCP_006	219231	S1200	Q05	M	26-30	true	100%	720 ms	33.1 ms	2 mm isotropic, 72 slices	5520 ms	89.5 ms	1.25 mm isotropic, 111 slices	1000 2000 3000
HCP_007	421226	S1200	Q13	M	31-35	true	100%	720 ms	33.1 ms	2 mm isotropic, 72 slices	5520 ms	89.5 ms	1.25 mm isotropic, 111 slices	1000 2000 3000
HCP_008	211417	Q3	Q03	M	36+	true	100%	720 ms	33.1 ms	2 mm isotropic, 72 slices	5520 ms	89.5 ms	1.25 mm isotropic, 111 slices	1000 2000 3000
HCP_009	902242	S1200	Q08	F	36+	true	100%	720 ms	33.1 ms	2 mm isotropic, 72 slices	5520 ms	89.5 ms	1.25 mm isotropic, 111 slices	1000 2000 3000
HCP_010	757764	S1200	Q13	F	36+	true	100%	720 ms	33.1 ms	2 mm isotropic, 72 slices	5520 ms	89.5 ms	1.25 mm isotropic, 111 slices	1000 2000 3000
HCP_011	180937	S500	Q06	M	36+	true	100%	720 ms	33.1 ms	2 mm isotropic, 72 slices	5520 ms	89.5 ms	1.25 mm isotropic, 111 slices	1000 2000 3000
HCP_012	792867	S900	Q12	M	36+	true	100%	720 ms	33.1 ms	2 mm isotropic, 72 slices	5520 ms	89.5 ms	1.25 mm isotropic, 111 slices	1000 2000 3000

Table 3.1: **HCP demographics and MRI imaging parameters.** The 12 participants were age and gender matched to the 12 patients for the first study. The HCP identification numbers are listed. Additionally, the release date of the data along with the acquisition year are listed. Finally, the DWI and functional MRI parameters are listed for each participant, and they were the same for all acquisition times.

preprocessed using the miniminally processed pipeline (Glasser et al., 2013; Van Essen et al., 2013).

3.1.1.2 Functional Connectivity Patient Cohort

Of the original 31 patients, a subset of 15 patients (P054, P055, P066, P069, P074, P079, P083, P084, P085, P089, P092, P096, P097, P099, P100) with more than 150 samples (i.e., TR count) for functional connectivity analysis were selected for the first and third studies. An additional 3 patients were excluded due to BOLD artifacts (patient P083), preprocessing errors (patient P097), or registration errors (patient P100). After these final exclusions there were 12 patients (see Table 3.2), which seven of these patients were male and five were female. All of these patients were presented with a post-resuscitation GCS during the acute stage of TBI which was transformed into an inferred GOS-E (Crone et al., 2018). Additionally, the GOS-E was assessed at the chronic stage of TBI. Together, the inferred GOS-E and chronic GOS-E were used to split 7 patients in the U2C group and 5 patients in C2C group.

3.1.1.3 Patients' Experimental Design

The 31 patients underwent two imaging sessions over the span of at least 158 days to at most 238 days. The first session occurred at most 37 days post injury (see Table 4.1), and the follow-up session took place 238 days post-injury. At each session the patient underwent (among other clinical and research sequences) anatomical (T1-weighted) and functional ($T2^*$-weighted) data protocols. T1-weighted images were acquired with a 3D MPRAGE sequence (repetition time [TR] = 1900 ms, echo time [TE] = 3.43, $1\times1\times1$ mm). BOLD functional data were acquired with a gradient-echo echo planar image (for the 12 patients with TR counts over 150 see Table 3.2 for the slice thickness, TR count, TE, and TR). Diffusion Weighted data were acquired with an echo planar sequence (for number of gradient directions, TR, TE, and slice thickness see Table 4.3) using a b-value of 1000 and acquiring an additional B0 image. Acute data were acquired on the in-patient 3 Tesla Siemens TimTrio system at the Ronald Reagan University Medical Center for patients P003, P005, P007, P014, P018, P021, P023, P024, P026, P027, P029, P039, and P066, and rest of the patients' acute data were acquired on a 3 Tesla Siemens Prisma system. All the chronic data were acquired on the out-patient 3 Tesla Siemens Prisma system also at the Ronald Reagan Medical Center at the University of California Los Angeles. The study was approved by the UCLA institutional review board (IRB). Informed consent was obtained from the legal surrogate, as per state regulations.

	Matched MRI	Acute TR Count	Chronic TR Count	Acute Slice Thickness	Chronic Slice Thickness	Acute TR	Chronic TR	Acute TE	Chronic TE
P054	Yes	200	200	3.4375x3.4375x3 mm, 40 Slices	3.4375x3.4375x3 mm, 40 Slices	3000 ms	3000 ms	25 ms	25 ms
P055	Yes	200	200	3.5 mm isotropic, 52 Slices	3.4375x3.4375x3 mm, 64 Slices	3000 ms	3000 ms	25 ms	25 ms
P066	No	200	200	3.4375x3.4375x3 mm, 64 Slices	3.4375x3.4375x3 mm, 50 Slices	3000 ms	3000 ms	25 ms	25 ms
P069	Yes	200	200	3.4375x3.4375x3 mm, 50 Slices	3.4375x3.4375x3 mm, 52 Slices	3000 ms	3140 ms	25 ms	25 ms
P074	Yes	200	200	3.4375x3.4375x3 mm, 50 Slices	3.4375x3.4375x3 mm, 50 Slices	3000 ms	3000 ms	25 ms	25 ms
P079	Yes	200	200	3.4375x3.4375x3 mm, 50 Slices	3.4375x3.4375x3 mm, 50 Slices	3000 ms	3000 ms	25 ms	25 ms
P084	Yes	200	200	3.4375x3.4375x3 mm, 50 Slices	3.4375x3.4375x4.25 mm, 37 Slices	3000 ms	2006 ms	25 ms	25 ms
P085	Yes	200	200	3.4375x3.4375x3 mm, 40 Slices	3.4375x3.4375x4.25 mm, 37 Slices	3000 ms	2006 ms	25 ms	25 ms
P089	Yes	200	200	3x3x3.99, 33 Slices	3.4375x3.4375x4.25 mm, 37 Slices	2000 ms	2006 ms	30 ms	25 ms
P092	Yes	300	300	3.4375x3.4375x4.25 mm, 37 Slices	3.4375x3.4375x4.25 mm, 37 Slices	2000 ms	2006 ms	25 ms	25 ms
P096	Yes	300	300	3.4375x3.4375x4.25 mm, 37 Slices	3.4375x3.4375x4.25 mm, 37 Slices	2000 ms	2006 ms	25 ms	25 ms
P099	Yes	300	300	3.4375x3.4375x4.25 mm, 37 Slices	3.4375x3.4375x4.25 mm, 37 Slices	2000 ms	2006 ms	25 ms	25 ms

Table 3.2: **Patients' functional MRI parameters.**. The functional MRI parameters are tabulated for each patient. These parameters' descriptions are the same as the DWI paramters's descriptions, except they are for the functional MRI imaging session. An additional parameter for the number to TRs are tabulated under TR count.

3.2 Data Preprocessing

3.2.1 BOLD data preprocessing

The functional data underwent a number of conventional preprocessing steps including brain extraction, slice timing correction, motion correction, band-pass filtering ($0.08 \leq \text{Hz} \leq 0.1$), and removal of linear and quadratic trends. A nuisance regression was employed to parcel out signals of non-interest including motion parameters, white matter, cerebral spinal fluid, and full-brain mean signal (which has been shown to alleviate the consequences of in-scanner motion; Power et al., 2012) within FSL (Jenkinson et al., 2002). Affine registration of the functional data to the standard template (MNI) was performed using Advanced Normalization Tools (ANTs; Avants et al., 2008, 2011). Our processing pipeline for the functional data are qualitatively similar to the minimally processed pipeline for the HCP data (Glasser et al., 2013; Van Essen et al., 2013). One important note is that our comparison of connectivity is within patients to within HCP participants. This should control for some of the differences between the pipelines, but not all of them.

3.2.2 DWI data preprocessing

The patients' diffusion data were preprocessed using the following pipeline: DWI preprocessing, registrations, probabilistic tractography with tractography thresholding. All of these processes were run using a bash script in parallel using the GNU Parallel package (Tange, 2011). These step are similar to the HCP pipeline, but as with the functional data there are differences between the pipelines, which should control for some of the differences found. However, an full exploration on the effects due to these differences are beyond the scope of this thesis. One last note, while the diffusion data was downloaded and preprocessed, we ran the the Bayesian estimation of the diffusion profile and probabilistic tractography for the patients and HCP participants.

DWI preprocessing. All preprocessing procedures were visually checked for optimal quality. The T1-weighted data were brain extracted (optiBET; Lutkenhoff et al., 2014) and

bias field corrected (BrainSuite BFC; Shattuck et al., 2001). The diffusion-weighted data were prepared for tractography with the following steps: 1) visual quality checking of raw images; 2) artifact checking/removal and motion correction with vector rotation (DTIprep; Oguz et al., 2014); 3) eddy current distortion correction followed by tensor fitting (i.e., linear fitting using weighted least squares) and estimation of diffusivity metrics (BrainSuite's BDP; Bhushan et al., 2012; Haldar and Leahy, 2013); 4) brain extraction of the b0 image (BET; Smith, 2002); and 5) GPU-enhanced Bayesian estimation of the diffusion profile with up to two principal directions per voxel (i.e., allowing for crossing/kissing streamlines) using FSLs bedpostx (Behrens et al., 2003b; Hernández et al., 2013).

Registrations. All registrations were visually checked for optimal quality. The following steps were conducted: 1) linear registration of the native diffusion data (b0 image) to the native T1-weighted data (ANTs IntermodalityIntrasubject; Avants et al., 2011); 2) nonlinear registration (ANTs) of the native T1-weighted data to the Montreal Neurological Institute (MNI) standard space (MNI Avg 152 T1 2x2x2mm standard brain); 3) forward or inverse transform concatenations (ANTs; Avants et al., 2011) to move between native diffusion, native T1, and the MNI template.

Probabilistic tractography. GPU-enhanced probabilistic tractography between all regions of the whole-brain atlas (i.e., iteratively seeding from each region to all other regions as targets) was conducted with the matrix1 option in FSLs probtrackx2 (Behrens et al., 2003b, 2007). A minimum distance of 4.8mm (i.e., 2 voxel widths) was set to prevent artificial streamlines passing through contiguous regions. The output matrix of streamline counts between all regions was thresholded to remove spurious streamlines with an optimization procedure that minimizes asymmetries between the seed/target assignments for each ROI-ROI pair (MANIA; Shadi et al., 2016).

3.3 Brain Network Construction

For each dataset (both the functional and diffusion data), a graph was constructed to provide a mathematical description of the brain as a functional network. Brain graphs were

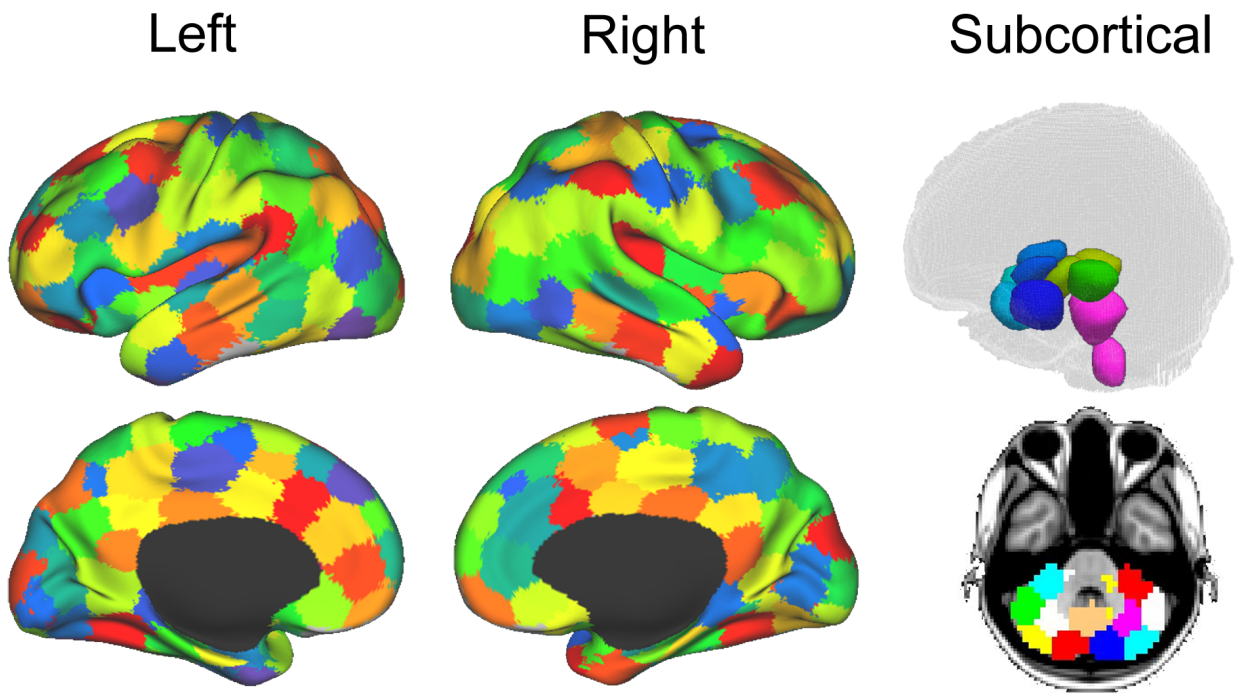

Figure 3.1: **Parcellation for structural and functional connectivity.** Cortical and subcortical parcellation of the brain data (Craddock et al., 2012). The imaging sessions' data sets were parcellated into 154 ROIs throughout the cortex, sub-cortical nuclei, cerebellum and brainstem. (Figure from Monti et al., 2013)

constructed in two steps. First, these data sets were parceled into 154 ROIs spanning the cortex, sub-cortical nuclei, cerebellum and brainstem (see Figure 3.1). This parcellation scheme, which was defined independently of our data, is made freely available by Craddock and colleagues (Craddock et al., 2012). Additionally, we used the Oxford thalamic connectivity atlas (Behrens et al., 2003a) to further refine the parcellation of the thalamus from 6 to 14 and we parcellated the basal ganglia into 6 ROIS (caudate, putamen, and globus pallidus each in the left and right hemispheres) for a total of 154 ROI (i.e., 134 Craddock ROIs, 6 basal ganglia ROIS and 14 Thalamic ROIs). While other parcellation schemes are available (e.g., Harvard-Oxford atlas, AAL atlas), the present one has two main advantages (cf., Monti et al., 2013). First, being functionally defined, it clusters spatially proximal voxels by the homogeneity of their functional connections as opposed to clustering voxels

by anatomical position which, as exemplified by the case of the precentral gyrus ROIs in both the AAL and the Harvard-Oxford atlases, might cluster together functionally distinct sub-regions. Second, at our chosen level of resolution, the Craddock ROIs have almost 50% more granularity as either structural atlas (i.e., 154 ROIs versus, 90 and 112 for the AAL and Harvard-Oxford atlases, respectively). Following parcellation, the average time-course of all voxel within each ROI were extracted and correlated across each pair of regions.

Functional connectivity was assessed with a partial correlation method using the Markov Network Toolbox (MoNeT; Narayan et al., 2015) in MATLAB. This approach, referred to as R3 (as in resampling, random penalization, and random effects), combines a penalized maximum likelihood estimation or graphical lasso procedure with a resampling-based (bootstrapped) model selection procedure, on whitened BOLD timeseries, to infer fully-data driven stable functional connectivity estimates at the single-subject (or group) level. Under this approach, each fMRI time series is repeatedly bootstrapped in order to estimate the within-subject variability and matrices of penalty parameters which reduce selection bias and variability. This method thus reduces the spurious connections from indirect sources arising from the high dimensionality of fMRI data often seen when using the conventional Pearsons r method. Using partial correlations with regularization parameters, the indirect sources are eliminated and the sparsity of each matrix is determined by the within subject variability. Thus, each functional data set returns a connectivity matrix that represents connectivity from direct sources, rather than indirect ones, and that is sparse, as determined on a single-subject basis through bootstrapping and regulatization. This latter point side-steps entirely the need for arbitrary and iterative thresholding approaches (Rubinov and Sporns, 2010). It is important to point out, however, another important difference between the partial correlations approach described above and the standard correlation approach to estimating brain networks as performed by most previous work (e.g., Boveroux et al., 2010; Monti et al., 2013; Schrouff et al., 2011). On the one hand, the conventional correlational approach has the advantage of allowing straightforward interpretation of the elements of adjacency matrices as strength of the functional connectivity between nodes. On the other hand, the matrices generated are fully connected and thus requiring application of a non-linear transformation

(e.g., thresholding) in order to render them sparse a condition necessary for application of many common graph theory metrics (Rubinov and Sporns, 2010). In contrast, the partial correlation method employed here returns a sparse matrix. However, it does so at the cost of losing interpretability of graph weights which can now be seen as the functional connectivity between two nodes i and j after controlling for the correlations with other nodes in the neighborhood (i.e., connected with) say i. For this reason, matrices obtained with this novel methodology are typically binarized, thus resulting in a sparse matrix of ones and zeros indexing the presence/absence of functional connectivity between each pair of nodes (i.e., ROIs).

3.3.1 Analyses

3.3.1.1 ERGM

For both the HCP participants' and patients' datasets, we ran 4 ERGM: complete model (see §2.2), structural model (i.e., all terms except GWESP), GWESP model (i.e., all terms except structural terms), and base model (i.e., all terms except GWESP and structural terms). We compared these 4 ERGMS in three combinations: base model to structural model (i.e., GWESP effect), base model to GWESP model (i.e,. structural effect), and GWESP model to complete model (i.e, interaction effect). The first comparison was to isolate the effects of leaving out structural terms discussed in problem #3. The second comparison was to isolate the effects of leaving out a term that accounts for triadic closure (i.e., the GWESP term) discussed in problem #2. Finally, the third comparison demonstrates the effects of leaving out the structural terms while still accounting for triadic closure (i.e., a combination of problem #2 and #3). We labeled on model as the full model and one as the partial model in each comparison.

To compare the affects of not accounting for specific terms, we tallied the change in PEs when the terms were omitted. If a PE was significant in the full model (i.e., the model with more terms for that specific comparison), but not the partial, we label this as a FN. FP was a PE that was significant in PM, but not the FM. We group the PEs based on whether

they belonged to the cortical regions or subcortical to see if within cortical connectivity was affected, within subcortical connectivity, or between cortical to subcortical connectivity.

These tallies of FP and FN were compared for differences between patients grouped based on their level of consciousness at each imaging session using a behavior assessment (see Chapter 4 for a complete description of the behavioral assessment used). This was to assess differences used in many cross sectional analyses for DOC patients (e.g., Boly et al., 2011; Crone et al., 2011, 2015; Fernández-Espejo et al., 2012; Kotchoubey et al., 2013; Sitt et al., 2014; Vanhaudenhuyse et al., 2010; Zhou et al., 2011). To mirror this in the HCP datasets, we compared the first resting state imaging to the second resting state imaging session.

3.3.1.2 ERGM model fits

Due to the large number of total ERGM conducted (192 in total across patients and HCP participants), we will only compare for two patients (i.e., P092 in acute stage TBI and P085 in chronic stage TBI) and HCP patients (i.e., HCP002 from the first and HCP008 resting state imaging sessions) for the complete and GWESP models assessed by using goodness of fit (GOF) plots (Hunter et al., 2008). After the model was estimated, a thousand simulations were run from the model statistics. These simulations were compared to the original graphs probabilities for each graph statistic. This is to ensure that the model represents a graph similar to the original data that it was modeled from. We will assess the overall model statistics from equation 4.1, edge shared partner distributions, and degree distributions.

3.3.1.3 Multinomial Regressions

Using the nnet package Venables and Ripley (2013) in R, we used the mlogit function to multinomial regressions to predict the differences between unconscious patients' FP and FN rates for the cortical groupings. The no error for all grouping was the reference group for the outcome variable and the acute conscious patients were the reference for the predictor variable. For the cortical group there were 6 possible categories predicted, which were FN

and FP for each grouping. The same comparisons were conducted for the HCP participants, but there was only one possible comparison between the first and second resting state scan. Finally, we transformed all the logits into odds ratios for reporting and interpretations.

3.4 Results

	Multinomial Regression: Cortical Nodal Labeling					
Comparison:	Interaction effect		GWESP effect		Structural effect	
	Constant	Rest2	Constant	Rest2	Constant	Rest2
False negatives for Cortical to Subcortical	0.00597***	1.49			0.00614***	1.97
	(0.355)	(0.458)			(0.355)	(0.435)
False positives for Cortical to Subcortical	0.0269***	0.716	0.039***	0.681	0.0338***	0.628
	(0.169)	(0.260)	(0.141)	(0.220)	(0.153)	(0.245)
False negatives for Within Cortical	0.0157***	0.614	0.001***	0.984	0.937***	0.797
	(0.220)	(0.355)	(0.708)	(1.001)	(0.198)	(0.296)
False positives for Within Cortical	0.0299***	1.09	0.031***	0.937	0.0515***	0.869
	(0.160)	(0.222)	(0.157)	(0.224)	(0.125)	(0.183)
False negatives for Within Subcortical	0.00448***	0.826	0.002***	0.656	0.00307***	1.73
	(0.409)	(0.607)	(0.578)	(0.914)	(0.501)	(0.628)
False positives for Within Subcortical	0.00149***	0.496	0.002***	<0.0001	0.000768***	1.97
	(0.708)	(1.23)	(0.578)	(<0.0001)	(1.00)	(1.23)
Observations	2904		2904		2904	
Log Likelihood	-1072.262		-1702.825		-1316.831	
Akaike Inf. Crit.	2168.524		1722.825		2657.662	
Note:					*$p<0.05$; **$p<0.01$; ***$p<0.001$	

Table 3.3: **The effect of imaging session day on FPs and FNs.** For the cortical nodal labeling, the FPs and FNs for each type of connectivity pattern were predicted for the first resting state imaging days. The change in logits and their standard errors in parentheses are listed for the interaction, GWESP and structural effect comparisons.

Consistent with the argument we made in the introduction (see §1.1.1), as shown in Table 3.4, the brain network construction using MoNeT resulted in with different estimated densities. Overall, the density varied between resting state session 1 and session 2 in all participants (except HCP011) within the range between 0.003 to 0.0175. Across participants, the densities ranged from 0.1676 to 0.2159. The structural connectivity, on the other hand, had less variability in the densities of the graphs across subjects from 0.0531 to 0.0632. For the patients, the density of the functional connectivity differed between resting acute session

	Acute	Chronic		Rest1	Rest2
P054			*HCP001*		
Functional Density	0.1524	0.1456	Functional Density	0.1799	0.1901
Structural Density	0.0648	0.0554	Structural Density	0.0534	NA
P055			*HCP002*		
Functional Density	0.1491	0.1395	Functional Density	0.1735	0.1854
Structural Density	0.0587	0.053	Structural Density	0.0543	NA
P066			*HCP003*		
Functional Density	0.1356	0.1344	Functional Density	0.1783	0.1702
Structural Density	0.0527	0.0535	Structural Density	0.0632	NA
P069			*HCP004*		
Functional Density	0.1341	0.1387	Functional Density	0.1862	0.1676
Structural Density	0.0637	0.0542	Structural Density	0.0531	NA
P074			*HCP005*		
Functional Density	0.1425	0.1306	Functional Density	0.1812	0.1787
Structural Density	0.056	0.0565	Structural Density	0.0576	NA
P079			*HCP006*		
Functional Density	0.1419	0.1329	Functional Density	0.1781	0.1748
Structural Density	0.0539	0.0546	Structural Density	0.0547	NA
P084			*HCP007*		
Functional Density	0.1511	0.1264	Functional Density	0.1919	0.1854
Structural Density	0.0557	0.0562	Structural Density	0.0538	NA
P085			*HCP008*		
Functional Density	0.1384	0.1274	Functional Density	0.2041	0.1996
Structural Density	0.0546	0.057	Structural Density	0.0556	NA
P089			*HCP009*		
Functional Density	0.1268	0.126	Functional Density	0.1829	0.1852
Structural Density	0.0548	0.0537	Structural Density	0.054	NA
P092			*HCP010*		
Functional Density	0.128	0.1299	Functional Density	0.1829	0.1826
Structural Density	0.0585	0.0598	Structural Density	0.0537	NA
P096			*HCP011*		
Functional Density	0.1039	0.137	Functional Density	0.1991	0.1991
Structural Density	0.057	0.0561	Structural Density	0.0543	NA
P099			*HCP012*		
Functional Density	0.1241	0.1385	Functional Density	0.2159	0.1984
Structural Density	0.0541	0.0535	Structural Density	0.0539	NA

Table 3.4: **Densities for the functional and structural connectivity.** The functional connectivity and structural connectivity was allowed to naturally vary based on the thresholding procedure (see §3.2). There is no clear difference within the patients when comparing acute and chronic stage of TBI for neither the structural or functional density. The HCP participants also show no clear difference between resting state imaging on day 1 compared to day 2.

	Complete Model					GWESP Model			
	Observed	*min*	*M*	*max*	*p*-value	*min*	*M*	*max*	*p*-value
HCP001 Rest1									
Inter-Frontoparietal Subcortical	11	5	10	19	1	3	8.600	14	0.200
Inter-Default Visual	82	65	78.700	90	0.800	65	77.400	88	0.200
Inter-Default Limbic	69	57	64.800	70	0.200	56	68	80	1
Inter-Subcortical Thalamus	14	13	16.500	20	0.200	3	13	21	1
Inter-Default Ventral Attention	79	75	86.100	100	0.200	62	78.300	86	1
HCP002 Rest1									
Edges	2,044	2,023	2,059.600	2,113	1	1,901	1,983.800	2,064	0.200
Inter-Limbic Thalamus	20	15	20.500	26	1	9	14.900	22	0.200
Within Subcortical	159	144	161.800	173	0.600	112	143.400	169	0.200
Gwesp (Fixed, λ=0.6	3,634.600	3,593.262	3,660.370	3,756.905	1	3,367.806	3,521.756	3,670.710	0.200
HCP003 Rest1									
Inter-Dorsal Attention Dorsa Attention	7	6	8.500	12	0.200	3	6.700	11	1
Inter-Subcortical Visual	10	6	8.300	14	0.200	4	10.300	18	0.800
HCP004 Rest1									
Within Thalamus	23	16	25.900	33	0.400	23	32.200	39	0.200
Within Subcortical	138	118	144.300	160	0.400	140	160.600	169	0
HCP005 Rest2									
Inter-Frontoparietal Somatomotor	45	29	38.800	45	0.200	30	43.300	50	1
Within Subcortical	174	156	184.100	200	0.200	148	167.400	176	0.600
HCP006 Rest2									
Inter-Frontoparietal Somatomotor	45	29	38.800	45	0.200	30	43.300	50	1
Within Subcortical	174	156	184.100	200	0.200	148	167.400	176	0.600
HCP008 Rest2									
Inter-Limbic Thalamus	26	19	23	30	0.400	16	20.800	29	0.200
Inter-Somatomotor Thalamus	75	64	73.800	87	0.800	60	67.900	76	0.200
Inter-Limbic Visual	28	15	27.100	37	0.800	18	21.900	27	0
HCP009 Rest1									
Inter-Limbic Subcortical	16	14	17.400	21	1	17	19.200	24	0
Inter-Frontoparietal Ventral Attention	46	35	46.700	52	0.800	45	49.900	57	0.200
Inter-Dorsal Attention Visual	28	21	28.200	38	1	20	24.200	34	0.200
HCP010 Rest1									
Inter-Basal Ganglia Default	33	24	31.700	44	0.400	25	29.200	32	0
Inter-Default Dorsal Attention	41	29	40.100	53	0.800	36	44.400	47	0.200
HCP010 Rest2									
Inter-Basal Ganglia Limbic	13	7	11.100	18	0.200	8	12.900	21	1
Within Temporal lobe	71	62	76	83	0.200	66	70.700	76	1
HCP012 Rest2									
Inter-Basal Ganglia Ventral Attention	18	17	20.800	30	0.200	12	16.200	24	0.600
Within Frontal lobe	332	318	339.700	354	0.200	311	336.400	350	0.600

Table 3.5: **Goodness of fit differences for the interaction effect comparison for graph statistics.** We are displaying the four worst fit differences for the two models in the interaction effect comparison. The observed column is the original data's values for each graph statistic, while the minimum, mean, maximum, and p-value for the simulated graphs based on each of the ERGM models are displayed. They are the biggest difference between the complete model and the GWESP model. Overall, all the patients' ERGM for the complete model and GWESP effect fit the data well based on the graph statistics modeled but the GWESP model had 4 p-values < 0.05.

	Complete Model					GWESP Model				Complete Model					GWESP Model			
	HCP001 Rest1					HCP001 Rest1				HCP008 Rest2					HCP008 Rest2			
	Observed	*min*	*M*	*max*	*p*-value	*min*	*M*	*max*	*p*-value	Observed	*min*	*M*	*max*	*p*-value	*min*	*M*	*max*	*p*-value
esp0	6	0	0	0	0	0	0.200	1	0	4	0	0	0	0	0	0	0	0
esp1	21	0	3.200	7	0	2	4.700	7	0	12	0	0.400	1	0	0	0.500	1	0
esp2	49	41	49.800	60	0.800	41	49	63	1	22	9	13.200	20	0	8	12	16	0
esp3	107	143	169	196	0	153	165.700	178	0	56	66	82.100	97	0	56	72	86	0.200
esp4	165	278	306.200	341	0	252	286.900	338	0	116	194	220.200	268	0	180	207.500	244	0
esp5	185	336	365.500	387	0	332	360.900	396	0	165	300	335.800	378	0	328	338.400	368	0
esp6	229	308	341.700	392	0	320	347.200	369	0	207	354	393.900	415	0	377	399.200	413	0
esp7	288	243	270.800	304	0.400	274	297.900	350	0.600	212	365	403.800	430	0	387	402.900	442	0
esp8	248	167	200.600	237	0	199	220.700	242	0	228	293	331.900	366	0	306	332.800	365	0
esp9	228	105	128.200	166	0	119	145	164	0	198	211	225.100	248	0	212	245.300	288	0
esp10	160	51	76.300	100	0	73	85.400	111	0	157	107	143.600	196	0.400	128	159.900	180	0.600
esp11	121	22	39.900	74	0	24	45.900	59	0	148	72	88.200	105	0	84	93.600	108	0
esp12	95	10	18.400	27	0	17	27.100	38	0	120	34	53.100	72	0	34	49.500	60	0
esp13	43	3	7.500	15	0	1	13.500	26	0	115	12	24.200	33	0	17	23.100	29	0
esp14	31	2	4.400	10	0	1	5.400	11	0	84	5	13	21	0	7	11.500	20	0
esp15	32	0	1.500	6	0	1	2.600	5	0	82	1	5.900	13	0	2	4.300	8	0
esp16	17	0	0.200	1	0	0	1.300	3	0	66	0	1.800	5	0	0	2.500	5	0
esp17	7	0	0.400	2	0	0	0.100	1	0	48	0	0.700	2	0	0	0.700	3	0
esp18	3	0	0.200	1	0	0	0	0	0	45	0	0	0	0	0	0.300	1	0
esp19	3	0	0	0	0	0	0.100	1	0	40	0	0.200	1	0	0	0.100	1	0

Table 3.6: **Goodness of fit differences for the interaction effect comparison for edge shared partners.** We are displaying the two worst fit differences for the two models in the interaction effect comparison. The observed column is the original data's values for each edge shared partner type, while the minimum, mean, maximum, and p-value for the simulated graphs based on each of the ERGM models are displayed. The edge shared partner types are based on the number of triangles sharing a common edge (e.g., the esp10 term has 10 triangles all sharing common edge). Overall, all the patients' ERGM for the complete model and GWESP effect did not fit the data well based on the graph statistics modeled because both models had at least than 11 of the 14 p-values < 0.05 for types of edge shared partner type.

	Complete Model					GWESP Model				Complete Model					GWESP Model			
	HCP001 Rest1					HCP001 Rest1				HCP008 Rest2					HCP008 Rest2			
	Observed	*min*	*M*	*max*	*p*-value	*min*	*M*	*max*	*p*-value	Observed	*min*	*M*	*max*	*p*-value	*min*	*M*	*max*	*p*-value
9	0	0	0.300	2	1	0	0.100	1	1	0	0	0	0	1	0	0	0	1
10	1	0	0.600	2	1	0	0.400	1	0.800	0	0	0	0	1	0	0	0	1
11	1	0	0.900	3	1	0	0.800	2	1	0	0	0	0	1	0	0	0	1
12	1	0	0.700	2	1	0	1.100	4	1	1	0	0.100	1	0.200	0	0.100	1	0.200
13	1	0	0.700	3	0.800	0	0.900	4	1	0	0	0.100	1	1	0	0	0	1
14	2	0	1.600	4	0.800	0	1.300	2	0.800	1	0	0.200	1	0.400	0	0	0	0
15	1	1	2	4	0.800	1	2.300	5	0.600	1	0	0.300	1	0.600	0	0.100	1	0.200
16	3	0	2.200	6	0.600	0	2.100	4	0.600	0	0	0.200	1	1	0	0.200	1	1
17	1	1	3.100	7	0.200	1	2.800	6	0.600	1	0	0.600	2	0.800	0	0.500	2	0.600
18	2	1	3	6	0.800	0	2.800	5	0.600	1	0	1	2	1	0	1	2	1
19	4	1	4.600	8	0.800	1	4.800	10	1	3	0	1.200	3	0.200	0	1.100	3	0.200
20	4	2	5.200	8	0.600	4	5.800	8	0.600	3	0	2.700	5	1	0	1.600	3	0.200
21	4	2	6.900	14	0.600	4	5.700	8	0.400	6	1	2.700	4	0	1	1.700	4	0
22	11	5	7.900	13	0.400	2	6.600	9	0	7	0	3.700	10	0.400	0	3.100	7	0.200
23	9	5	9.700	18	1	3	8.500	13	1	3	1	4.300	7	1	2	5.800	12	0.400
24	8	5	8.900	16	1	6	10.100	16	0.400	5	4	6.200	9	0.600	5	7.700	12	0.200
25	9	1	8.600	14	1	7	10	14	1	10	5	8.500	14	0.600	3	7.700	13	0.600
26	8	8	10.500	13	0.600	3	7.900	10	1	6	7	9.400	13	0	4	7.100	11	1
27	11	5	10.700	16	1	5	9	15	0.400	6	3	9.500	13	0.400	3	8	14	1
28	11	5	8.700	13	0.800	4	9.200	16	0.600	12	7	10.100	14	0.600	7	10.400	16	0.400
29	10	7	10.500	15	1	3	9.500	16	1	5	6	9.200	13	0	6	9.700	15	0
30	10	1	7.400	10	0.400	6	9	12	0.800	6	6	10.100	15	0.200	7	11.600	20	0
31	10	1	6	8	0	4	6.800	12	0.400	5	7	11.700	16	0	5	10	16	0.200
32	4	3	5.300	8	0.800	4	6.100	9	0.200	7	5	9.200	14	0.800	5	11	17	0.400
33	7	1	5.200	11	0.800	2	6.100	10	1	10	5	8.700	14	0.600	4	10.800	16	1
34	3	1	4.700	8	0.800	3	5.400	8	0.400	5	1	8	13	0.400	6	9.700	14	0
35	5	1	3.700	7	0.800	0	3.700	8	0.600	10	3	5.700	10	0.200	3	6.400	9	0
36	4	1	2.600	5	0.800	1	3.700	8	1	9	3	6.300	9	0.200	2	5.700	11	0.400
37	2	0	2.200	5	1	0	2.400	5	1	5	2	5.800	9	1	3	6	9	0.800
38	0	0	1.900	4	0.200	0	1.600	3	0.200	5	1	4.400	7	1	1	4.400	7	1
39	1	0	1.700	4	0.800	0	1.600	3	0.800	2	2	4.400	7	0.200	0	2.300	5	1

Table 3.7: **Goodness of fit differences for the interaction effect comparison for the degree distribution.** We are displaying the two worst fit differences for the two models in the interaction effect comparison. The observed column is the original data's values for each nodal degree, while the minimum, mean, maximum, and p-value for the simulated graphs based on each of the ERGM models are displayed. Overall, all the patients' ERGM for the complete model and GWESP effect fit the data well based on the graph statistics modeled because there were only 3 to 5 p-values < 0.05.

ERGM Structural Terms and GWESP term for Functional Connectivity for HCP participants												
	HCP001 Rest1	HCP001 Rest2	HCP002 Rest1	HCP002 Rest2	HCP003 Rest1	HCP003 Rest2	HCP004 Rest1	HCP004 Rest2	HCP005 Rest1	HCP005 Rest2	HCP006 Rest1	HCP006 Rest2
Degree	0.003	−0.0001	0.006	0.007	0.006	0.006	−0.002	0.007	−0.001	−0.005	0.003	0.00003
	(0.002)	(0.005)	(0.003)	(0.004)	(0.006)	(0.005)	(0.003)	(0.005)	(0.004)	(0.004)	(0.003)	(0.005)
Efficiency	−0.031	0.047	0.189	0.114	0.068	0.153	−0.161	0.431*	−0.199	−0.227	−0.044	−0.073
	(0.085)	(0.203)	(0.144)	(0.131)	(0.228)	(0.210)	(0.114)	(0.217)	(0.163)	(0.143)	(0.102)	(0.104))
Clustering Coefficient	0.074	−0.020	−0.235	−0.122	−0.151	−0.077	−0.184	−0.298	−0.157	−0.082	−0.132	0.092
	(0.101)	(0.212)	(0.241)	(0.134)	(0.232)	(0.213)	(0.138)	(0.211)	(0.164)	(0.181)	(0.131)	(0.212)
Latent Cluster 1	−0.041	0.158**	0.113	0.068	−0.003	0.034	0.011	0.039	0.170*	0.027	−0.002	0.004
	(0.052)	(0.053)	(0.059)	(0.057)	(0.077)	(0.063)	(0.067)	(0.107)	(0.079)	(0.056)	(0.052)	(0.052))
Latent Cluster 2	−0.036	0.197**	0.291***	0.049	0.061	0.054	0.101	0.022	0.052	−0.019	0.038	0.092
	(0.072)	(0.069)	(0.063)	(0.072)	(0.058)	(0.072)	(0.061)	(0.051)	(0.050)	(0.082)	(0.076)	(0.096)
GWESP(fixed, $\lambda = 0.6$)	3.549***	4.660***	3.543***	3.707***	3.843***	3.057***	4.222***	2.760***	4.581***	3.205***	3.946***	4.057***
	(0.279)	(0.351)	(0.240)	(0.299)	(0.262)	(0.212)	(0.327)	(0.199)	(0.319)	(0.266)	(0.289)	(0.270)
Note:												*$p<0.05$; **$p<0.01$; ***$p<0.001$

Table 3.8: **Structural metrics effects on functional connectivity and triadic closure in functional connectivity for HCP participants.** The effects for structural connectivity's degree, local efficiency, clustering coefficient, and nodematch latent clustering on the functional connectivity from the complete models. The LATEX code to create this table was produced by the R package called texreg (Leifeld, 2013).

ERGM Structural Terms and GWESP term for Functional Connectivity for HCP participants												
	HCP007 Rest1	HCP007 Rest2	HCP008 Rest1	HCP008 Rest2	HCP009 Rest1	HCP009 Rest2	HCP010 Rest1	HCP010 Rest2	HCP011 Rest1	HCP011 Rest2	HCP012 Rest1	HCP012 Rest2
Degree	−0.001	−0.003	0.004	0.004	0.006	−0.001	0.002	0.009***	0.006	0.013***	0.006	0.009*
	(0.003)	(0.004)	(0.004)	(0.004)	(0.004)	(0.004)	(0.004)	(0.003)	(0.004)	(0.004)	(0.005)	(0.005)
Efficiency	−0.330***	−0.277**	−0.056	−0.007	−0.273	−0.304*	0.012	0.116	−0.0005	−0.002	−0.287	0.138
	(0.125)	(0.126)	(0.171)	(0.176)	(0.189)	(0.179)	(0.140)	(0.139)	(0.213)	(0.217)	(0.239)	(0.229)
Clustering Coefficient	0.339	0.232	−0.113	0.272	0.389	0.368*	−0.370	0.102	−0.158	−0.015	0.169	−0.072
	(0.208)	(0.209)	(0.221)	(0.228)	(0.237)	(0.204)	(0.253)	(0.246)	(0.315)	(0.317)	(0.274)	(0.271)
Latent Cluster 1	0.090*	−0.008	0.203***	0.121*	0.086*	−0.081	0.013	−0.039	−0.152	0.090	0.005	0.084*
	(0.050)	(0.049)	(0.057)	(0.063)	(0.052)	(0.318)	(0.051)	(0.052)	(0.151)	(0.142)	(0.050)	(0.050)
Latent Cluster 2	0.076	0.069	0.168***	0.015	−0.114	−0.002	0.001	−0.061	−0.004	−0.001	0.019	0.069
	(0.070)	(0.074)	(0.052)	(0.053)	(0.079)	(0.064)	(0.068)	(0.069)	(0.050)	(0.053)	(0.071)	(0.074)
GWESP(fixed, $\lambda = 0.6$)	5.441***	3.791***	7.485***	5.060***	2.786***	2.760***	4.611***	5.454***	5.050***	3.704***	7.656***	4.842***
	(0.409)	(0.302)	(0.584)	(0.431)	(0.252)	(0.199)	(0.313)	(0.343)	(0.424)	(0.364)	(0.687)	(0.425)
Note:												*p<0.05; **p<0.01; ***p<0.001

Table 3.9: **Structural metrics effects on functional connectivity and triadic closure in functional connectivity for HCP participants.** The effects for structural connectivity's degree, local efficiency, clustering coefficient, and nodematch latent clustering on the functional connectivity from the complete models. The LATEX code to create this table was produced by the R package called texreg (Leifeld, 2013).

Figure 3.2: **HCP participants comparison revealing the interaction effect.** Each graph represents the difference between the complete model and GWESP model. These parameter estimates are generated from the same connectivity matrix for both the complete model and GWESP model. The numerical values for each parameter estimate is the difference between the two models. The FPs are the parameter estimates that were significant in the GWESP model, but they were not significant in complete. The FNs are the parameter estimates that were not significant in the GWESP model, but they were significant in the complete model. The difference between the two models are the inclusion of structural connectivity nodal covariates.

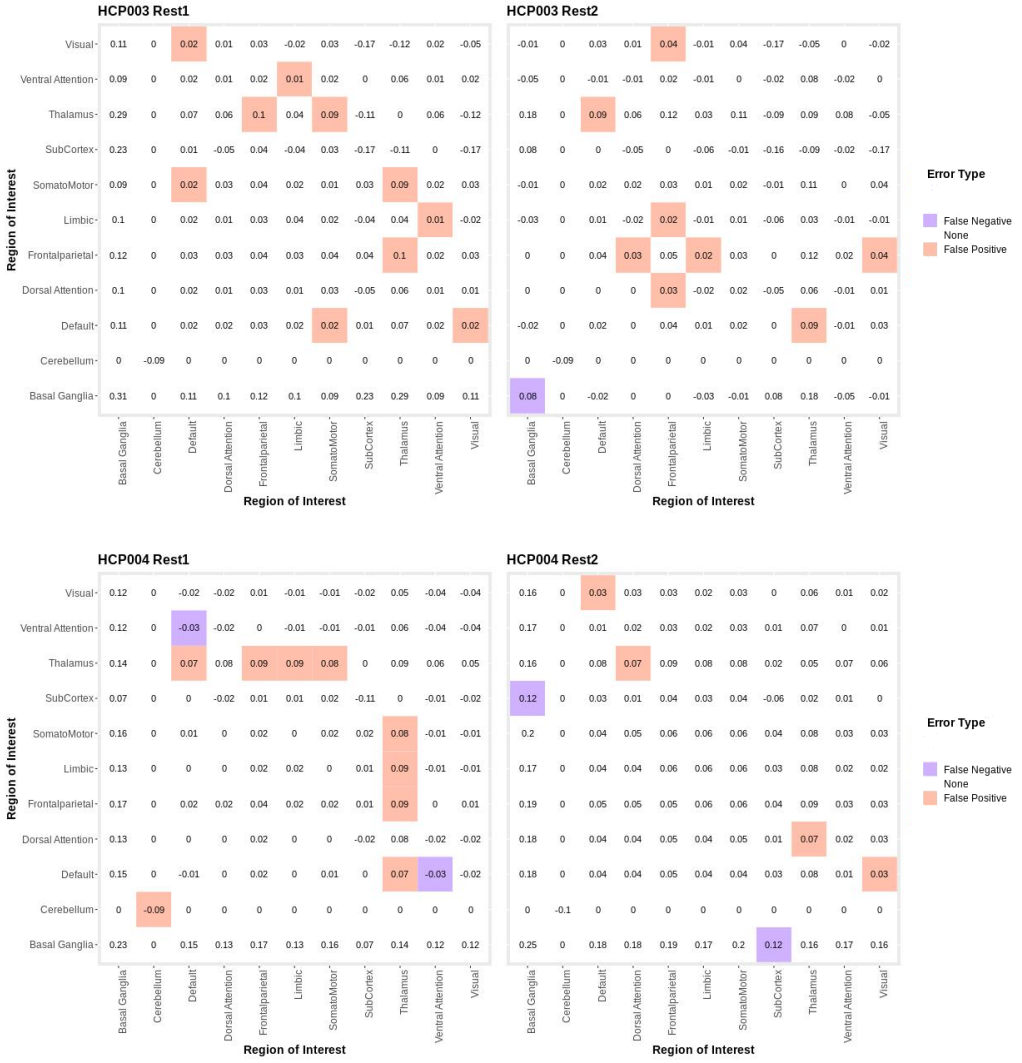

Figure 3.3: **HCP participants comparison revealing the interaction effect.** Each graph represents the difference between the complete model and GWESP model. These parameter estimates are generated from the same connectivity matrix for both the complete model and GWESP model. The numerical values for each parameter estimate is the difference between the two models. The FPs are the parameter estimates that were significant in the GWESP model, but they were not significant in complete. The FNs are the parameter estimates that were not significant in the GWESP model, but they were significant in the complete model. The difference between the two models are the inclusion of structural connectivity nodal covariates.

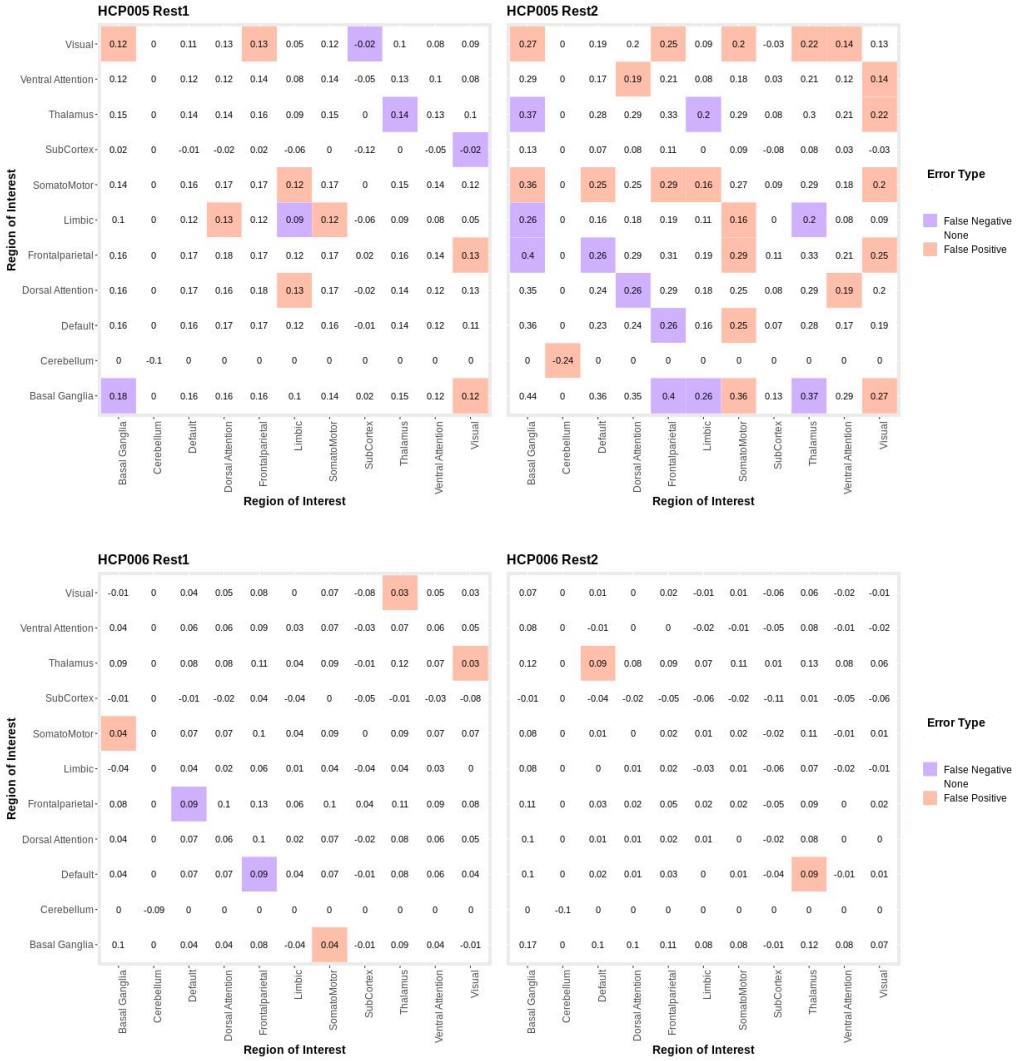

Figure 3.4: **HCP participants comparison revealing the interaction effect.** Each graph represents the difference between the complete model and GWESP model. These parameter estimates are generated from the same connectivity matrix for both the complete model and GWESP model. The numerical values for each parameter estimate is the difference between the two models. The FPs are the parameter estimates that were significant in the GWESP model, but they were not significant in complete. The FNs are the parameter estimates that were not significant in the GWESP model, but they were significant in the complete model. The difference between the two models are the inclusion of structural connectivity nodal covariates.

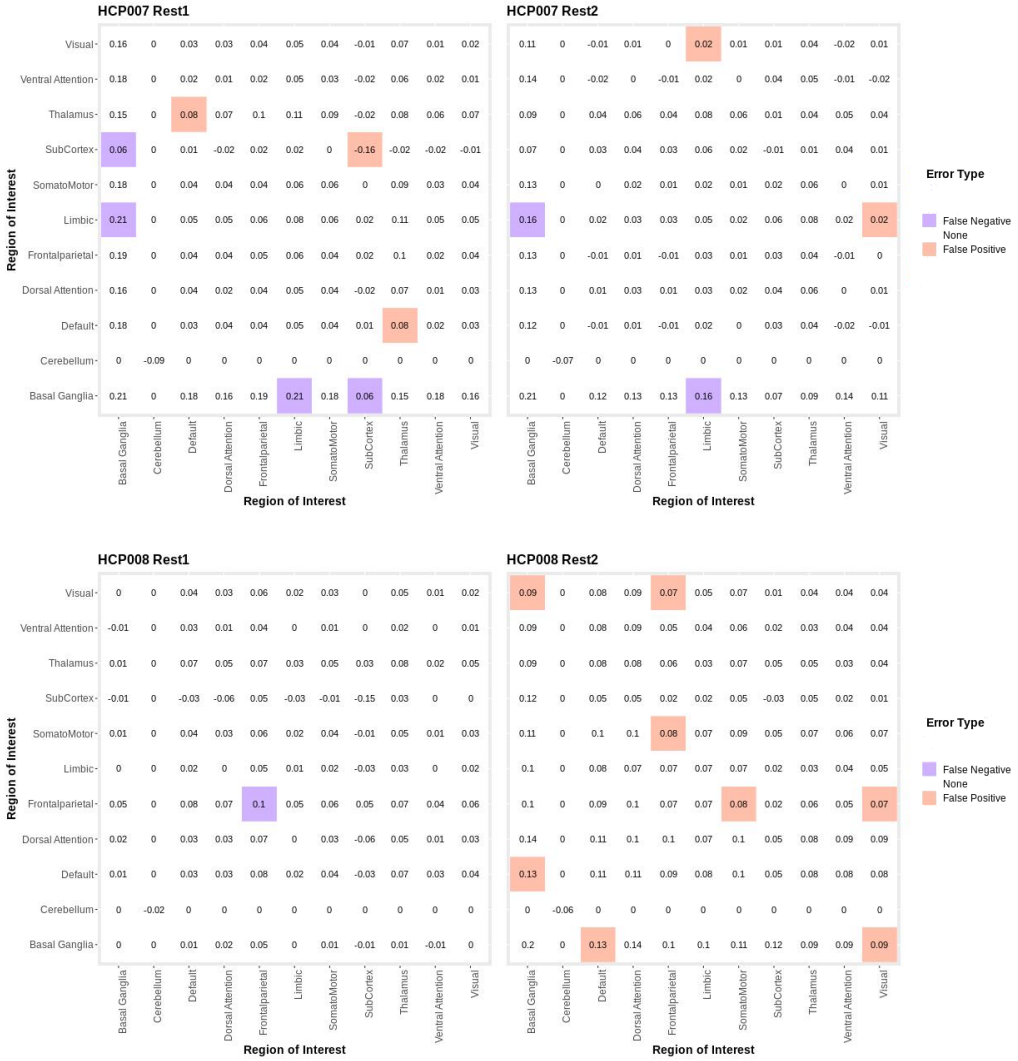

Figure 3.5: **HCP participants comparison revealing the interaction effect.** Each graph represents the difference between the complete model and GWESP model. These parameter estimates are generated from the same connectivity matrix for both the complete model and GWESP model. The numerical values for each parameter estimate is the difference between the two models. The FPs are the parameter estimates that were significant in the GWESP model, but they were not significant in complete. The FNs are the parameter estimates that were not significant in the GWESP model, but they were significant in the complete model. The difference between the two models are the inclusion of structural connectivity nodal covariates.

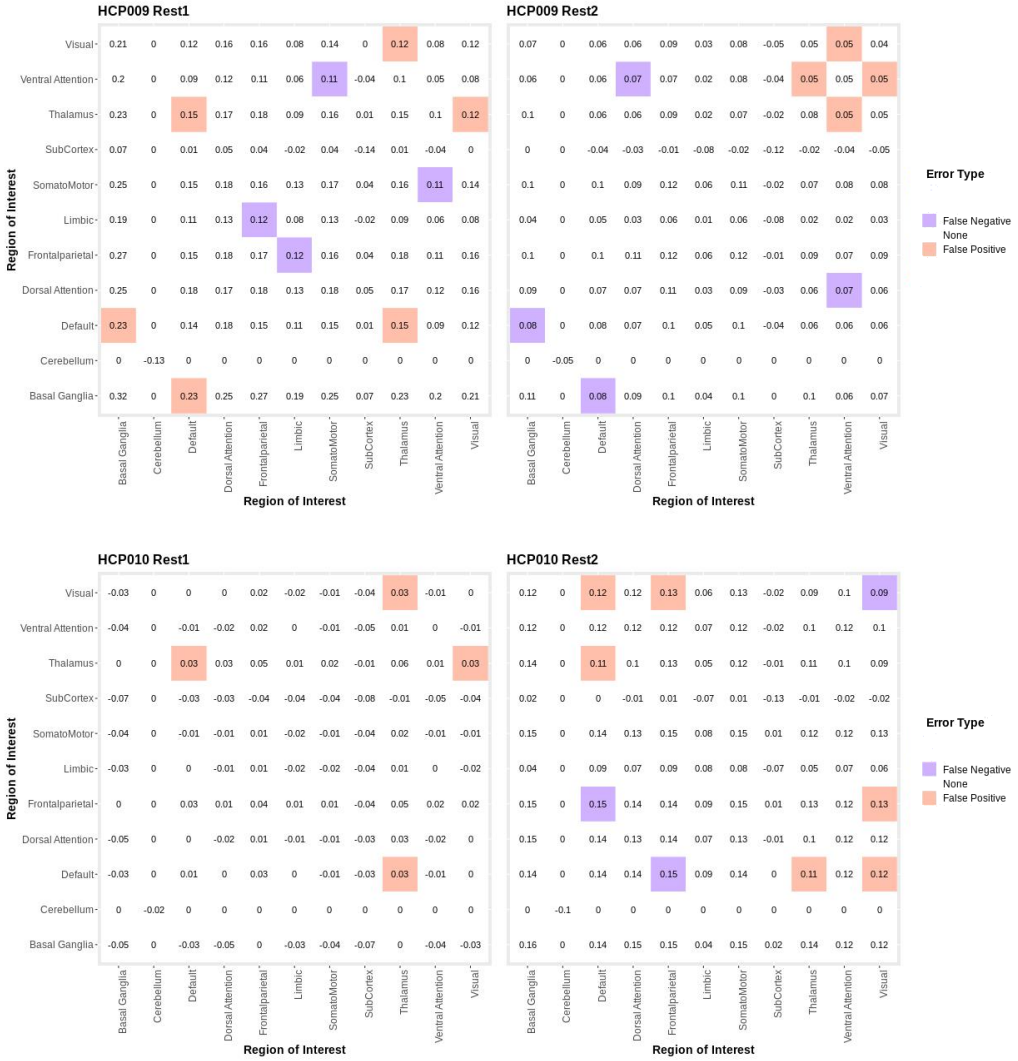

Figure 3.6: **HCP participants comparison revealing the interaction effect.** Each graph represents the difference between the complete model and GWESP model. These parameter estimates are generated from the same connectivity matrix for both the complete model and GWESP model. The numerical values for each parameter estimate is the difference between the two models. The FPs are the parameter estimates that were significant in the GWESP model, but they were not significant in complete. The FNs are the parameter estimates that were not significant in the GWESP model, but they were significant in the complete model. The difference between the two models are the inclusion of structural connectivity nodal covariates.

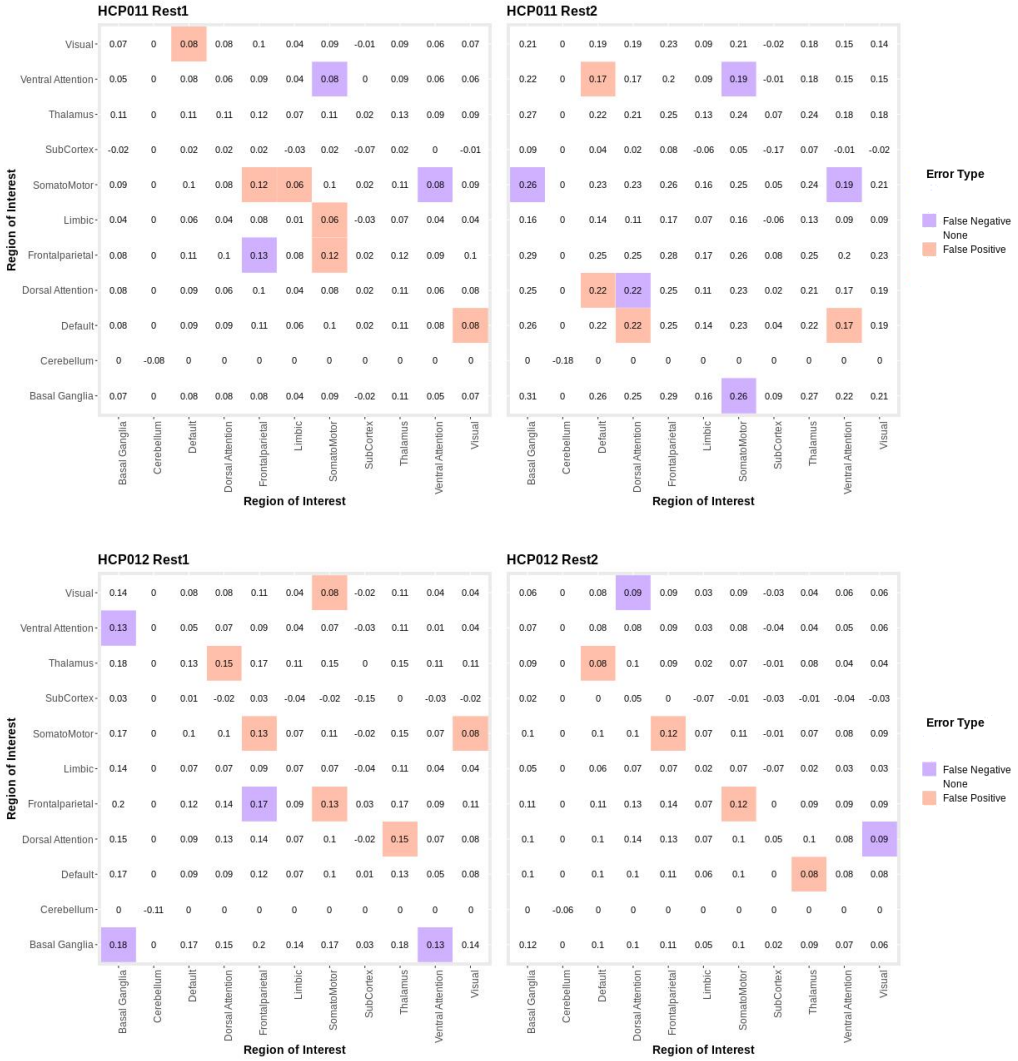

Figure 3.7: **HCP participants comparison revealing the interaction effect.** Each graph represents the difference between the complete model and GWESP model. These parameter estimates are generated from the same connectivity matrix for both the complete model and GWESP model. The numerical values for each parameter estimate is the difference between the two models. The FPs are the parameter estimates that were significant in the GWESP model, but they were not significant in complete. The FNs are the parameter estimates that were not significant in the GWESP model, but they were significant in the complete model. The difference between the two models are the inclusion of structural connectivity nodal covariates.

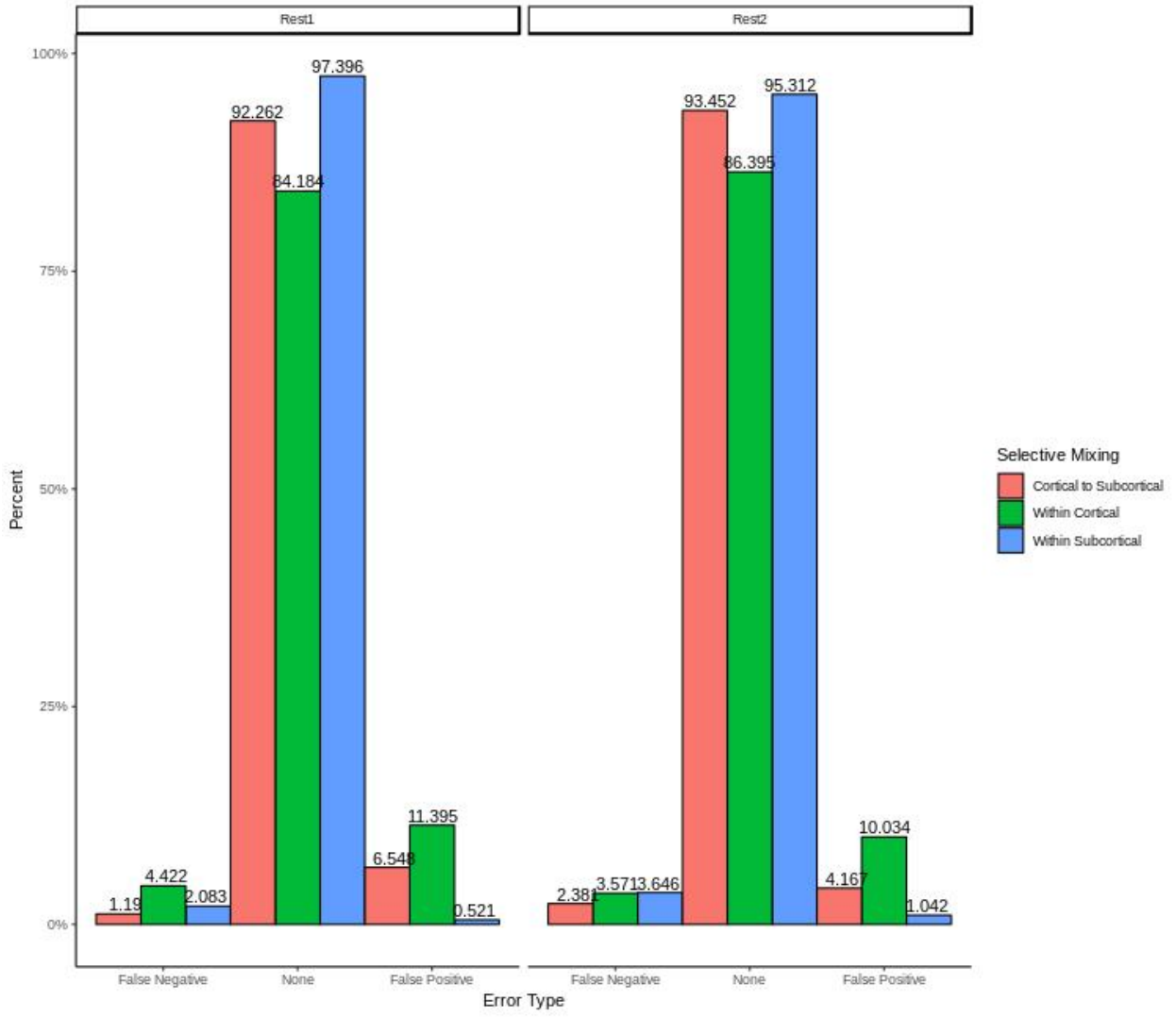

Figure 3.8: **HCP participants comparison revealing the interaction effect.** This figure shows the FN and FP effects for a different exogenous nodal labeling of cortical compared to subcortical regions for each resting state imaging session separated by one day.

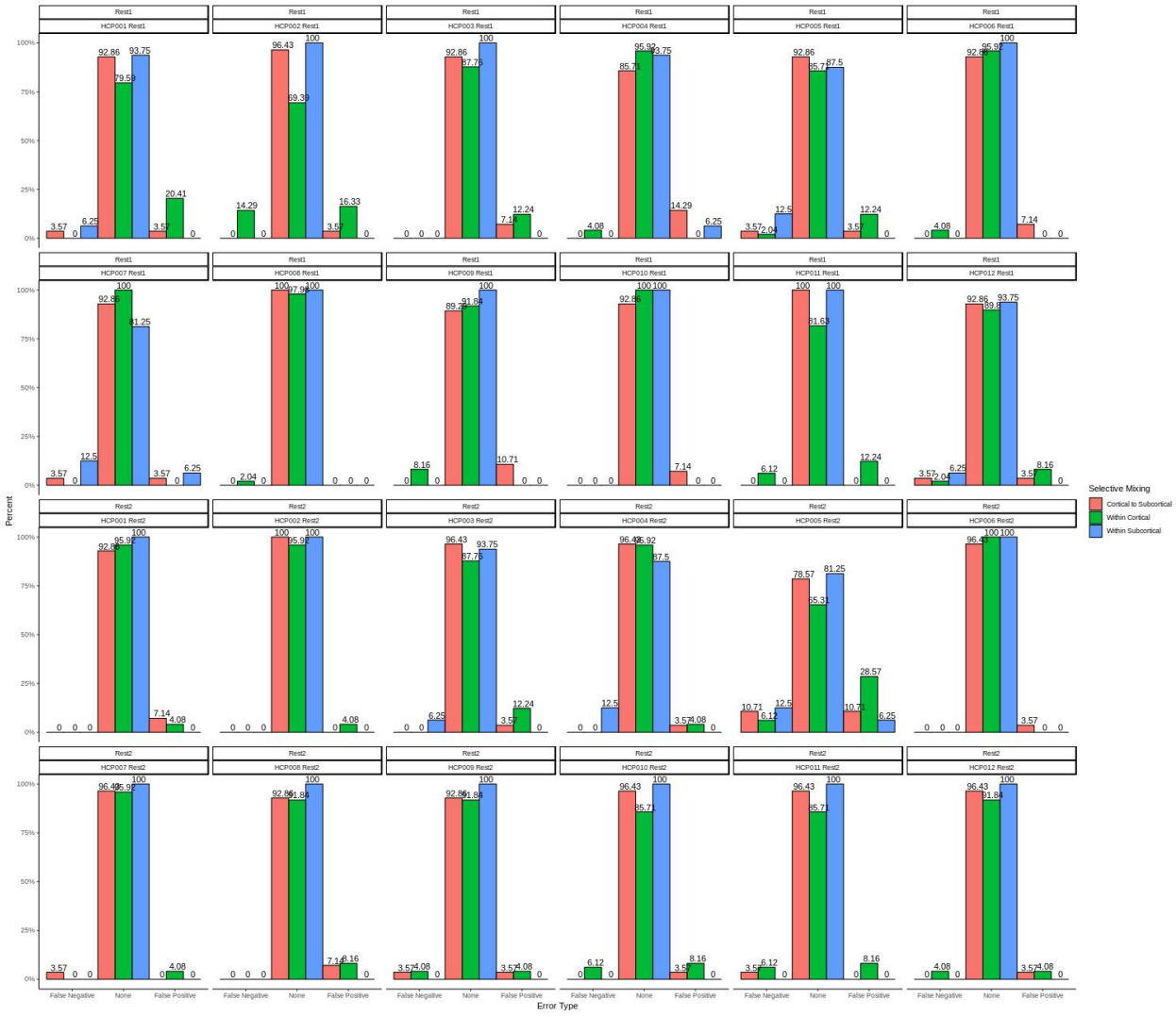

Figure 3.9: **HCP participants comparison revealing the interaction effect.** These are individual participants' FN and FP rates for the selective mixing of the cortical nodal labeling.

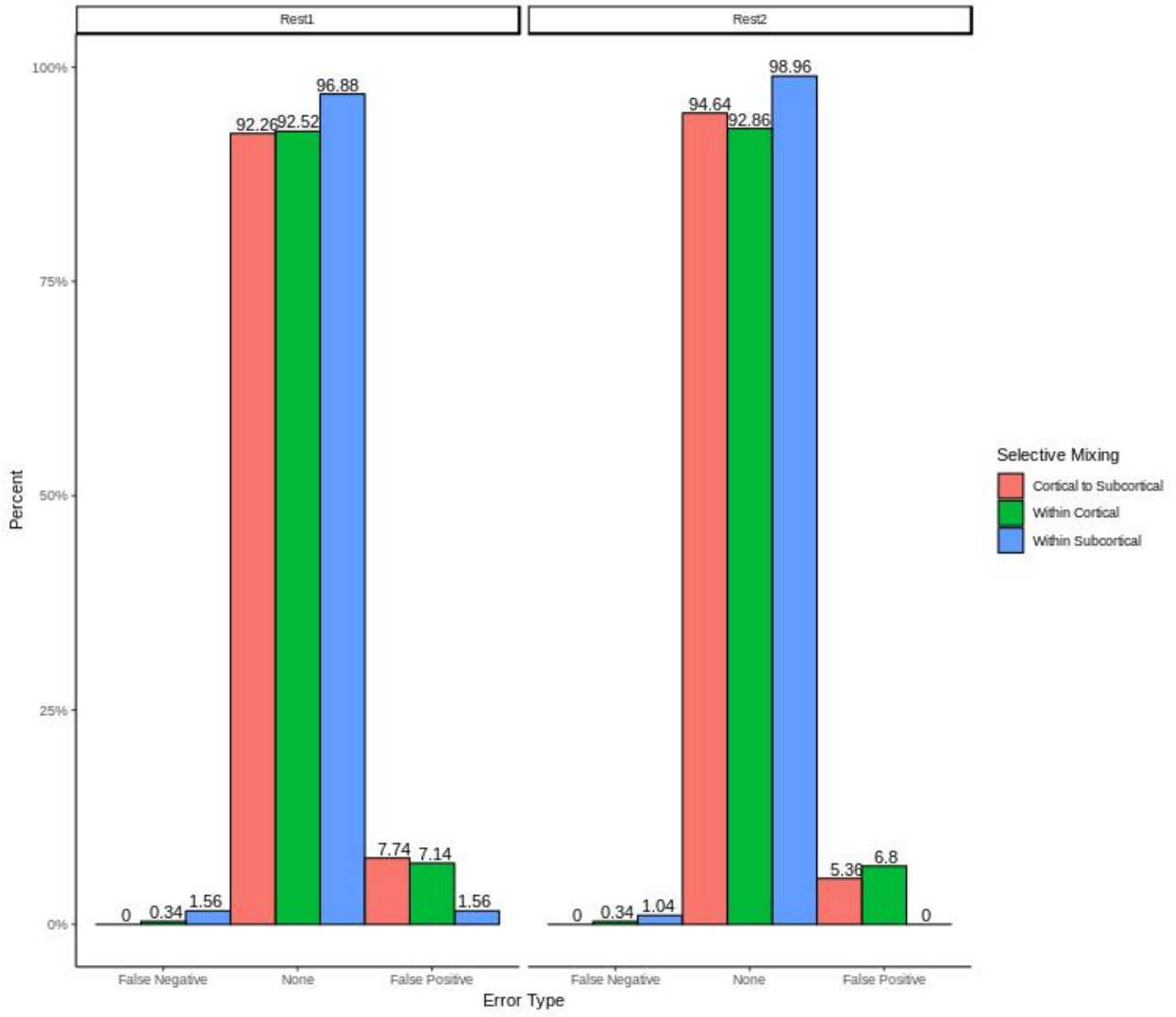

Figure 3.10: **HCP participants comparison revealing the GWESP effect.** This figure shows the FN and FP effects for a different exogenous nodal labeling of cortical compared to subcortical regions for each resting state imaging session separated by one day.

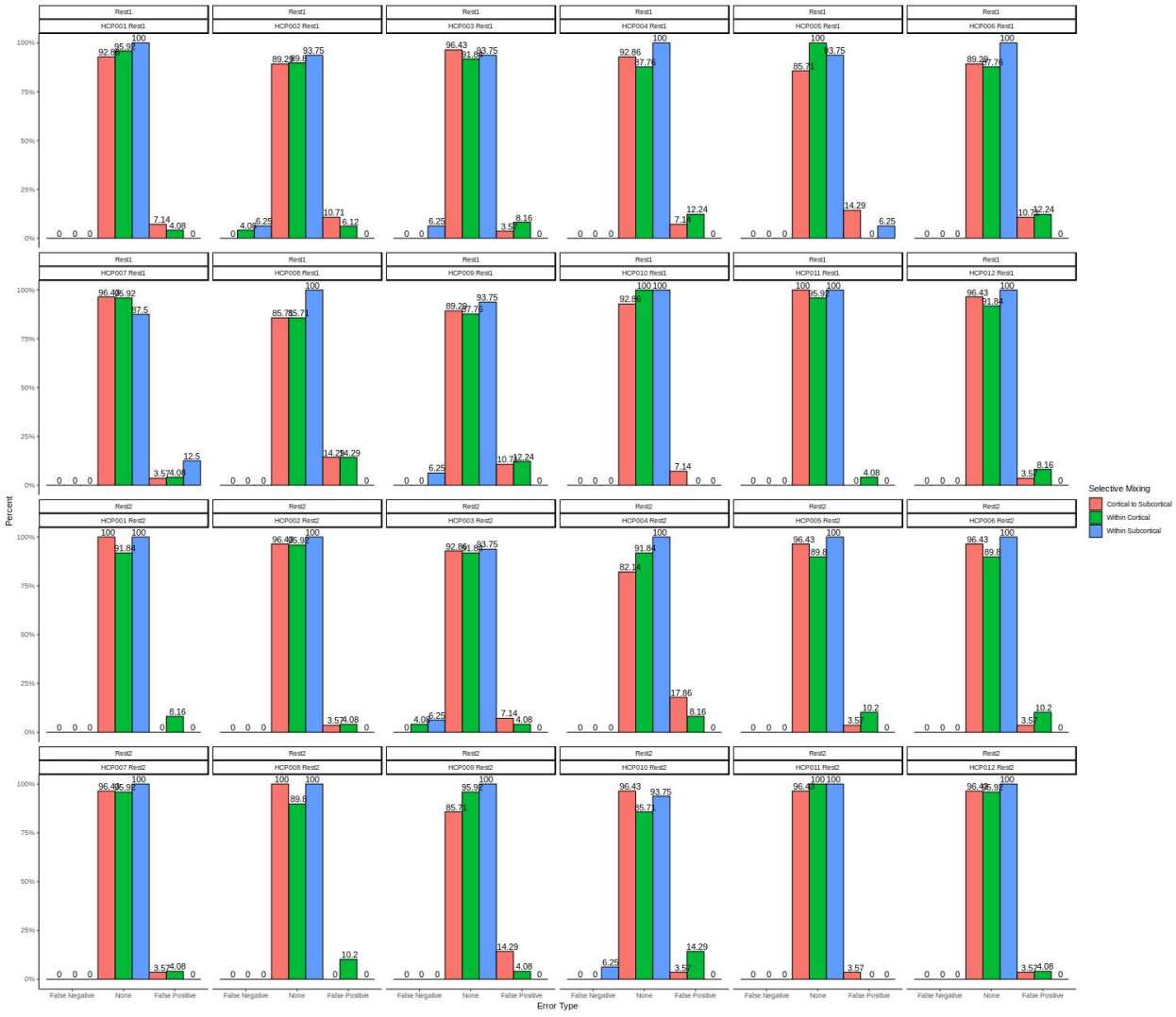

Figure 3.11: **HCP participants comparison revealing the GWESP effect.** These are individual participants' FN and FP rates for the selective mixing of the cortical nodal labeling.

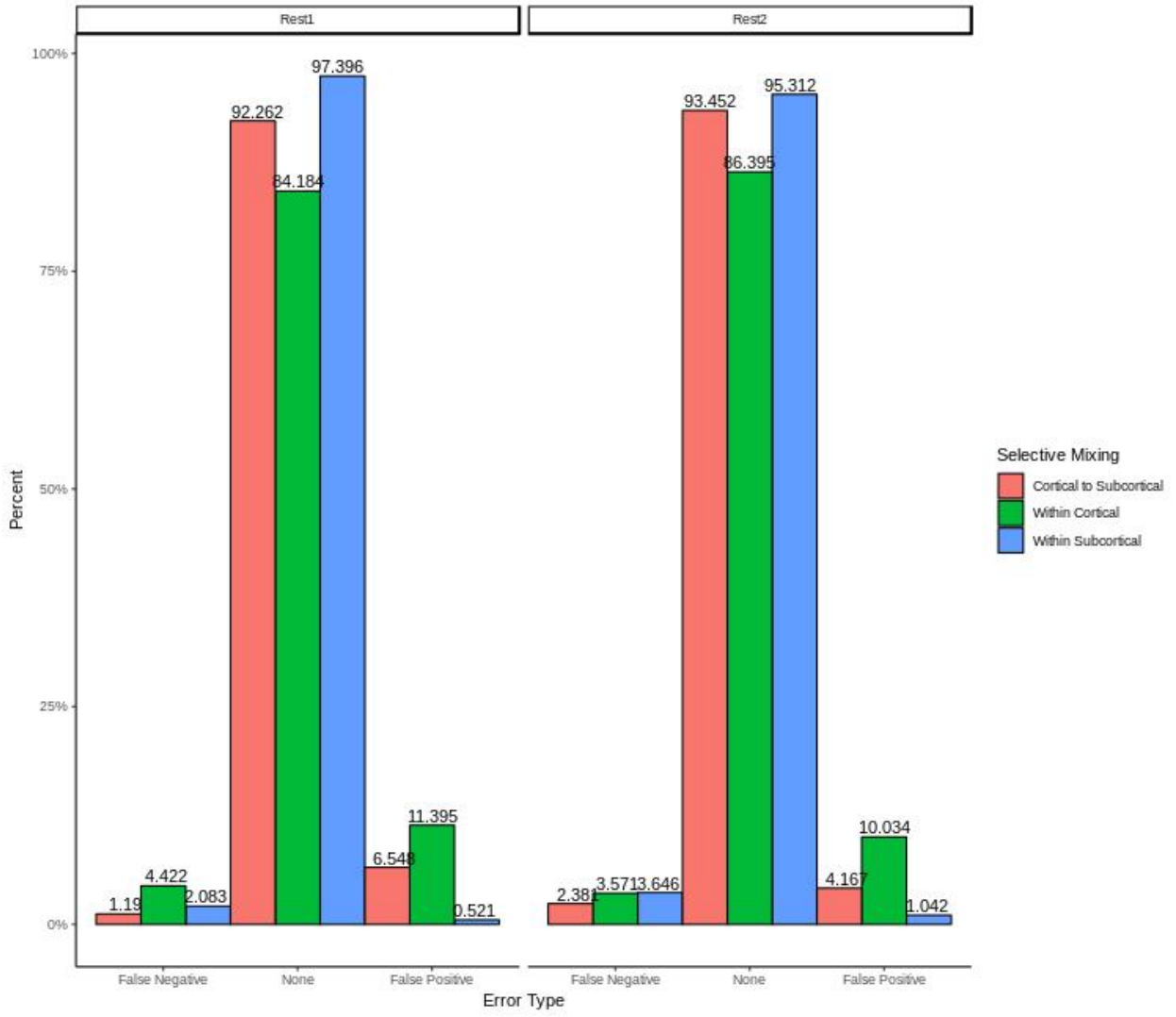

Figure 3.12: **HCP participants comparison revealing the structural effect.** This figure shows the FN and FP effects for a different exogenous nodal labeling of cortical compared to subcortical regions for each resting state imaging session separated by one day.

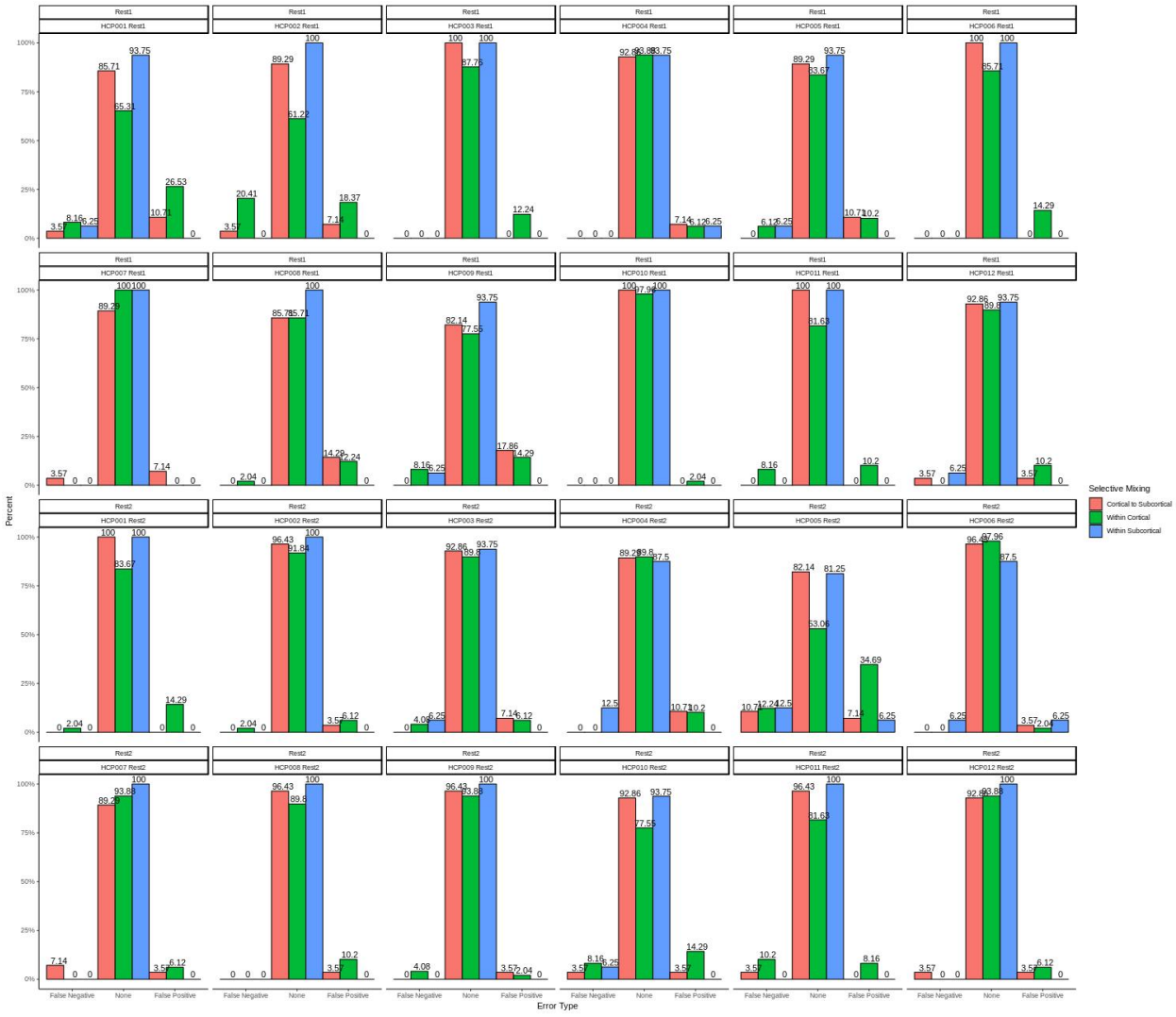

Figure 3.13: **HCP participants comparison revealing the structural effect.** These are individual participants' FN and FP rates for the selective mixing of the cortical nodal labeling.

and chronic session in all patients within the range between 0.0019 to 0.0331. Across patients, the densities ranged from 0.1039 to 0.1524. The structural connectivity, on the other hand, had less variability across acute and chronic imaging sessions in the densities(i.e., a difference between 0.005 to 0.0095) and graphs across subjects from 0.0527 to 0.0648.

In both HCP participants and patients,we assessed the functional connectivity types with ERGM using four models (i.e., base, structural, GWESP, and complete) to reveal the FPs and FNs that result from the omissions of the structural terms (i.e., the structural effect), triadic closure term (i.e., the GWESP effect), and both structural and triadic closure (i.e., the interaction effect). Leaving out the structural terms, the HCP participants all had either FP or FNs for cortical/subcortical connectivity (see Figure 3.12 and 3.13). Using multinomial regression we tested for differences in FP and FN rates between their two resting state imaging, the structural effect, GWESP effect and interaction effect comparisons all revealed no significant change odds ratios for the resting state imaging session performed on day 2 compared to day 1. Despite these lack of differences in resting state imaging days, all patients had FP or FN rates for leaving out the triadic closure term (see Figure 3.10 and 3.11), and for the interaction effect of leaving out both the structural and GWESP terms (see Figure 3.8 and 3.9). Overall, the HCP participants did not have differing rates FP and FN, but their parameter estimates did change in magnitude (see Figure 3.2, 3.3, 3.4, 3.5, 3.6, and 3.7.

The omission of structural terms generate FPs or FNs for all patients (see Figure 3.24 and 3.25) did produce a 0.401 times decrease in FN for cortico-subcortical connectivity and a 0.321 times decrease for FP in within cortical connectivity for conscious chronic compared to conscious acute stage of TBI patients (see column 3, in Table 3.10). A similar pattern was found for unconscious patients compared to conscious acute patients, where there was a significant 0.274 times decrease in FN for cortico-subcortical connectivity and a 0.274 times significant decrease for FP in within cortical connectivity. For the GWESP (see Figure 3.22 and 3.23), only the chronic patients had a significant decrease in FP for within subcortical connecitivty and significant decrease in FP for within cortical connectivity compared to acute patients (see column 2, in Table 3.10). Finally, the interaction effect of leaving out GWESP

and structural terms (see Figure 3.20 and 3.21) produced FPs and FNs significant decreases in odds ratios of 0.277 times, 0.366 times, 0.259 times, and 0.431 times for FNs in cortico-subcortical connectivity, FNs and FPs for within cortical, and FP for within subcortical, respectively. Overall, the patients with DOC did have differing rates FP and FN and their parameter estimates did change in magnitude (see Figure 3.14, 3.15, 3.16, 3.17, 3.18, and 3.19.

	Multinomial Regression: Cortical Nodal Labeling								
Comparison:	Interaction effect			GWESP effect			Structural effect		
	Constant	Unconscious	Chronic	Constant	Unconscious	Chronic	Constant	Unconscious	Chronic
False negatives for Cortical to Subcortical	0.0272***	0.277***	1.16	NA	NA	NA	0.0183***	0.274*	0.401*
	(0.271)	(0.491)	(0.317)	(NA)	(NA)	(NA)	(0.319)	(0.594)	(0.450)
False positives for Cortical to Subcortical	0.0350***	0.575	1.14	0.05628***	0.83284	0.94166	0.00733***	0.685	1.00
	(0.240)	(0.348)	(0.281)	(0.188)	(0.254)	(0.225)	(0.502)	(0.709)	(0.594)
False negatives for Within Cortical	0.0447***	0.366***	1.31	0.01313***	0.69403	0.23741*	0.0201***	1.31	1.09
	(0.213)	(0.352)	(0.246)	(0.380)	(0.537)	(0.629)	(0.305)	(0.376)	(0.356)
False positives for Within Cortical	0.0485***	0.259***	1.18	0.05816***	0.60447	1.05868	0.0366***	0.274**	0.321***
	(0.205)	(0.378)	(0.239)	(0.185)	(0.269)	(0.218)	(0.228)	(0.422)	(0.339)
False negatives for Within Subcortical	0.0136***	0.370	0.551	NA	NA	NA	0.0256***	0.636	0.746
	(0.381)	(0.629)	(0.507)	(NA)	(NA)	(NA)	(0.271)	(0.389)	(0.335)
False positives for Within Subcortical	0.00583***	0.431*	2.43	0.00750***	0.86763	0.10388*			
	(0.579)	(0.915)	(0.628)	(0.502)	(0.673)	(1.12)			
Observations	2904			2904			2904		
Log Likelihood	-1749.64			-1381.539			-1024.384		
Akaike Inf. Crit.	3535.28			2799.077			2078.769		

Note: $^{*}p<0.05$; $^{**}p<0.01$; $^{***}p<0.001$

Table 3.10: **The effect of level of consciousness and stage of TBI on FPs and FNs.** For the cortical nodal labeling, the FPs and FNs for each type of connectivity pattern were predicted for unconscious patients compared to all conscious patients. The change in odds rations and their standard errors in parentheses are listed for the interaction, GWESP and structural effect comparisons.

	Complete Model					GWESP Model			
	Observed	*min*	*M*	*max*	*p*-value	*min*	*M*	*max*	*p*-value
P054 Acute									
Edges	1,796	1,702	1,780.300	1,839	0.800	1,793	1,839.300	1,886	0.200
Intra-Limbic	19	15	21.300	28	0.400	18	22.100	28	0.200
Inter-Somatomotor-Ventral Attention	56	50	57.700	69	1	54	63.300	74	0.200
GWESP (fixed, λ=0.45)	2,766.980	2,614.125	2,741.347	2,834.899	0.800	2,761.997	2,835.273	2,908.383	0.200
P084 Acute									
Inter-Frontoparietal-Somatomotor	40	28	39	52	1	6	10.400	16	0.200
Inter-Frontoparietal-Thalamus	16	13	18.250	28	0.700	13	18.200	22	0.200
P084 Chronic									
Inter-Dorsal Attention-Limbic	9	9	11.300	14	0.200	2	8	12	1
Within Subcortical	153	151	159	172	0.200	127	144.300	161	0.600
P085 Acute									
Inter-Dorsal Attention-Ventral Attention	12	6	9.700	15	0.200	10	15	21	0.800
Within Occipital Lobe	65	53	60.900	77	0.200	53	63.200	71	1

Table 3.11: **Goodness of fit differences for the interaction effect comparison for graph statistics.** We are displaying the four worst fit differences for the two models in the interaction effect comparison. The observed column is the original data's values for each graph statistic, while the minimum, mean, maximum, and p-value for the simulated graphs based on each of the ERGM models are displayed. None of these are bad fits, but they are the biggest difference between the complete model and the GWESP model. Overall, all the patients' ERGM for the complete model and GWESP effect fit the data well based on the graph statistics modeled because neither model produced any p-values < 0.05 for any graph statistic.

	Complete Model					GWESP Model				Complete Model					GWESP Model			
	P054 Acute					P054 Acute				P084 Chronic					P084 Chronic			
	Observed	*min*	*M*	*max*	*p*-value	*min*	*M*	*max*	*p*-value	Observed	*min*	*M*	*max*	*p*-value	*min*	*M*	*max*	*p*-value
esp0	4	0	0.100	1	0	0	0	0	0	16	0	0.700	2	0	0	1.600	4	0
esp1	20	1	3.200	6	0	1	3.200	6	0	63	42	56.800	73	0.800	50	58.500	67	0.400
esp2	58	50	65	83	0.600	54	74	89	0.400	140	198	231.700	254	0	182	226.200	258	0
esp3	140	226	245.900	269	0	224	252.800	292	0	243	311	341.300	371	0	326	347.500	391	0
esp4	213	357	385	410	0	326	359.100	383	0	275	311	335.200	365	0	316	332.900	353	0
esp5	255	362	384	406	0	360	380.300	401	0	260	200	237.600	277	0.400	217	240.600	267	0.200
esp6	275	276	311.200	351	0	261	292.500	326	0.600	201	113	142.900	167	0	124	149.600	174	0
esp7	245	176	205	231	0	170	198.300	231	0	143	51	76.700	95	0	67	80.100	94	0
esp8	197	89	116.100	147	0	81	110.600	135	0	72	26	35.600	47	0	20	35.700	46	0
esp9	158	54	64.200	78	0	40	60.900	79	0	40	7	14.600	26	0	11	14.700	25	0
esp10	93	26	34.800	45	0	17	28.500	41	0	17	3	7	15	0	3	5.400	9	0
esp11	68	6	14.600	22	0	9	12.900	22	0	12	0	2.500	6	0	0	1.800	3	0
esp12	28	4	6	9	0	1	4.300	7	0	6	0	1	3	0	0	1.100	4	0
esp13	24	1	2.700	5	0	0	2.200	4	0	1	0	0.500	1	1	0	0.100	1	0.200
esp14	11	0	0.900	3	0	0	0.600	3	0	0	0	0	0	1	0	0	0	1

Table 3.12: **Goodness of fit differences for the interaction effect comparison for edge shared partners.** We are displaying the two worst fit differences for the two models in the interaction effect comparison. The observed column is the original data's values for each edge shared partner type, while the minimum, mean, maximum, and p-value for the simulated graphs based on each of the ERGM models are displayed. The edge shared partner types are based on the number of triangles sharing a common edge (e.g., the esp10 term has 10 triangles all sharing common edge). Overall, all the patients' ERGM for the complete model and GWESP effect did not fit the data well based on the graph statistics modeled because both models had at least than 11 of the 14 p-values < 0.05 for types of edge shared partner type.

	Complete Model					GWESP Model				Complete Model					GWESP Model			
	P054 Acute					P054 Acute				P084 Chronic					P084 Chronic			
	Observed	*min*	*M*	*max*	*p*-value	*min*	*M*	*max*	*p*-value	Observed	*min*	*M*	*max*	*p*-value	*min*	*M*	*max*	*p*-value
0	0	0	0.100	1	1	0	2.600	4	0.200	0	0	0.100	1	1	0	0.200	1	1
1	0	0	0.100	1	1	0	0	0	1	0	0	0	0	1	0	0.100	1	1
2	0	0	0	0	1	0	0	0	1	0	0	0.100	1	1	0	0.200	1	1
3	0	0	0.200	1	1	0	0.100	1	1	0	0	0	0	1	0	0.200	2	1
4	0	0	0	0	1	0	0.200	1	1	0	0	0	0	1	0	0.100	1	1
5	0	0	0.100	1	1	0	0.400	1	1	0	0	0.100	1	1	0	0.600	2	1
6	0	0	0.400	2	1	0	0.300	2	1	0	0	1.100	2	0.600	0	0.500	2	1
7	0	0	0.300	2	1	0	0.200	1	1	0	0	0.900	3	0.800	0	0.900	4	1
8	0	0	0.500	2	1	0	0.500	2	1	0	0	1.600	4	0.400	0	1.800	4	0.600
9	1	0	0.600	2	1	0	0.600	1	1	1	1	3.300	7	0.400	0	2	6	1
10	0	0	0.900	3	1	0	1.100	3	0.600	1	1	2.700	5	0.200	1	3.600	8	0.200
11	0	0	1	5	1	0	1.300	2	0.200	3	0	3.900	8	0.800	1	4	5	0.600
12	1	0	1.900	5	1	0	1.800	3	0.800	3	1	6	10	0.600	3	5.200	7	0.400
13	0	1	3.300	6	0	1	2.900	6	0	5	3	5.900	10	0.800	3	6.800	13	0.600
14	2	0	3	8	1	0	3.600	6	0.600	4	2	6.700	12	0.600	2	5.800	8	0.400
15	2	2	4.200	8	0.400	2	4.600	7	0.400	8	5	9	12	0.600	5	7.400	11	1
16	2	1	4.100	7	0.400	1	5	7	0.200	10	7	10.800	14	0.800	6	8.400	11	0.400
17	6	2	5.600	10	0.800	2	5.300	9	1	13	9	11.100	13	0.400	4	9.400	12	0
18	5	1	5.600	11	1	4	6.500	9	0.400	17	8	10.100	13	0	3	10.500	15	0
19	15	3	7.400	10	0	3	6.900	12	0	13	6	9.200	14	0.200	6	10.800	15	0.400
20	12	4	8.300	15	0.200	2	7.600	11	0	13	7	8.300	11	0	7	9.100	12	0
21	9	5	8.200	12	0.800	4	9	12	0.800	21	6	10.100	15	0	6	10.200	14	0
22	10	6	9.100	12	1	2	8.100	12	0.800	11	5	8.800	14	0.600	6	9.800	15	0.600
23	18	5	8.900	14	0	7	9.400	14	0	9	3	7.600	10	1	4	8	12	1
24	11	6	9.900	17	0.800	2	7.900	11	0.400	5	3	7.100	13	0.600	3	8.700	15	0.600
25	8	3	9.500	15	0.800	5	9.700	14	0.800	8	1	5.800	8	0.400	4	7.700	11	1
26	11	3	8.200	14	0.600	5	10.200	14	1	3	3	6	9	0.200	1	4.400	7	0.600
27	7	4	7.600	12	1	2	7	11	1	3	1	3.600	7	1	2	4.600	8	0.800
28	12	4	8.400	10	0	4	7.400	11	0	1	1	3.400	8	0.400	1	3.300	8	0.400
29	9	1	5.700	10	0.400	3	6.400	12	0.600	2	0	2.500	6	1	0	3.300	6	0.400

Table 3.13: **Goodness of fit differences for the interaction effect comparison for the degree distribution.** We are displaying the two worst fit differences for the two models in the interaction effect comparison. The observed column is the original data's values for each nodal degree, while the minimum, mean, maximum, and p-value for the simulated graphs based on each of the ERGM models are displayed. Overall, all the patients' ERGM for the complete model and GWESP effect fit the data well based on the graph statistics modeled because there were only 3 to 5 p-values < 0.05.

ERGM Structural Terms and GWESP term for Functional Connectivity for Unconscious Patients in Acute Sessions

	P054 Acute	P054 Chronic	P055 Acute	P055 Chronic	P066 Acute	P066 Chronic	P069 Acute	P069 Chronic	P079 Acute	P079 Chronic	P084 Acute	P084 Chronic	P096 Acute	P096 Chronic
Degree	0.003	−0.0001	0.006	0.007	0.006	0.006	−0.002	0.007	−0.001	−0.005	0.003	0.00003	0.003	0.002
	(0.002)	(0.005)	(0.003)	(0.004)	(0.006)	(0.005)	(0.003)	(0.005)	(0.004)	(0.004)	(0.003)	(0.005)	(0.004)	(0.005)
Efficiency	−0.031	0.047	0.189	0.114	0.068	0.153	−0.161	0.431*	−0.199	−0.227	−0.044	−0.073	−0.245	−0.099
	(0.085)	(0.203)	(0.144)	(0.131)	(0.228)	(0.210)	(0.114)	(0.217)	(0.163)	(0.143)	(0.102)	(0.104)	(0.171)	(0.229)
Clustering Coefficient	0.074	−0.020	−0.235	−0.122	−0.151	−0.077	−0.184	−0.298	−0.157	−0.082	−0.132	0.092	−0.008	0.275
	(0.101)	(0.212)	(0.241)	(0.134)	(0.232)	(0.213)	(0.138)	(0.211)	(0.164)	(0.181)	(0.131)	(0.212)	(0.236)	(0.288)
Latent Cluster 1	−0.041	0.158**	0.113	0.068	−0.003	0.034	0.011	0.039	0.170*	0.027	−0.002	0.004	0.087	0.062
	(0.052)	(0.053)	(0.059)	(0.057)	(0.077)	(0.063)	(0.067)	(0.107)	(0.079)	(0.056)	(0.052)	(0.052)	(0.063)	(0.681)
Latent Cluster 2	−0.036	0.197**	0.291***	0.049	0.061	0.054	0.101	0.022	0.052	−0.019	0.038	0.092	0.125	0.799
	(0.072)	(0.069)	(0.063)	(0.072)	(0.058)	(0.072)	(0.061)	(0.051)	(0.050)	(0.082)	(0.076)	(0.096)	(0.076)	(0.594)
Latent Cluster 3														0.074
														(0.054)
Latent Cluster 4														0.155
														(0.084)
(GWESP fixed, $\lambda = 0.45$)	6.870***	4.568***	2.589***	3.462***	4.733***	7.490***	2.116***	3.742***	3.254***	2.649***	2.639***	3.196***	2.629***	3.175***
	(0.382)	(0.306)	(0.192)	(0.229)	(0.269)	(0.410)	(0.133)	(0.257)	(0.230)	(0.189)	(0.195)	(0.218)	(0.176)	(0.220)

Note: $^{*}p<0.05$; $^{**}p<0.01$; $^{***}p<0.001$

Table 3.14: **Structural metrics effects on functional connectivity and triadic closure in functional connectivity for acute, unconscious patients and chronic conscious patients.** The effects for structural connectivity's degree, local efficiency, clustering coefficient, and nodematch latent clustering on the functional connectivity from the complete models. The LATEX code to create this table was produced by the R package called texreg (Leifeld, 2013).

	ERGM Structural Terms and GWESP term for Functional Connectivity for Conscious Patients in Acute Sessions									
	P074 Acute	P074 Chronic	P085 Acute	P085 Chronic	P089 Acute	P089 Chronic	P092 Acute	P092 Chronic	P099 Acute	P099 Chronic
Degree	0.014***	0.006	0.005	0.007	0.001	0.005	0.005	0.007*	0.004	0.003
	(0.004)	(0.005)	(0.005)	(0.005)	(0.005)	(0.005)	(0.004)	(0.003)	(0.004)	(0.007)
Efficiency	0.022	0.097	0.164	0.067	0.030	−0.301	0.206	0.066	−0.143	−0.070
	(0.122)	(0.136)	(0.132)	(0.197)	(0.221)	(0.272)	(0.177)	(0.130)	(0.122)	(0.275)
Clustering Coefficient	0.062	0.054	−0.144	0.055	−0.276	0.432	−0.210	0.026	0.261	−0.012
	(0.210)	(0.235)	(0.145)	(0.292)	(0.285)	(0.383)	(0.159)	(0.239)	(0.156)	(0.301)
Latent Cluster 1	0.012	−0.012	0.083	0.240***	−0.030	0.127*	−0.067	0.089	0.028	0.037
	(0.056)	(0.076)	(0.055)	(0.059)	(0.065)	(0.058)	(0.119)	(0.057)	(0.070)	(0.094)
Latent Cluster 2	0.023	0.013	0.125	0.227***	−0.086	0.108	−0.059	0.088	0.039	0.151*
	(0.071)	(0.060)	(0.070)	(0.063)	(0.069)	(0.074)	(0.054)	(0.071)	(0.064)	(0.061)
Latent Cluster 3										0.401*
										(0.196)
Latent Cluster 4										0.659
										(0.567)
Latent Cluster 5										11.672
										NA
Latent Cluster 6										0.545
										(0.342)
(GWESP fixed, $\lambda = 0.45$)	5.848***	3.240***	2.503***	2.888***	2.560***	1.912***	2.396***	2.912***	2.574***	2.640***
	(0.322)	(0.222)	(0.168)	(0.194)	(0.169)	(0.150)	(0.166)	(0.185)	(0.175)	(0.200)
Note:										*$p<0.05$; **$p<0.01$; ***$p<0.001$

Table 3.15: **Structural metrics effects on functional connectivity and triadic closure in functional connectivity for acute and chronic conscious patients.** The effects for structural connectivity's degree, local efficiency, clustering coefficient, and nodematch latent clustering on the functional connectivity from the complete models. The LATEX code to create this table was produced by the R package called texreg (Leifeld, 2013).

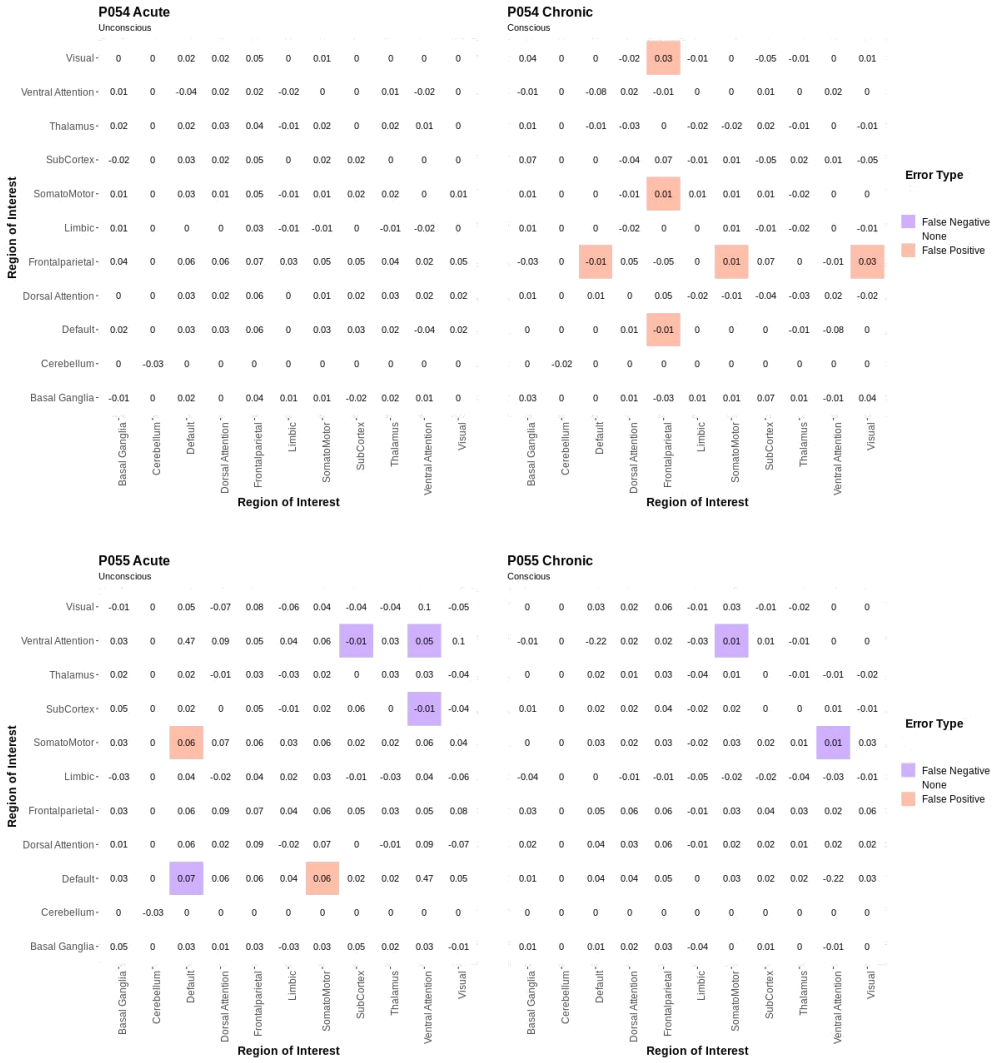

Figure 3.14: **Patient comparison revealing the interaction effect.** Each graph represents the difference between the complete model and GWESP model. These parameter estimates are generated from the same connectivity matrix for both the complete model and GWESP model. The numerical values for each parameter estimate is the difference between the two models. The FPs are the parameter estimates that were significant in the GWESP model, but they were not significant in complete. The FNs are the parameter estimates that were not significant in the GWESP model, but they were significant in the complete model. The difference between the two models are the inclusion of structural connectivity nodal covariates.

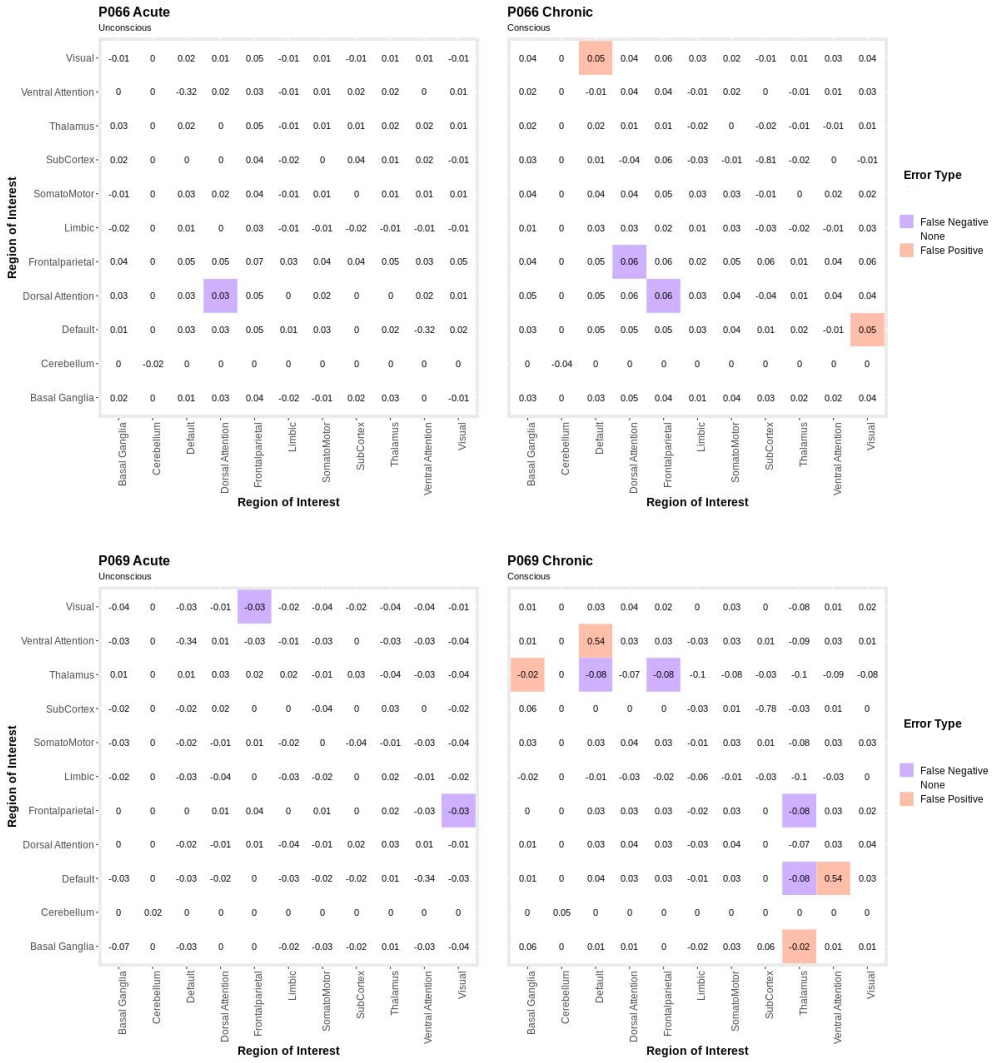

Figure 3.15: **Patient comparison revealing the interaction effect.** Each graph represents the difference between the complete model and GWESP model. These parameter estimates are generated from the same connectivity matrix for both the complete model and GWESP model. The numerical values for each parameter estimate is the difference between the two models. The FPs are the parameter estimates that were significant in the GWESP model, but they were not significant in complete. The FNs are the parameter estimates that were not significant in the GWESP model, but they were significant in the complete model. The difference between the two models are the inclusion of structural connectivity nodal covariates.

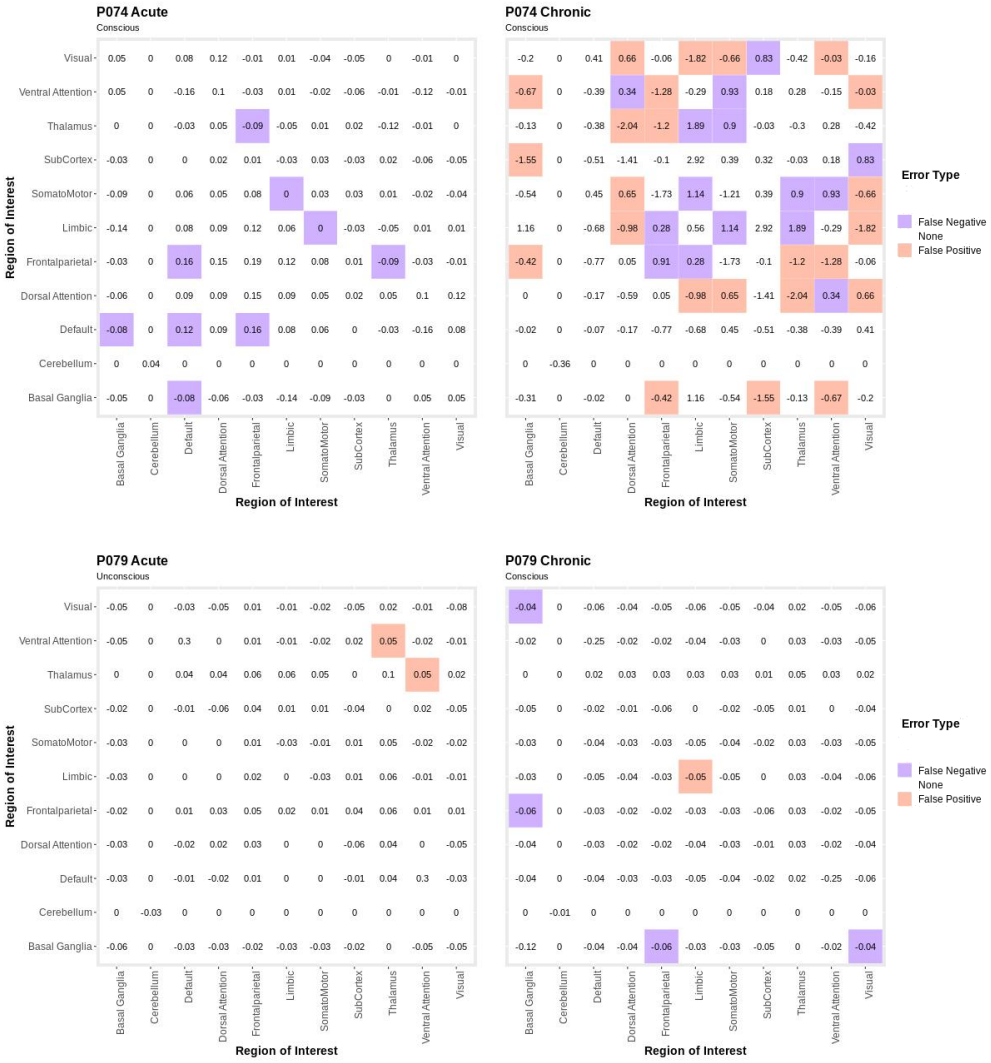

Figure 3.16: **Patient comparison revealing the interaction effect.** Each graph represents the difference between the complete model and GWESP model. These parameter estimates are generated from the same connectivity matrix for both the complete model and GWESP model. The numerical values for each parameter estimate is the difference between the two models. The FPs are the parameter estimates that were significant in the GWESP model, but they were not significant in complete. The FNs are the parameter estimates that were not significant in the GWESP model, but they were significant in the complete model. The difference between the two models are the inclusion of structural connectivity nodal covariates.

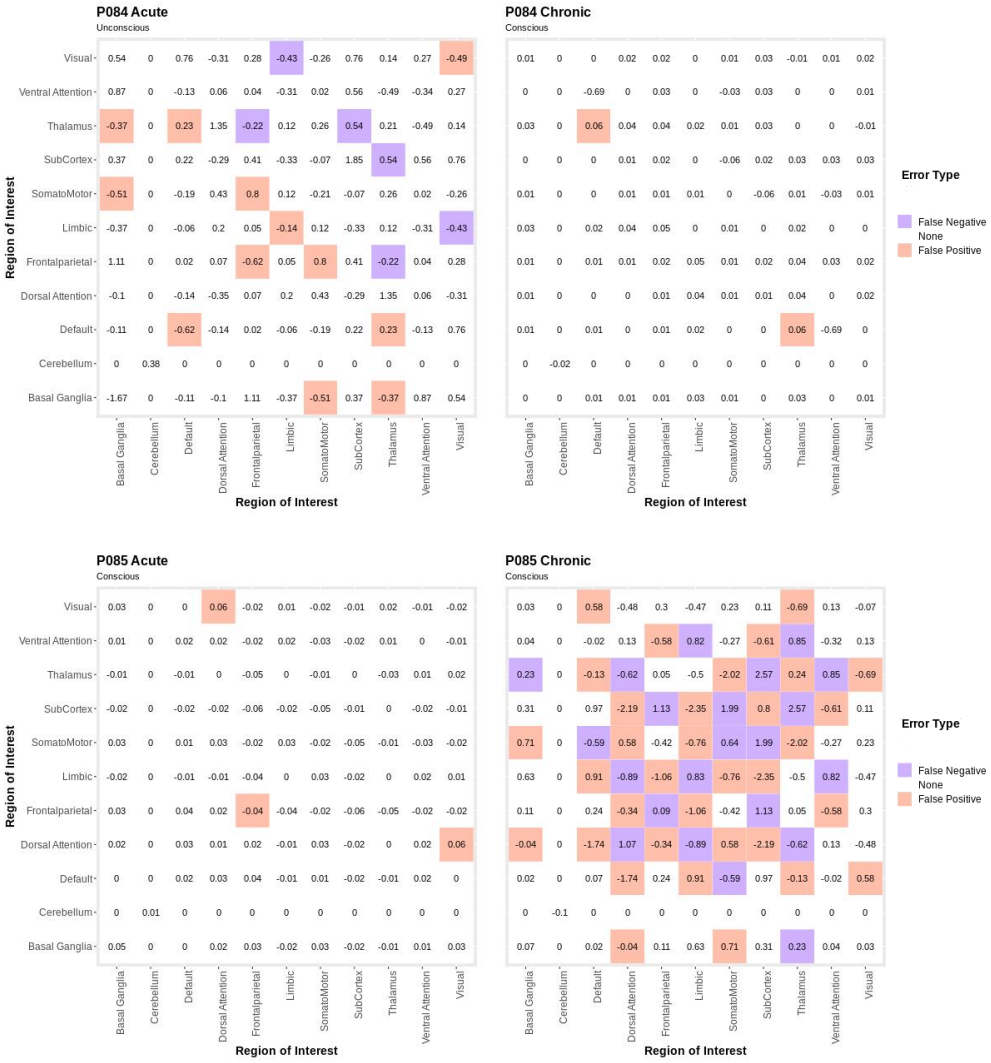

Figure 3.17: **Patient comparison revealing the interaction effect.** Each graph represents the difference between the complete model and GWESP model. These parameter estimates are generated from the same connectivity matrix for both the complete model and GWESP model. The numerical values for each parameter estimate is the difference between the two models. The FPs are the parameter estimates that were significant in the GWESP model, but they were not significant in complete. The FNs are the parameter estimates that were not significant in the GWESP model, but they were significant in the complete model. The difference between the two models are the inclusion of structural connectivity nodal covariates.

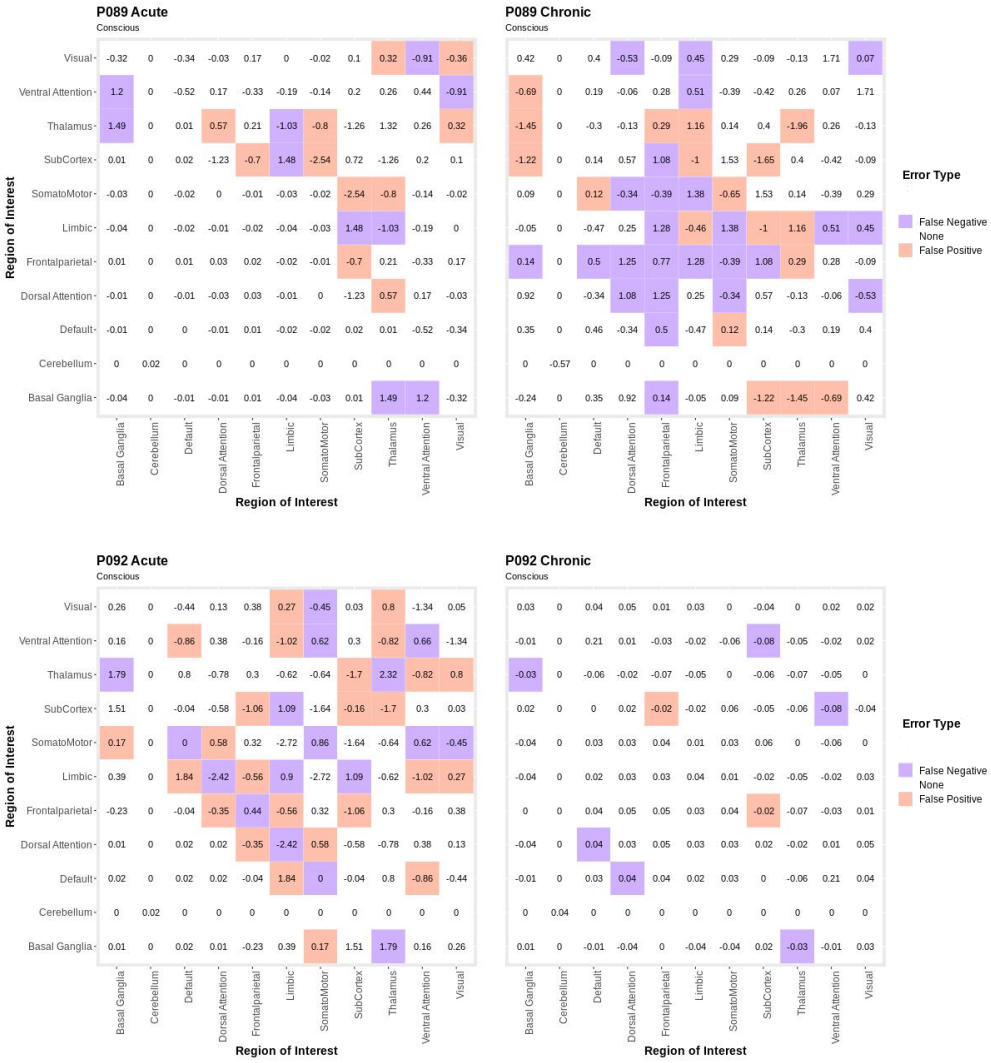

Figure 3.18: **Patient comparison revealing the interaction effect.** Each graph represents the difference between the complete model and GWESP model. These parameter estimates are generated from the same connectivity matrix for both the complete model and GWESP model. The numerical values for each parameter estimate is the difference between the two models. The FPs are the parameter estimates that were significant in the GWESP model, but they were not significant in complete. The FNs are the parameter estimates that were not significant in the GWESP model, but they were significant in the complete model. The difference between the two models are the inclusion of structural connectivity nodal covariates.

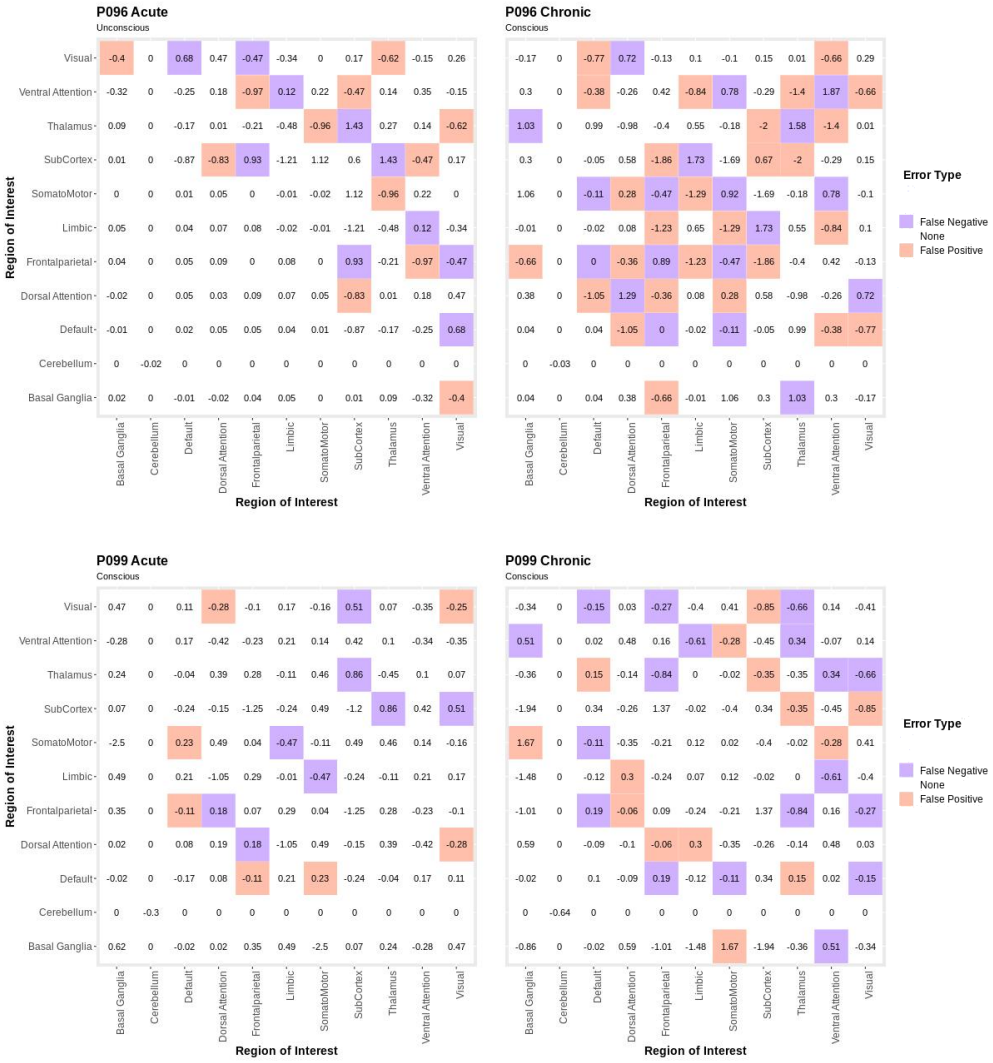

Figure 3.19: **Patient comparison revealing the interaction effect.** Each graph represents the difference between the complete model and GWESP model. These parameter estimates are generated from the same connectivity matrix for both the complete model and GWESP model. The numerical values for each parameter estimate is the difference between the two models. The FPs are the parameter estimates that were significant in the GWESP model, but they were not significant in complete. The FNs are the parameter estimates that were not significant in the GWESP model, but they were significant in the complete model. The difference between the two models are the inclusion of structural connectivity nodal covariates..

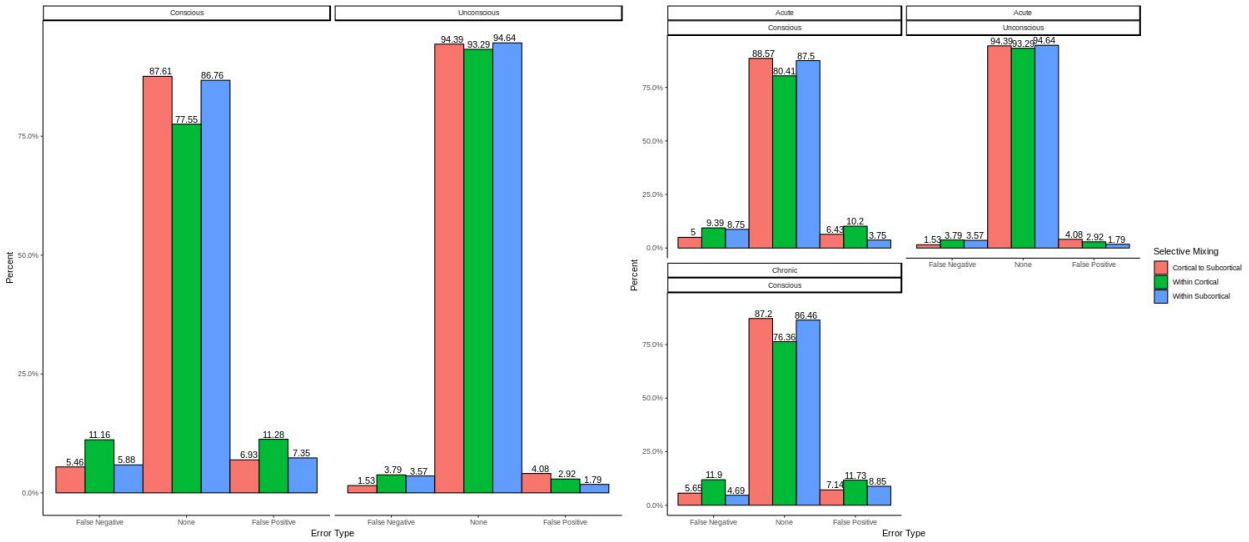

Figure 3.20: **Patients comparison revealing the interaction effect.**The differences in FN and FP effects for an exogenous nodal labeling of cortical compared to subcortical regions and their selective mixing. The right figure displays the FN and FP for the selective mixing of the cortical nodal labeling when the patients are divided into their stage of TBI and their level of consciousness assessed by behavioral metrics (i.e., GOS-E).

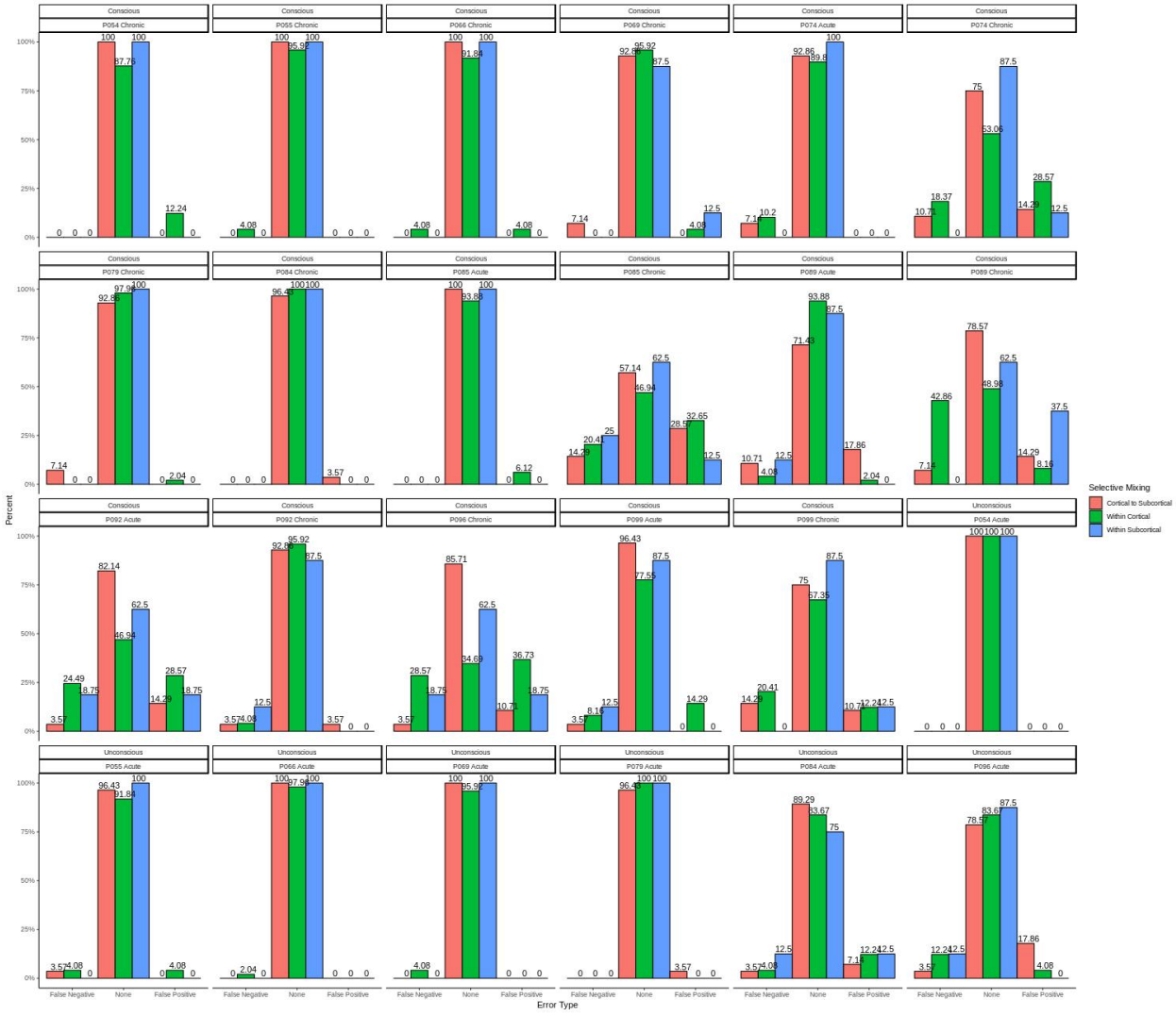

Figure 3.21: **Patients comparison revealing the interaction effect.** These are individual patients' FN and FP rates for the selective mixing of the cortical nodal labeling.

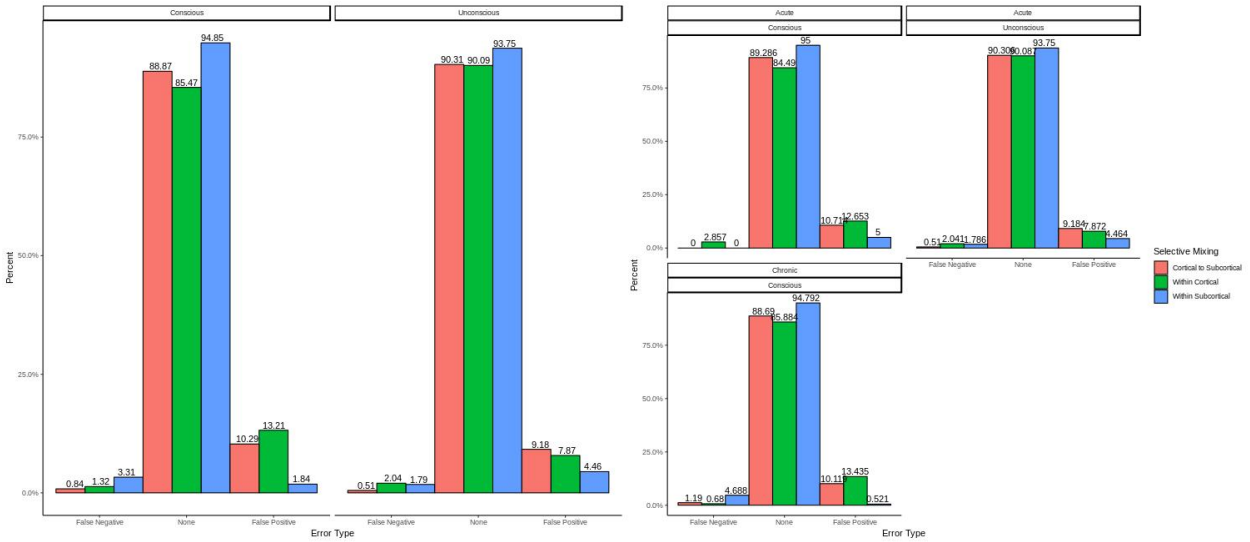

Figure 3.22: **Patients comparison revealing the GWESP effect.** The differences in FN and FP effects for an exogenous nodal labeling of cortical compared to subcortical regions and their selective mixing. The right figure displays the FN and FP for the selective mixing of the cortical nodal labeling when the patients are divided into their stage of TBI and their level of consciousness assessed by behavioral metrics (i.e., GOS-E).

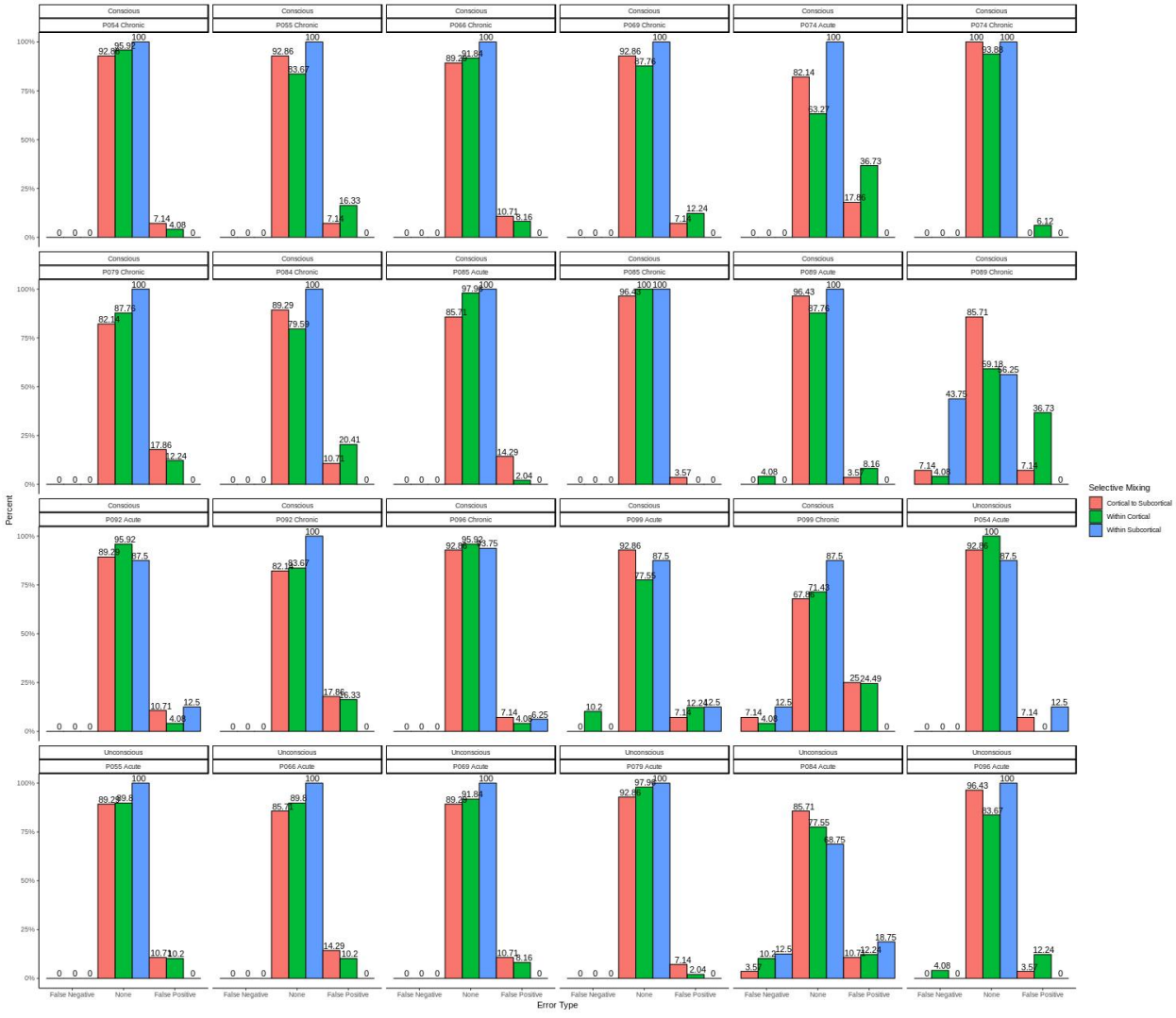

Figure 3.23: **Patients comparison revealing the GWESP effect.** These are individual patients' FN and FP rates for the selective mixing of the cortical nodal labeling.

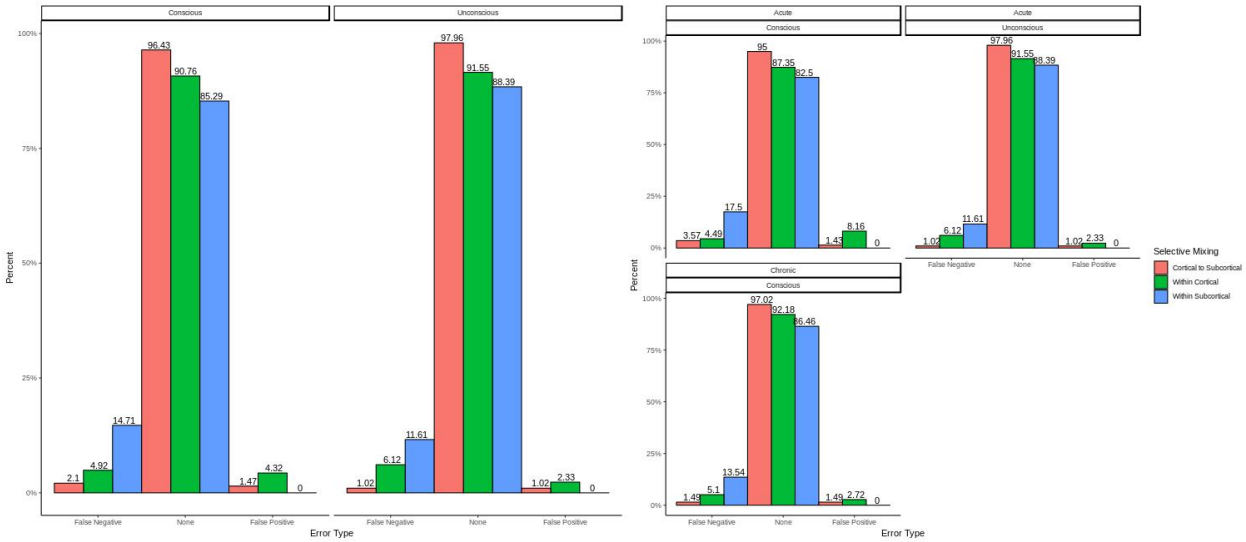

Figure 3.24: **Patients comparison revealing the structural effect.**The differences in FN and FP effects for an exogenous nodal labeling of cortical compared to subcortical regions and their selective mixing. The right figure displays the FN and FP for the selective mixing of the cortical nodal labeling when the patients are divided into their stage of TBI and their level of consciousness assessed by behavioral metrics (i.e., GOS-E).

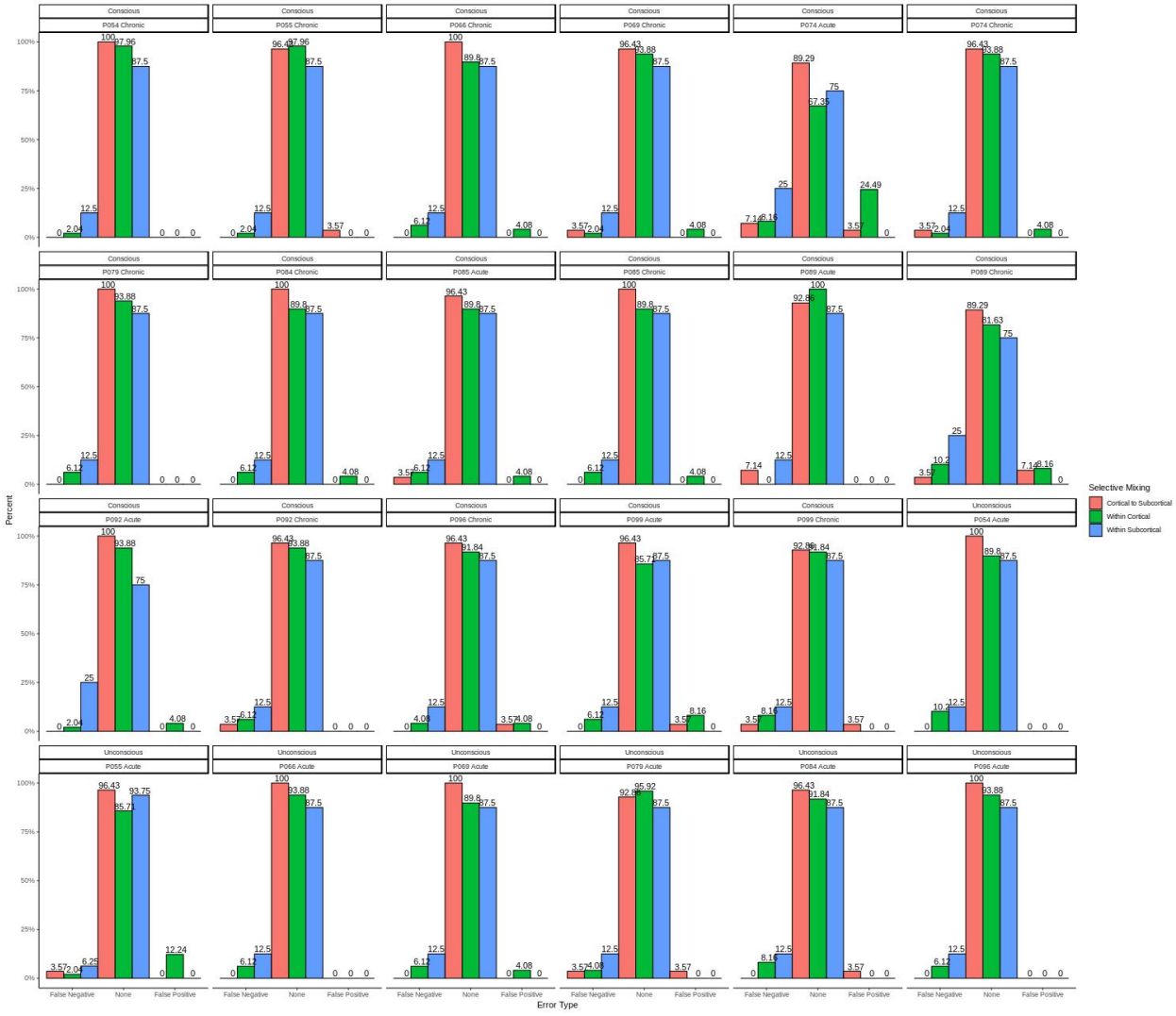

Figure 3.25: **Patients comparison revealing the structural effect.** These are individual patients' FN and FP rates for the selective mixing of the cortical nodal labeling.

3.5 Discussion

As our longitudinal data shows, consistent with results from other domains of neuroscience (see Milham et al., 2012; Nielsen et al., 2013), brain graphs are susceptible to having different "natural" levels of density at which they are the most stable and which might thus be ideal to estimate network properties. In the HCP data, the densities ranged from 0.1676 to 0.215. While in patient data, over the progression of 6 months post injury, as the patient recovered consciousness and cognitive function, the natural brain graphs had differences in density between 0.0019 to 0.0331. Additionally, the densities varied across subjects between 0.1039 to 0.1524. These density differences were revealed thanks to the use of MoNeT (Narayan et al., 2015), a tool which combines a penalized maximum likelihood estimation with a resampling-based (bootstrapped) model selection procedure in order to find the most stable level of sparse brain graph given a set of time-dependent measurements (e.g., fMRI data). On the one hand, these differences might well reflect important aspects of network dynamics in the recovery of consciousness post severe brain injury in patients or natural variation across participants for the HCP participants. On the other hand, regardless of the ultimate interpretation of the finding in of itself, had we employed the standard approach and enforced equal density across brain graphs in order to allow comparability (Rubinov and Sporns, 2010; van Wijk et al., 2010), these differences would have been obscured and would have introduced a bias in the direct comparison of topological properties across graphs. Ultimately, an accurate estimation of the connectivity is necessary to correctly model the connectivity. ERGM allows for controlling the density without having to fix the density for all graphs. This allows for data driven approaches to allow the density to vary based on the stability of the connectivity estimates. This natural variance could reveal differences in graph statistics that would otherwise be masked by fixing density. Overall, this result further demonstrates that, when arbitrarily enforcing equal density across graphs, we are in fact biasing our results towards the graphs with natural density closest to the threshold employed. While we show this in the context of time, it immediately translates to cross-sectional analyses that are also typical of the field of DOC (e.g., healthy controls versus

patients), with the prediction that the more different the natural density across groups, the greater the bias in the results.

Even if the density is allowed to vary, the other problems of interrelated connectivity measures (i.e., problem #2) and leaving out structural terms (i.e., problem #3) affect the analyses. The interpretations of connectivity differences depends on the generative processes (Goodreau et al., 2009) involved in generating the observed connectivity. Research questions involving specific types of cortical and subcortical connectivity (e.g., cortico-cortico vs thalamo-cortical connectivity; Laureys et al., 2000a,b; Vanhaudenhuyse et al., 2010; Boly et al., 2009, 2011; Crone et al., 2014; Amico et al., 2017; Crone et al., 2018) are questions of selective mixing (i.e., specific connectivity patterns differences in patients associated with within cortical, within subcortical or between cortical and subcortical connectivity). However, network connectivity is the result of multiple generative processes, which together produce the structure in the graph being analyzed. If there differences found within the selective mixing of cortical and subcortical connectivity, but the other generative process are not accounted for, the attribution to selective mixing is inaccurate. There needs to be an account for other generative process (e.g., triadic closure) or other covariate (e.g., structural connectivity differences in patients) which could have affected the selective mixing within functional connectivity that are theoretically relevant to the research. Otherwise, there is a risk of misinterpretation of causes for connectivity differences.

Overall, both the patients and HCP participants had non-zero rates for FP and FN, if a triadic closure, structural term, or both are omitted. We wanted to investigate rate differences for within patient populations and within healthy volunteers because rate differences would lead to lead biased conclusions about important types of connectivity differences between groups of patients. A general trend was that patients and participants all had some effect of leaving out the terms, but patients had rate differences for unconscious compared to conscious patients and conscious acute stage TBI compared to conscious, chronic stage TBI patients. As discussed below, we believe this is due to the difference in the terms omitted within the patient population specific to DOC and/or their differences in levels of consciousness, but the HCP participant population does not have these differences.

Leaving out a known interrelated measures (e.g., GWESP term for triadic closure term; see column 2 in Table 3.10) increases risks for differences in rates in FN for within cortical connectivity and FP within subcortical connectivity for comparisons between acute and chronic stage TBI patients. As we discussed in the introduction, triadic closure is one the key generative processes (Goodreau et al., 2009) present most graphs, but more importantly these differences in FP an FN rates could be due to the importance of triadic closure to consciousness. Integrated information theory propose that functional specificity and integration are necessary for producing the necessary connectivity to support consciousness, in which triadic closure is likely to play a key role. Furthermore, clustering coefficients have been used to differentiate patients with DOC (using structural connectivity; Tan et al., 2019) and for differentiating levels of consciousness while undergoing anesthesia (Monti et al., 2013). Due to the empirical findings of different levels of triadic closure within patient groups and the theoretical importance of triadic closure to consciousness, the best way to avoid these FP and FN rate differences is to model the selective mixng and triad closure processes in a single model.

The effects of omitting the structural terms (see column 3 in Table 3.10) affected the FP rates differently for the unconscious patients in their acute stage of TBI and the conscious patients in the chronic stage of their TBI for both within cortical connectivity and between subcortical and cortical connectivity. These effects are quite problematic for DOC research due to the interest in comparing cortico-cortico and thalamo-cortical connectivity (e.g., Laureys et al., 2000a,b; Vanhaudenhuyse et al., 2010; Boly et al., 2009, 2011; Crone et al., 2014; Amico et al., 2017; Crone et al., 2018) and its importance to consciousness. Due to the inherent nature of structural damage affecting the structural connectivity, the inclusion of structural terms into a model assessing functional connectivity will help to avoid the FP and FN rate differences between patient in acute and chronic stage of TBI, and the difference in rates between unconscious and conscious patients.

The effect of leaving out both the structural terms and the GWESP term (see column 1 in Table 3.10) has differing rates in: FNs for cortico-subcortical connectivity, FN and FPs for within cortical connectivity, and FPs for within subcortical connectivity. Since all these

effects are for unconscious patients, it affects all of DOC research for all three possible types of comparisons between cortical and subcortical connectivity. As can be seen in Table 3.10, the combination of leaving both terms is not just a simple combination of leaving out each term, but it has specific impacts for unconscious patients. A possible explanation is that for unconscious patients have structural connectivity alterations from their TBI that affected the patients' triadic closure, but these differences are masked by not accounting for patients' structural connectivity metrics. These types of interactions are key reasons for including all the generative processes in a graph and other key contributing factors like structural connectivity metrics for patients. The estimation of the connectivity differences depends on the structure in the graphs. If there is unaccounted factors, which affect one patient group more than another, the interpretation of results will be not accurately represent the generative processes associated with the connectivity differences between the patient groups.

Overall, investigating the network differences in patient populations is plagued by all three problems that we outlined. We strongly suggest to account for triadic closure and structural terms when investigating the functional connectivity differences between patient populations. We did not compare the patients to the HCP data due to the differences in quality of BOLD imaging and imaging parameters. However, we suspect that there would be differences similar to comparing the groups of patients because the underlying cause of these FP and FN is the importance in generating structure in the brain. Patient populations differ in this structure, which would be reflected by difference in sociality, selective mixing, and triadic closure. Leaving out one of these generative processes will affect the rest (Goodreau et al., 2009). Additionally, the structural terms are specifically important to DOC due to the TBI resulting in structural damage that is part of the recovery process. While there may be alternatives to solving the three of the four problems we outlined (i.e., problem#1, #2, and #3), we chose to use ERGM due to the flexibility it provides to model all the generative processes and other covariates of interest (e.g., size of regions of interest or amount of atrophy within an region of interest). This flexible framework would allow researchers to generate models that fit their specific needs and research questions.

3.5.1 Limitations and Future Studies

While we have demonstrated that all three problems would have affected this analysis, we did not fit the data well for the specific effects of triadic closure. The GWESP term matched the overall observed values (see Table 3.11 for patients, and for HCP participants, see Table 3.5), but our fits were sub-optimal for most specific edge shared partners (see Table 3.12 and 3.6 for HCP and patietns, respectively). The edge shared partners are a type of triadic closure that measures the number of triangles that share an edge. The effect of these poor fits are not well understood in our field. There is not any work that we are aware of, which explains specific amounts of triadic closure and their neural mechanisms. There is some work describing larger scale interpretations of outcome metrics (e.g., local and global clustering cofficient; Rubinov and Sporns, 2010, 2011) or to characteristic network blocks (i.e., motifs; Sporns and Ktter, 2004), but these accounts are for general interpretations without linking them to key neural mechanism. More theoretical work is needed to understand how these generative processs (i.e., sociality, selective mixing, and triadic closure) arise from neural mechanisms.

Finally, our structural terms only having a few significant terms for patients and participants (see Table 3.14, 3.15, 3.8, and 3.9). Yet, structural connectivity can be used to predict functional connectivity (Bettinardi et al., 2017; Mess et al., 2015), which we expected to have additional relationships found between degree, local efficiency, clustering coefficient and latent clustering of structural connectivity, and the functional connectivity. We only accounted for the structural terms by using measures of centrality and higher order clustering terms (e.g., clustering coefficient and latent space clusters). This is the equivalent of parcelling out the effects of structural connectivity on functional connectivity, similar to using covariates in a regression analysis to control for confounding effects. We have not truly estimated the effects of structural connectivity on functional connectivity. There are structural effects which could account for generative processes that we are attributing to the functional connectivity. For example, if a three nodes have two structural edges, does the functional close this triad? A process like this would represent a possible structural and

functional relationship from triad closure from the combination of structural and functional connectivity. In the future, a method is needed that accounts for the social processes that generate the complex interactions between structural and functional connectivity.

CHAPTER 4

The formation and dissolution of structural connectivity in patients with DOC: Extricating the return of complex behavior and consciousness

4.1 Methods

This second study uses a larger cohort of 31 patients to assess the dynamic changes of network properties for structural connectivity occurring over observations (e.g., time, clinical groups). STERGM was used to assess the differences in recovery from TBI for two groups of patients with differing levels of consciousness in the acute stage of their TBI whom differ in levels of consciousness, but both have the return of other complex behavior (Crone et al., 2018).

4.1.1 Structural Connectivity Patient Cohort

There were 31 patients that had at least one MRI session during the first two weeks since injury and at least one MRI session at least 158 days after injury. This cohort was mostly male (n=24) with seven female patients. At the time of injury, 14 male patients were below the age of 35 years old with the remaining ten over the age of 36. There were four female patients below the age of 25 and the remaining three were over 36 years old. The acute imaging sessions for 20 of the patients were held before 10 days post-injury with the remaining 11 between 10 and 37 days post-injury (see Table 4.1). The chronic imaging sessions were conducted between 158 and 238 days post-injury. During the acute session, patients were evaluated with a post-resuscitation Glasgow Coma Scale (GCS; Teasdale and Jennett, 1974). The GCS has three subscales: eyes opening (E), verbal response (V), and

motor response (M). Crone and colleagues 2018 used the GCS subscales of V and M to transform the GCS scores into the Glasgow Outcome Scale – Extended (GOS-E; Wilson et al., 1998). A patient with a GCS V subscale of less than or equal 3 and a GCS M subscale of less than or equal to 4 were assigned an inferred GOS-E of 2, while a patient with higher scores for GCS V and M were assigned an inferred GOS-E of 3. While DoC diagnoses are typically not made at such an acute stage, a patient with a GOS-E of 2 is consistent with a vegetative state (VS; see Table 4.2 for a description of VS), and patient with a GOS-E of 3 has recovered from VS. This allows organizing patients into two groups (see Table 4.1): VS at acute stage of TBI with recovering consciousness (U2C) at chronic stage of TBI and conscious at acute stage of TBI with maintaining consciousness (C2C) at the chronic stage of TBI. Both groups recovered cognitive functions transitioning from the acute to chronic stage of TBI, but the U2C group recovered consciousness going from acute to chronic stages of TBI, while the C2C group maintained consciousness. In total, the U2C group had 16 patients and the C2C group had 15 patients.

4.1.2 Parameter Selection

The selection procedure of parameter estimates is a three step process. First, we chose different mixing terms based on another exogenous nodal labeling of ROIs using their anatomical location within the four cerebral lobes (i.e, frontal, occipital, parietal, and temporal) and four subcortical divisions (i.e., basal ganglia, cerebellum, subcortex, and thalamus). Our STERGM model was specified with four terms, where the $P_\theta(Y = y)$:

$$= \frac{\exp(\theta_1 \text{edges} + \theta_2 \text{nodemix(lobes)} + \theta_2 \text{nodematch(laterality)} + \theta_4 \text{gwesp(alpha} = \lambda))}{c(\theta)} \tag{4.1}$$

The edges and GWESP terms (the decay parameter differs, but the interpretation is the same) are the same as the previous model (see §2.2). The still represents the intra- and inter-connectivity of the exogenous nodal labeling, but there are less terms because there are only 8 nodal labels compared to 11 (see §2.2). The nodematch for laterality term creates

	Gender	Cause of Injury	Age at Injury	Acute TSI	Chronic TSI	Delta TSI	Acute GCS	Acute GOS-E	Chronic GOS-E	Group
P003	Male	Blunt Trauma	31-35	3	238	235	8 (E:2, V:1, M:5)	3	4	C2C
P005	Male	Blunt Trauma	18-25	1	200	199	3 (E:1, V:1, M:1)	2	8	U2C
P006	Male	Blunt Trauma	36+	2	176	174	8 (E:2, V:1, M:5)	3	8	C2C
P007	Male	Automobile Accident	31-35	4	261	257	7 (E:1, V:1, M:5)	3	4	C2C
P014	Male	Fall	36+	3	194	191	7 (E:1, V:1, M:5)	3	3	C2C
P018	Male	Fall	36+	28	182	154	11 (E:4, V:1, M:6)	3	6	C2C
P021	Male	Fall	18-25	10	176	166	8 (E:2, V:1, M:5)	3	4	C2C
P022	Male	Fall	31-35	3	186	183	3 (E:1, V:1, M:1)	2	3	U2C
P023	Female	Automobile Accident	18-25	1	184	183	10 (E:4, V:1, M:5)	3	5	C2C
P024	Male	Bicycle vs Automobile	36+	24	207	183	8 (E:2, V:1, M:5)	3	5	C2C
P026	Male	Automobile Accident	18-25	2	194	192	3 (E:1, V:1, M:1)	2	3	U2C
P027	Male	Automobile Accident	18-25	2	196	194	3 (E:1, V:1, M:1)	2	5	U2C
P029	Female	Fall	36+	19	187	168	6 (E:4, V:1, M:1)	2	5	U2C
P039	Male	Automobile Accident	18-25	19	180	161	3 (E:1, V:1, M:1)	2	4	U2C
P051	Male	Automobile Accident	18-25	8	233	225	5 (E:1, V:1, M:3)	2	8	U2C
P054	Female	Fall	36+	25	186	161	7 (E:2, V:1, M:4)	2	8	U2C
P055	Male	Fall	36+	1	195	194	6 (E:1, V:1, M:4)	2	4	U2C
P066	Male	Bicycle vs Automobile	36+	0	222	222	7 (E:2, V:1, M:4)	2	5	U2C
P069	Male	Fall	36+	1	186	185	7 (E:2, V:1, M:4)	2	8	U2C
P074	Female	Automobile Accident	18-25	1	180	179	8 (E:1, V:2, M:5)	3	8	C2C
P079	Female	Pedestrian vs Automobile	18-25	2	181	179	7 (E:3, V:3, M:1)	2	7	U2C
P083	Male	Pedestrian vs Automobile	18-25	1	180	179	3 (E:1, V:1, M:1)	2	8	U2C
P084	Female	Automobile Accident	18-25	5	183	178	3 (E:1, V:1, M:1)	2	3	U2C
P085	Female	Fall	36+	2	177	175	15 (E:4, V:5, M:6)	3	7	C2C
P086	Male	Fall	36+	26	221	195	6 (E:1, V:1, M:4)	3	5	C2C
P089	Male	Fall	36+	17	181	164	10 (E:2, V:1, M:5)	3	3	C2C
P092	Male	Automobile Accident	18-25	1	158	157	10 (E:4, V:1, M:5)	2	4	U2C
P096	Male	Automobile Accident	26-30	37	176	139	3 (E:1, V:1, M:1)	3	4	C2C
p097	Male	NA	18-25	17	170	153	8 (E:2, V:1, M:5)	3	6	C2C
P099	Male	Bicycle vs Automobile	18-25	18	184	166	8 (E:2, V:1, M:5)	3	8	C2C
P100	Male	NA	36+	4	173	169	8 (E:2, V:1, M:5)	2	5	U2C

Table 4.1: **Patients' demographics.** For the 31 patients, the following demographics for each patient is tabulated: gender, cause of injury, age at injury, time since injury for the acute imaging session (Acute TSI), time since injury for the chronic imaging session (Chronic TSI), and the difference in time between the two imaging sessions (Delta TSI). Additionally for each patient, the level of consciousness at the acute imaging session (Acute GSC) and chronic imaging session (Chronic GOS-E) are tabulated. The acute GOS-E is inferred from the GCS scores after the acute imaging session. Finally, these GOS-E scores are used to group patients into two different recovery groups: unconscious to conscious (U2C) and conscious to conscious (C2C) groups. For a full description of the groups and inferred GOS-E see section §4.1.1.

Behavior	Score	Interpretation
Death	1	
Vegetative State	2	A condition of unawareness with some reflex functions and spontaneous eye openings.
Lower Severe Disability	3	A patient with mental and/or physical disabilities who needs more than 8 hours of assistance for daily activities.
Upper Severe Disability	4	A patient with mental and/or physical disabilities who needs less than 8 hours of assistance for daily activities.
Lower Moderate Disability	5	A patient with some mental disabilities (e.g., aphasia, epilepsy or memory deficits). They do not need assistance for daily activities, but they are unable to return to work or school.
Upper Moderate Disability	6	A patient with some mental disabilities (e.g., aphasia, epilepsy or memory deficits). They do not need assistance for daily activities, and they are able to return to work or school.
Lower Good Recovery	7	Patient is able to resume work and daily activities, but may have minor mental and physical deficits which affect work and/or daily activities.
Upper Good Recovery	8	Patient is able to resume work and daily activities without being disrupted by mental or physical deficits.

Table 4.2: **Glasgow Outcome Scale – Extended (GOS-E) description.** The behavior, score, and interpretation of the GOS-E scores (Wilson et al., 1998).

three parameter estimates based on the laterality of each ROI (i.e., within left hemispher, within right hemisphere or within medial). The medial term was not estimable for many subjects, and was omitted from the model. This first step resulted in the STERGMs having a varying number of terms for the formation (between 29 and 33 terms for each patient) and dissolution models (between 21 and 29 terms for each patient) because some of the mixing terms were not able to be estimated due to the low number of tie counts for the intra- and inter-connectivity which were omitted from each patient's models.

In the second step, after the estimation of the STERGMs, we eliminated the mixing terms which were estimatable for the mean parameter estimate, but the standard errors were not able to be estimated. This was also due to a lack of tie counts for mixing terms. These tie counts were higher than the other terms omitted, but still not enough to get a true estimate of the variance of the ties across the MCMCs. This reduced the original 29 to 33 terms for each patient down to the 13 parameter estimates (i.e., edges, fronto-basal ganglia, within frontal lobe, fronto-parietal, within parietal lobe, thalamo-basal ganglia, thalamo-frontal, within Thalamus, within left hemisphere, within right hemisphere, GWESP, parieto-occipital, and within temporal lobe) for the formation model and 11 parameter estimates (i.e., all of the formation model's parameter estimates except fronto-basal ganglia and thalamo-frontal) for the dissolution models. The exclusion criterion for these parameter estimates was that each parameter estimate had to have at least 30 patients with estimable standard errors.

The final step of the selection of parameter estimates for the regression models was

	Matched MRI	Acute Bvec	Chronic Bvec	Acute Slice Thickness	Chronic Slice Thickness	Acute TR	Chronic TR	Acute TE	Chronic TE
P003	No	31	29	2x2x3 mm, 50 Slices	2x2x3 mm, 50 Slices	8000 ms	8000 ms	95 ms	90 ms
P005	No	32	27	2x2x3 mm, 50 Slices	2x2x3 mm, 50 Slices	8300 ms	8000 ms	95 ms	95 ms
P006	No	32	30	2x2x3 mm, 50 Slices	2x2x3 mm, 50 Slices	8000 ms	8000 ms	95 ms	95 ms
p007	No	26	29	2x2x3 mm, 50 Slices	2x2x3 mm, 50 Slices	8000 ms	8000 ms	95 ms	95 ms
P014	No	30	30	2x2x3 mm, 50 Slices	2x2x3 mm, 50 Slices	8000 ms	8000 ms	95 ms	95 ms
P018	No	30	29	2x2x3 mm, 50 Slices	2x2x3 mm, 50 Slices	9000 ms	8000 ms	95 ms	95 ms
P021	No	31	32	2x2x3 mm, 50 Slices	2x2x3 mm, 50 Slices	8000 ms	8000 ms	95 ms	95 ms
P022	Yes	32	27	2x2x3 mm, 50 Slices	2x2x3 mm, 50 Slices	8000 ms	8000 ms	95 ms	95 ms
P023	No	25	31	2x2x3 mm, 50 Slices	2x2x3 mm, 50 Slices	8000 ms	8000 ms	95 ms	95 ms
P024	No	32	28	2x2x3 mm, 50 Slices	2x2x3 mm, 50 Slices	8000 ms	8000 ms	95 ms	95 ms
P026	No	31	28	2x2x3 mm, 50 Slices	2x2x3 mm, 50 Slices	8000 ms	8000 ms	95 ms	95 ms
P027	No	31	28	2x2x3 mm, 50 Slices	2x2x3 mm, 50 Slices	8000 ms	8000 ms	95 ms	95 ms
P029	No	31	32	2x2x3 mm, 50 Slices	2x2x3 mm, 50 Slices	8000 ms	8000 ms	95 ms	95 ms
P039	No	29	30	2 mm isotropic, 75 Slices	2 mm isotropic, 75 Slices	9700 ms	9700 ms	90 ms	95 ms
P051	Yes	63	58	2x2x3 mm, 50 Slices	2.125x2.125x2 mm, 75 Slices	9000 ms	9700 ms	90 ms	90 ms
P054	Yes	64	63	2 mm isotropic, 69 Slices	2.125x2.125x2 mm, 69 Slices	9000 ms	9000 ms	90 ms	90 ms
P055	Yes	56	56	2x2x3 mm, 50 Slices	2.125x2.125x2 mm, 81 Slices	8000 ms	9000 ms	96 ms	90 ms
P066	No	41	38	2 mm isotropic, 81 Slices	2 mm isotropic, 69 Slices	9300 ms	9000 ms	90 ms	90 ms
P069	Yes	59	61	2 mm isotropic, 69 Slices	2.125x2.125x2 mm, 77 Slices	9000 ms	9900 ms	90 ms	90 ms
P074	Yes	58	62	2 mm isotropic, 69 Slices	2.125x2.125x2 mm, 69 Slices	9000 ms	9000 ms	90 ms	90 ms
P079	Yes	64	62	2 mm isotropic, 69 Slices	2.125x2.125x2 mm, 69 Slices	9000 ms	9000 ms	93 ms	90 ms
P083	Yes	64	56	2 mm isotropic, 69 Slices	2.125x2.125x2.1 mm, 69 Slices	9000 ms	9000 ms	90 ms	90 ms
P084	Yes	64	62	2 mm isotropic, 69 Slices	2x2x3 mm, 52 Slices	9000 ms	9000 ms	90 ms	90 ms
P085	Yes	54	62	2 mm isotropic, 69 Slices	2x2x3 mm, 52 Slices	10100 ms	9000 ms	90 ms	90 ms
P086	Yes	57	60	2 mm isotropic, 78 Slices	2x2x3 mm, 52 Slices	8100 ms	9000 ms	90 ms	90 ms
P089	Yes	60	62	2x2x3 mm, 50 Slices	2 mm isotropic, 72 Slices	9500 ms	9500 ms	90 ms	90 ms
P092	Yes	61	63	2 mm isotropic, 78 Slices	2 mm isotropic, 75 Slices	10100 ms	9500 ms	90 ms	90 ms
P096	Yes	45	60	2 mm isotropic, 78 Slices	2 mm isotropic, 78 Slices	10100 ms	10100 ms	90 ms	90 ms
P097	Yes	48	59	2 mm isotropic, 73 Slices	2 mm isotropic, 78 Slices	10100 ms	10100 ms	90 ms	90 ms
P099	Yes	62	64	2 mm isotropic, 78 Slices	2 mm isotropic, 78 Slices	10100 ms	10100 ms	90 ms	90 ms
P100	Yes	63	62	2 mm isotropic, 78 Slices	2 mm isotropic, 78 Slices	10100 ms	10100 ms	90 ms	90 ms

Table 4.3: **Patients' DWI parameters.**. The following parameters for each DWI imaging session (i.e., acute and chronic) varied from patient to patient due to clinical requirements: the number of gradient directions (Bvec), the slice thickness, the repetition time (TR), and the echo times (TE). Additionally, the matched MRI indicates which patients had the same MRI system in both the acute and chronic imaging sessions.

based on compatible hypotheses for the structural connectivity from theories of consciousness (global neuronal workspace theory [GNW]; Dehaene et al. 1998, Dehaene and Changeux 2005, Dehaene and Changeux 2011, Dehaene et al. 2014, higher-order thought theory [HOT]; Lau 2007, Lau 2011, Lau and Rosenthal 2011, and integrated information theory [IIT]; Oizumi et al. 2014, Tononi 2008, Tononi and Koch 2015, Tononi et al. 2016) or recovery of complex behavior (mesocircuit hypothesis; Schiff, 2010). Hypotheses based on the dynamic competition between assemblies of cells (Crick and Koch, 2003), the presence of synchronized long-range activity in specific frequency bands (Engel and Singer, 2001; Tallon-Baudry, 2009), and recurrent connectivity (Lamme and Roelfsema, 2000; Lamme, 2006, 2010) were exlcuded because DTI data cannot detect dynamic competition between assemblies of cells, cannot detect specific frequency bands, or discriminate between recurrent connectivity compared to other types of connectivity (i.e., DTI connectivity is undirected). Importantly, GNW, HOT, and IIT are theories of consciousness that describe the key physical substrates for consciousness, not the recovery of consciousness. The mesocircuit hypothesis describes recovery of complex behavior and the recovery of consciousness. Neither the mesocircuit hypothesis nor the theories of consciousness (i.e., GNW, HOT, and IIT) provide a full description of the important physical substrates for the recovery of consciousness, but we will test their hypotheses based on the important physical substrates of consciousness and complex behavior.

For all theories, we assumed that a loss of consciousness in DOC patients also causes a lack of consciousness awareness because a patients in a VS or unresponsive awareness syndrome have wakefulness in the absence of any behavioral sign of awareness of the self or the environment. If the lack of awareness for the environment is truly absent (i.e., assuming the behavioral signs are accurate), they also lack consciousness awareness. Next, we assumed that these theories would suggest that the important physical substrates of consciousness is also the important physical substrates for recovery of consciousness. Additionally, none of these theories/hypothesis differentiate between the formation and dissolution/perservance of connectivity, which we assumed equally important for the parameter estimates chosen for this model because either the formation, or dissolution/perservance of connectivity could

represent a reorganization process in patients with severe TBI. Finally, we described only some of the predictions for types of connectivity for each theory, which are relevant to the possible connectivity specified by our STERGM.

GNW builds upon global worskspace theory's posited role of the reverberation and spread of neural activity across fronto-parietal association regions (Baars, 1993, 2002; Baars et al., 2003; Baars, 2005) by additionally proposing the role of specific, recurrent thalamo-cortical loops. Taken together for GNW, we assert the key physical substrates for supporting a global workspace would be fronto-parietal, thalamo-frontal, and thalamo-parietal connectivity. Additionally, a globabl workspace is integrating multiple regions which would result in changes in integrative connectivity.

HOT of consciousness posit that consciousness is a higher-order process (i.e., a type of metacognition) different from first-order perceptual representations (e.g., information processing in sensory or ventral-temporal regions; Lau and Rosenthal, 2011). This form of metacognition determine the reliability of the first-order representation (Lau, 2007), which is conscious awareness (Ko and Lau, 2012; Maniscalco and Lau, 2016). The higher-order representations are posited within the frontal lobe (e.g, dorsolateral prefrontal cortex; Lau and Passingham, 2006; Rounis et al., 2010). Finally, the higher-order representations require the first-order representation, which would entail connectivity between frontal and temporal regions. Taken together, the physical substrates of consciousness for HOT is approximated here by the within frontal lobe connectivity and fronto-temporal connectivity.

IIT posits a mathematical framework specifying that the level consciousness is identical to the integrated information of system (Φ^{max}), and the contents of consciousness are identical to a physical systems' maximal irreducible conceptual structure (MICS; Oizumi et al., 2014; Tononi and Koch, 2015; Tononi et al., 2016). Due to current computational limitations, neither the Φ^{max} nor the MICS can be computed for biologically relevant systems (Tegmark, 2016), but the more general properties of integration and differentiation (Tononi, 2008) have been assessed using path based and clustering metrics (Monti et al., 2013). Typically path based measures are used to test integration (Monti et al., 2013), but we used the edges term, which accounts for the overall density of the graph over and above the rest of the terms in our

model. While the overall density of a graph is not directly related to integration, an increase in density will increase overall integration, but as posit by IIT (Tononi, 2008), too much integration reduce the overall level of consciousness. The lack of path based metrics in our model is due to path based metrics being affected by multiple generative processes, which we are trying to extricate using STERGM. Additionally, the superior parietal lobule may play an important role in generating the integrated information as discovered using perturbational complexity index (PCI Casali et al., 2013; Casarotto et al., 2016; Comolatti et al., 2018) to discriminate states of consciousness (e.g., sleep, anesthesia, DOC) with unprecedented accuracy. PCI is not a 1-to-1 translation of the mathematical framework (Sitt et al., 2013; Nagaraj and Virmani, 2017), but it is "based upon" the core ideas of IIT of integration and differentiation. As per GNW's integration test, we will use an edge term, and our clustering term is the GWESP metric (for a full description, see Chapter 2, §2.2). Finally, the within parietal lobe connectivity will be included due to the findings using PCI.

According to the mesocircuit hypothesis, there are cortical-striatopallidal thalamocortical loop systems which are responsible for complex behavior including consciousness (Schiff, 2010). The thalamus and basal ganglia (internal globus pallidus and striatum) are key subcortical sites that can have larger scale connectivity in cortical regions (e.g., frontal, parietal, temporal and occipital regions). Given the large number of regions posited, we will include the within thalamic and basal ganglia connectivity along with the thalamo-frontal and thalamo-basal ganglia connectivity.

Considering the regions and types of connectivity posited by the theories of consciousness and mesocircuit hypothesis, we built two regression models with the following 9 parameter estimates (edges, fronto-basal ganglia, within frontal lobe, fronto-parietal, within parietal lobe, thalamo-basal ganglia, thalamo-frontal, within Thalamus, and GWESP) for the formation model and 7 parameters (edges, within frontal lobe, fronto-parietal, within parietal lobe, thalamo-basal ganglia, within Thalamus, and GWESP) for the dissolution model. The fronto-temporal connectivity and within basal ganglia connectivity were eliminated due to too few patients with estimable SEs.

4.1.3 Analyses

Using the 9 and 7 parameter estimates discussed in the previous section as predictor variables, we took the mean parameter estimates of the STERGM and divided them by the standard errors to include the variability into the predictor variables. Additionally, we regressed the average number Bvecs and matched MRI (see Table 4.3 to control for the different scanning parameters and scanning systems in the acute and chronic imaging sessions. These residualized predictor variables were used in both the normal and logistic regression analyses. Next, we ran six additional regressions for both the logistic and normal regression to assess the need to covary the age, time since injury and gender of patient, but none of the covariates were significantly related to either outcome variable. Thus, we did not include the covariates into either logistic or normal regression. We also performed three stepwise procedures (i.e., forward selection, backwards elimination, and bidirectional elimination) that were used to produce the most parsimonious models based on the Akaike information criterion (AIC) for both the logistic regressions. The penalty multiplier for each degree of freedom (df) used in a model for AIC is 2. We also tested these models using Bayesian information criterion (BIC) which the penalty multiplier for the dfs is the $\log(df)$. The BIC and AIC penalty multipliers converged on the same models, so we only report the AIC. Finally, we ran a t-tests with equal variances assumed to assess the differences between the delta GOS-E for both the patients in the dissolution and formation models to test if the patients recovered at different rates according to the GOS-E. For this test, the null hypothesis is a difference of -1 (instead of 0) because the U2C recovery group's acute inferred GOS-E was 2 and the C2C recovery group was 3.

Using a generalized linear models in R (Chambers et al., 1992; Dobson and Barnett, 2008; McCullagh, 2018; Venables and Ripley, 2013), we fit two logistic regression analyses (one for the formation model and one for the dissolution model) to determine which residualized predictor variables were more associated with the going from C2C (reference group) to U2C group (see Table 4.1). A positive coefficient can be interpreted as more predictive of the U2C group and a negative coefficient is more predictive of the C2C group. These group

differences will be assessed by a follow up analysis of the delta GOS-E to investigate the type of formation or dissolution driving the change. It is important to note that the coefficients from this regression all are important for predicting consciousness because they are affected by each other due to collinearity. Additionally, a lack of significance does not necessarily mean no group difference, it means that the difference is less likely to be uniquely attributable to that specific type of connectivity, but it is still important to report and interpret these coefficients.

Using a generalized linear models in R (Chambers et al., 1992; Dobson and Barnett, 2008; McCullagh, 2018; Venables and Ripley, 2013), the two normal regressions analyses (one for the formation model and one for the dissolution model) used the interaction between residualized predictor variables and the patient recovery group variable (i.e., U2C and C2C groups, see Table 4.1) to predict the delta GOS-E. Only the interaction between the residualized predictor variables and the recovery groups were included in the model because the delta GOS-E does not account for different recovery groups which have an important effect on the interpretation of delta GOS-E. For example, a delta GOS-E of 1 for a patient in the C2C group indicates a increase in cognitive function (see Table 4.2), but a 1 for a patient in the U2C group indicates that patient transitioned from VS to a more recovered state of consciousness and regained some cognitive functions. Thus, the normal regression models will have two coefficients for each residualized predictor variable which allows for the association of the residualized predictor variables for each recovery group to be established. The model's connectivity PEs were chosen to match the logistic regression because we want to explore the group differences found in the logistic regression for the type of relationship with a change in GOS-E.

In the formation model, for the C2C group, a positive coefficient was interpreted as an increase of formation of connectivity that predicts an increase in cognitive function measured by a behavioral assessment. While in the dissolution model, for the C2C group, a positive coefficient was interpreted as the perseverance of connectivity that predicts an increase in cognitive function. Continuing with the C2C group in the formation model, a negative coefficient was interpreted as increase in cognitive function as the formation connectivity

becomes less likely. This is due to delta GOS-E ≥ 0 for all patients and the formation model only indicates the likelihood of the formation of connectivity (i.e., negative parameter estimate is a reduced likelihood of formation, see §2.1). In other words, patients in the C2C group did not decrease in their cognitive function and this is related to the reduced likelihood of the formation of a specific type of connectivity. While in the dissolution model, for the C2C group, a negative coefficient was interpreted as an increase in cognitive function as there is a decrease in connectivity (i.e., a dissolution of connectivity). The U2C group's interpretation of coefficients will only add the change in consciousness in combination with the increase in cognitive function.

The interpretations of both regressions together extricate the return consciousness and complex behavior. For the U2C group, a significant parameter estimate in both the logistic and normal regression indicate that connectivity type predicts the return of consciousness because it predicts the difference between the two recovery groups (i.e., return of consciousness) and it predicts the type of formation (i.e., either a tendency for increased formation or a tendency for resistance to formation) or dissolution (i.e., either a tendency for perseverance or a tendency dissolution of connectivity) that is related to the more likely return of consciousness. This is because both groups recovered complex behavior, but the U2C group recovered from an unconscious state, while the C2C group began in a conscious state. For the C2C group, a significant parameter in both regressions indicate that connectivity type predicts the return of complex behavior because it is predicts the return of complex behavior instead of consciousness (i.e., indicative of C2C group in logistic regression) and it predicts the type of formation or dissolution that is related to the return of complex behavior. If the logistic regression has a significant coefficient, but the normal regression does not, the relationship between return of behavior and consciousness for formation or dissolution types cannot be determined. If the normal regression has a significant coefficient, but the logistic does not have a significant coefficient, the relationship is between the return of consciousness and the type of formation is likely, but not as likely as having a significant group difference between the U2C and C2C groups in the logistic regression.

Finally, t-test with equal variances assumed were preformed on the counts of connectivity

during the acute stage of TBI for each parameter estimate. On the one hand, if the recovery groups had larger counts of connectivity in the acute stage of TBI, this could lead to an increase in dissolution/perseverance of connectivity. On the other hand, if the recovery group had reduced counts of connectivity in the acute stage of TBI, this could lead to an increase in formation connectivity. If the recovery groups had equal counts of connectivity in the acute stage of TBI, the formation and dissolution/perseverance connectivity should be equally likely. One important note, the edge counts for the edges term were tested by assessing differences in overall density, and the edge counts for the GWESP were tested using triangle counts because the edges and GWESP terms are model specific. This would require an ERGM analysis for each patient, but only STERGM for each patient was conducted.

4.2 Results

In the all the regression models, for the both formation and dissolution models, the stepwise procedure converged on the same results for the backwards elimination and the bidirectional elimination, but the forward selection resulted in the full model. Since the backwards elimination and bidirectional elimination converged on the same model, we chose the model based on the bidirectional elimination. For the formation model, the bidirectional elimination excluded the edges term, fronto-basal-ganglia connectivity, and GWESP term (see Table 4.4). For the dissolution model, the bidirection elimination excluded all terms, except edges and GWESP terms (see Table 4.4). The t-test with equal variances assumed was not significant for the patients in the formation model (M_{U2C} = 3.923, M_{C2C} = 2.500, df = 25, t-statistic = -0.596, CI_{lB} = -2.898, CI_{UB} = 0.052, p-value = 0.56) nor the dissolution model (M_{U2C} = 3.467, M_{C2C} = 2.214 , df = 27, t-statistic = -0.356, CI_{lB} = -2.706, CI_{UB} = 0.201, p-value =0.724).

The formation model's logistic regression resulted in a significant negative coefficient for within frontal lobe connectivity (β = -2.062, df = 20, SE = 0.981, p = 0.0355) and a significant positive coefficient for within thalamic connectivity (β = 1.459, df = 20, SE = 0.689, p = 0.0342; see Table 4.4, the formation after stepwise column). There were also

positive coefficients for fronto-parietal connectivity (β = 1.369, df = 20, SE = 0.0775, p = 0.0774), within parietal lobe connectivity (β = 1.512, df = 20, SE = 0.871, p = 0.0825), and thalamo-frontal connectivity (β = 0.889, df = 20, SE = 0.507, p = 0.0798). Finally, there was a negative coefficient for thalamo-basal ganglia connectivity (β = -1.202, df = 20, SE = 0.689, p = 0.0665). The dissolution model's logistic regression had a positive coefficient for the GWESP term (β = 1.349, df = 26, SE = 0.653, p = 0.0507) and for the edges term (β = 0.519, df = 26, SE = 0.313, p = 0.0973; see Table 4.4, the dissolution after stepwise column).

For the U2C group, the formation model's normal regression resulted in a significant negative coefficient for the within frontal lobe connectivity (β = -2.668, df = 15, SE = 0.968, p = 0.019). Additionally, there were a significant positive coefficient for the within parietal lobe connectivity (β = 3.013, df = 15, SE = 1.148, p = 0.016; see Table 4.4 and positive coefficients for the fronto-parietal connectivity (β = 2.397, df = 15, SE = 1.235, p = 0.010), for thalamo-basal ganglia connectivity (β = 0.034, df = 15, SE = 1.026, p = 0.5849), for thalamo-frontal connectivity (β = 0.481, df = 15, SE = 0.880, p = 0.585), and within thalamic connectivity (β = 1.697, df = 15, SE = 1.037, p = 0.104). For the C2C, there was negative coefficients for the fronto-parietal connectivity (β = -0.025, df = 15, SE = 1.074, p = 0.982), for the within parietal lobe connectivity (β = -1.432, df = 15, SE = 1.395, p = 0.321), for the thalamo-basal ganglia connectivity (β = -0.124, df = 15, SE = 0.805, p = 0.2700), for the thalamo-frontal connectivity (β = -0.240, df = 15, SE = 0.879, p = 0.763), and for the within thalamic connectivity (β = -0.431, df = 15, SE = 0.986, p = 0.682). Finally, there was a positive coefficient for the within frontal lobe connectivity (β = 0.696, df = 15, SE = 0.908, p = 0.455).

In the dissolution model for the U2C group, the normal regression resulted in a significant positive coefficient for the edges term (β = 1.283, df = 24, SE = 0.517, p = 0.02006) and the GWESP term (β = 4.178, df = 24, SE = 1.288, p = 0.00334). For the C2C group, there were negative coefficients for the edges term (β = -0.021, df = 24, SE = 0.605, p = 0.97225) and the GWESP term (β = -0.548, df = 24, SE = 1.039, p = 0.60269).

When comparing the acute imaging sessions counts of connectivity for the patients in

the U2C and C2C, the results of the t-tests with equal variances were not significant for any parameter estimate in the formation nor the dissolution model (see Table 4.6). For the U2C in the formation model, there were on average more edge counts within frontal lobe, within parietal lobe, for fronto-basal ganglia, and for fronto-thalamo. While the C2C group, had on average more edges within thalamus, for thalamo-basal ganglia, and triangles. For the U2C group in the dissolution model, there was on average more edge for all the terms except the thalamo-basal ganglia connectivity.

	Logistic Regression With Group C2C As The Reference Group			
	Formation		Dissolution	
	(Before Stepwise)	(After Stepwise)	(Before Stepwise)	(After Stepwise)
Edges	0.123		1.216	0.519*
	(0.330)		(0.961)	(0..313)
Fronto-Basal Ganglia Connectivity	−0.491			
	(0.481)			
Within Frontal Lobe Connectivity	−2.048*	−2.062**	0.430	
	(1.077)	(0.981)	(0.682)	
Fronto-Parietal Connectivity	1.906**	1.369*	0.475	
	(0.968)	(0.775)	(0.699)	
Within Parietal Lobe Connectivity	1.000	1.512*	0.017	
	(0.939)	(0.871)	(0.626)	
Thalamo-Basal Ganglia Connectivity	−1.335*	−1.202*	0.177	
	(0.748)	(0.655)	(0.259)	
Thalamo-Frontal Connectivity	0.911	0.889*		
	(0.562)	(0.507)		
Within Thalamus Connectivity	1.554**	1.459**	−0.379	
	(0.725)	(0.689)	(0.482)	
GWESP	−0.011		2.209	1.276*
	(0.588)		(1.381)	(0.653)
Constant	−0.408	−0.408	−9.887	−6.587*
	(0.568)	(0.568)	(6.213)	(3.429)
Observations	27	27	29	29
Log Likelihood	−11.488	−12.467	−16.613	−17.644
Akaike Inf. Crit.	42.975	38.933	49.226	41.288

Note: $^{*}p<0.1$; $^{**}p<0.05$; $^{***}p<0.01$

Table 4.4: **Logistic regression with group C2C as the reference group.** There were two logistic regression models fit for each the formation and dissolution models: full model (before stepwise column) and final model (after stepwise column). The LATEX code to create this table was produced by the R package called texreg (Leifeld, 2013).

	Normal Regression Using GOS-E Change from Acute to Chronic	
	Formation	Dissolution
Group C2C:Edges		−0.021
		(0.605)
Group U2C:Edges		1.283**
		(0.517)
Group C2C:Within Frontal Lobe Connectivity	0.696	
	(0.908)	
Group U2C:Within Frontal Lobe Connectivity	−2.668**	
	(0.968)	
Group C2C:Fronto-Parietal Connectivity	−0.025	
	(1.074)	
Group U2C:Fronto-Parietal Connectivity	2.397*	
	(1.268)	
Group C2C:Within Parietal Lobe Connectivity	−1.432	
	(1.395)	
Group U2C:Within Parietal Lobe Connectivity	3.013**	
	(1.148)	
Group C2C:Thalamo-Basal Ganglia Connectivity	1.118	
	(0.976)	
Group U2C:Thalamo-Basal Ganglia Connectivity	0.034	
	(1.026)	
Group C2C:Thalamo-Frontal Connectivity	−0.124	
	(0.805)	
Group U2C:Thalamo-Frontal Connectivity	0.481	
	(0.880)	
Group C2C:Within Thalamus Connectivity	−0.431	
	(1.029)	
Group U2C:Within Thalamus Connectivity	1.697	
	(1.037)	
Group C2C:GWESP		−0.548
		(1.039)
Group U2C:GWESP		4.178***
		(1.288)
Observations	27	29
Log Likelihood	−65.329	−77.524
Akaike Inf. Crit.	154.66	163.048

Note: $^{*}p<0.1$; $^{**}p<0.05$; $^{***}p<0.01$

Table 4.5: **Normal Regression using GOS-E change from acute to chronic as the dependent variable.** There were two normal regression models fit for each the formation and dissolution models: full model (before stepwise column) and final model (after stepwise column). The LATEX code to create this table was produced by the R package called texreg (Leifeld, 2013).

	C2C.Mean	U2C Mean	*df*	*t*-Statistic	Lower Bound CI	Upper Bound CI	*p*-value
Formation Edge Type							
Within Frontal Lobe	142.357	142.615	25	−0.064	−8.633	8.116	0.950
Fronto-Basal Ganglia	15.643	17.231	25	−0.682	−6.383	3.207	0.502
Fronto-Parietal	30.929	31.462	25	−0.402	−3.263	2.197	0.691
Within Parietal Lobe	65.714	66.077	25	−0.195	−4.196	3.471	0.847
Thalamo-Basal Ganglia	23.500	22.846	25	0.272	−4.306	5.613	0.788
Fronto-Thalamo	4	4.385	25	−0.164	−5.215	4.446	0.871
Within Thalamus	46.571	44.615	25	0.847	−2.800	6.712	0.405
Density	0.056	0.056	25	−0.317	−0.004	0.003	0.754
Triangles	868.571	864.308	25	0.044	−196.410	204.938	0.965
Dissolution Edge Type							
Within Frontal Lobe	140.143	142.333	27	−0.584	−9.881	5.501	0.564
Fronto-Parietal	30.786	31.333	27	−0.424	−3.196	2.101	0.675
Within.Parietal Lobe	66	67.133	27	−0.607	−4.965	2.698	0.549
Thalamo-Basal Ganglia	24.929	24.267	27	0.291	−4.010	5.334	0.774
Within Thalamus	46	46.133	27	−0.054	−5.173	4.907	0.957
Density	0.056	0.057	27	−0.509	−0.004	0.003	0.615
Triangles	881.143	886.400	27	−0.059	−188.453	177.938	0.953

Table 4.6: **Group differences of PEs used in the logistic and normal regressions for acute stage of TBI.** For the formation model and dissolution model, none of the PEs had different average counts for the U2C and C2C recovery groups. The LATEX code to create this table was produced by the R package called texreg (Leifeld, 2013).

4.3 Discussion

The main goal of this study was predict the recovery of consciousness while controlling for the recovery of complex behavior. Using the methods developed by Crone and colleagues 2018, we identified two groups of patients, which were unconscious at the acute time point with recovering consciousness in the chronic time point (U2C) and conscious at both time points (C2C). We used two types of regression to predict the connectivity types associated with recovery of consciousness (i.e., connectivity predicting the U2C group) or complex behavior (i.e., connectivity predicting the C2C group) using logistic regression. The normal regression was used a follow up analysis to discern the the type of formation (i.e., a positive coefficient indicating tendency for increased formation and tendency for a negative coefficient indicating resistance to formation) or dissolution (i.e., i.e., tendency for a positive coefficient indicating perseverance of connectivity and tendency for a negative coefficient indicating a dissolution of connectivity) of connectivity associated with the group differences found in the logistic regression. We tested for group differences recovery rates of consciousness and complex behavior assessed via delta GOS-E, neither of the tests were significant for the formation model nor the dissolution model, and the mean delta GOS-E were by 1.253 higher in the U2C group for the formation model and 1.253 higher in the U2C group for the dissolution model, which indicates that the difference between the U2C and C2C recovery groups initial acute GOS-E is the driving change in the differences of the mean delta GOS-E for these two groups.

The recovery of consciousness was predicted by formation of within thalamic connectivity (see Table 4.4), but the type of formation (i.e., increased formation or resistance) was not dissociable using delta GOS-E (see Table 4.5). The level of overall thalamic damage in patients are a key marker of VS (Adams et al., 2000; Lutkenhoff et al., 2013, 2015), and in increase for formation could indicate a recovery process of the thalamus for patients recovering consciousness because an increase of thalamic atrophy is associate with a worse recovery of complex behavior and consciousness (Lutkenhoff et al., 2013, 2015). Additionally, an tendency for an increase in formation could result in an increase in overall white matter

tract integrity within the thalamus, which is consistent with previous findings Fernández-Espejo et al. (2011). Finally, an increase in formation for within thalamic connectivity would affect the economy of cortical-striatopallidal thalamocortical loop system resulting in a change specific to recovery of consciousness compared to an overall change in complex behavior predicted by the mesocircuit hypothesis (Schiff, 2010).

The increased formation of within parietal lobe connectivity is likely to predict the return of consciousness. This increase in formation would change the underlying structural architecture which could be a factor in the difference of complexity found in discriminating DOC patients using PCI (Casali et al., 2013; Casarotto et al., 2016; Comolatti et al., 2018). The formation of fronto-parietal and thalamo-frontal connectivity are likely to predict the return of consciousness, but the type of formation underlying this change is unclear. Formation in both the fronto-parietal and thalamo-frontal connectivity are part of the larger thalamo-cortical recurrent loop predicted by GNW, which are necessary for establishing a global workspace. The link between thalamo-frontal connectivity and recovery of consciousness is consistent with previous findings that the degree of intact thalamo-frontal anatomical connectivity is related to recovery of consciousness assessed by behavioral measures (Zheng et al., 2017). Finally, the change in formation for thalamo-frontal connectivity is part of the cortical-striatopallidal thalamocortical loop system (Schiff, 2010), which is another change specific to recovery of consciousness.

The perseverance of overall density predicting the return of consciousness could be linked to a protective factor for patients recovering consciousness against forming too edges, which could result in too much integration and an overall loss of integrated information (Tononi, 2008). The perseverance of triadic closure (i.e., the GWESP term) is likely to predict patients recovering consciousness is inconsistent with a recent finding that decrease in transitivity (a type of triadic closure) has been associated with a patient transitioning from VS to MCS, and an increase has been associated in a second patient whom remained in VS (Tan et al., 2019). Our GWESP term accounts for the triadic closure over and above all the other types of generative processes (i.e., sociality and selective mixing) involved producing networks because it is modeled with terms that control for sociality (i.e., the edges term) and

selective mixing (e.g., the nodemix terms for lobes), while Tan and colleagues 2019 choice of transitivity was tested independently, which does not control for the other generative processes of sociality and selective mixing that could affect the an increase in transitivity (see §1.1.2 for a detailed description). This perseverance of triadic closure could be linked to an increase in differentiation (Tononi, 2008), which would increase the amount of integrated information in the main complex responsible for consciousness (Oizumi et al., 2014; Tononi and Koch, 2015; Tononi et al., 2016).

The return of complex behavior was predicted the formation of within frontal lobe connectivity, and this group difference was due to the U2C group having a tendency for resistance to formation, while the C2C group did not have any dissociable type of formation assessed via delta GOS-E (see Table 4.5). The resistance to formation in the U2C recovery group could be indicative of a interaction between the recovery of consciousness and recovery of complex behavior. There could be a resistance to formation for recovering from a VS to another state of DOC. This could be driving the resistance to formation for the U2C recovery group, but the C2C recovery group did not have this factor. However, there is not enough evidence to fully support this possibility because the C2C group did not have a discernible type of within lobe frontal connectivity. Finally, the formation of thalamo-basal connectivity is likely to predict the return of complex behavior(the mesocircuit hypothesis; Schrouff et al., 2011), but the type of formation is underlying this change is unclear.

These findings should not be interpreted as testing the theories of consciousness or mesocircuit hypothesis, rather we used the theories and mesocircuit hypothesis to form a feature set of possible connectivity types associated with both recovery of consciousness and complex behavior. First, we assumed that GNW, HOT, and IIT would describe the same physical substrates to the recovery of consciousness as the physical substrates for consciousness; however, additional hypotheses specific to the recovery of conscious with regard to the formation and dissolution are needed to establish the role of formation and dissolution for higher-order representations, a global workspace, and integrated information. Second, we only extracted a few hypotheses from each theory that were testable in our model. GNW predicts that thalamo-cortical recurrent loops are necessary for the establishing the globabl workspace,

but our connectivity based on DTI cannot discern feedfordward, feedback, or recurrent loops. Furthermore, we did not test for overall thalamo-cortical connectivity because we only had thalamo-frontal and fronto-parietal connectivity in our model. For HOT, we were only able to test the within frontal regions, and we were not able to test fronto-temporal regions due to too many subjects had non-estimable SEs for that particular connectivity. Additionally, within frontal lobe connectivity contains dorsolateral prefrontal cortex, but it also contains all other regions within the frontal lobe, which might important for complex behavior, while the dorsolateral prefrontal cortex alone may be important for conscious awareness. For IIT, we only tested the general properties of differentiation via triadic closure (i.e., the GWESP term). While triadic closure could play a role in differentiation, it is not likely to fully explain the brains ability to different multiple states. Given all these caveats, it would be too speculative to assess the theories of consciousness.

4.3.1 Limitations and Future Studies

One limitation in this study is the number of subjects compared to the number of terms in our logistic and normal regression. We had 29 observations for our dissolution model and 27 observations for our formation model for either the logistic regression, which estimated seven and three coefficients respectively, for our formation and dissolution models. We were limited to the number of observations due to excluding patients for multiple factors (e.g., failed quality control checks and lack of a chronic DWI imaging session). Finally, we only estimated the transition from acute stage to chronic stage of TBI using a single network from each stage. This is a coarse grained resolution of time for the recovery of consciousness. The formation and dissolution of connectivity occurred throughout the approximately 180 days between each imaging session. These processes were not captured and could change the original STERGM PEs. Finally, we only assessed these 31 patients for their structural connectivity, but a joint analysis of the functional and structural connectivity is needed to gain a deeper understanding of the overall connectivity involved in the recovery of consciousness (see Chapter 5).

These analyses need to be run with a larger cohort of patients to discover whether or not the group differences between the recovery groups for fronto-parietal, within parietal lobe, thalamo-frontal, and thalamo-basal ganglia are still present. Additionally, collecting multiple DWI imaging sessions in acute and chronic stage of TBI will allow for a more fine grained estimation of the formation and dissolution of connectivity. Furthermore, having multiple time points for each stage of TBI would allow for comparisons between acute stage of TBI recovery and chronic stage of TBI recovery, which could differ.

CHAPTER 5

Increased formation of functional connectivity within thalamic and basal ganglia in patients recovering consciousness

5.1 Methods

This study included 12 patient (i.e., the same cohort in study #1, see Chapter 3) subset of the 31 patients which had sufficient quality of functional imaging sessions to assess the dynamic changes of network properties for functional connectivity using STERGM. The other 19 patients had either had too few data points during the functional imaging session for a reliable assessment of their functional connectivity or their functional imaging session failed at one or more steps in BOLD preprocessing (see §3.2) or network construction (see §3.3). Of the 12 patients, 7 were in the U2C recovery group and 5 were in the C2C recovery group. The connectivity matrices from each patient's acute and chronic time points were analyzed for their network dynamics using the STERGM graph statistics (see Chapter 2, §2.2).

Since there were only 12 patients, we were unable to perform statistical tests for group differences between the U2C and C2C recovery groups using logistic normal (see Chapter 4, §4.1.3). Instead, we leveraged the ability ERGM and STERGM assess single graphs (for ERGM) or single group of graphs (STERGM). Additionally, we coded the significance of the combination of PE across the formation and dissolution models because STERGM identifies these as independent processes, but together they are describing a single process of recovery from severe TBI that forms a group of restructuring. This group of restructuring (i.e, coded

significance) has 8 different possible types based on the sign and significance parameter estimates for both the formation and dissolution.

The first two types of restructuring involve the formation of edges. A strong formation (SF) have significant positive PEs that includes both the formation and dissolution models, and a weak formation (WF) that has only a significant positive PE in the formation model. SF is a type of restructuring characterized by a higher tendency to form edges and still maintain the original edges from the acute stage of TBI, which differs from weak formation (WF) because there is purely formation of edges without perseverance or dissolution of edges. Another type of restructuring involves both the dissolution and formation of edges (i.e., significant positive PE for formation and significant negative PE for dissolution), which is an overall reorganization of connectivity (RC). Next, there is resistance for formation (RF) that only has significant negative PE, which is characterized by networks forming less edges than at chance levels (i.e., 50 % chance).

The next two types of restructuring involve the dissolution of edges. Strong dissolution (SD) occurs when there is a significant negative PE for both formation and dissolution models, and weak dissolution (WD) occurs when there is only a significant PE in the dissolution model. The key difference between these two types of restructuring is that the WD still has edges forming at chance, while the SD has a resistance to edge formation in combination with the dissolution of edges. Finally, the last two types of restructuring involve the perseverance of edges. Strong perseverance (SP) has a significant positive PE for the dissolution model and a significant negative PE for the formation model, and weak perseverance (WP) only contains a significant positive PE for the dissolution model.

We summarized the results based on the percentage of patients from each recovery group which has the 8 types of restructuring of connectivity discussed. We focused on the 9 PEs (within frontal lobe connectivity, within parietal lobe connectivity, within basal ganglia, within thalamic connectivity, fronto-parietal connectivity, thalamo-fronto connectivity, thalamo-basal ganglia connectivity, the edges term, and the GWESP term) from the theories of consciousness (i.e., GNW, HOT, and IIT) and mesocircuit hypothesis.

5.2 Results

For the U2C recovery group, 57.14% of the patients had SF (see Figure 5.1) within the basal ganglia connectivity, and 42.86% had WF (see Figure 5.2) for a total of 100 % with increased formation of connectivity. Also, 100% of the patients had SF for within thalamic connectivity. There were also 42.86% patients that had WF and 28.57% had WP for the within frontoparietal network. For the thalamo-basal ganglia connectivity, 28.57% of the patients had WF (see Figure 5.2), and 14.29% had WP. For the within frontal lobe, 71.43% of the patients with SF and 14.29% had WP. The same 71.43% of the patients had SF for with parietal lobe and the same 14.29% had WP, but another 14.29% had WF for a total of 85.72% with significant formation (see Table 5.1). Finally, 71.43% of the patients had RF and 28.57% had SD for the edges term, and 100% of the patients had SF for the GWESP term.

For the C2C recovery group, 60% of the patients had WP for the within basal ganglia connectivity, and 20% had SF (see Figure 5.3). For the within thalamic connectivity, 40% of the patients had SF and anther 40% had WP, while 20% had WF for a total of 60% with increased formation. For the within frontoparietal network, 60% of the patients had SF, 20% had WP, and 20% had WF (see Figure 5.4) for a total of 80% with increased formation. The thalamo-frontoparietal connectivity had RF in 20% of the patients. In 40% of the patients, there was SF for the within frontal lobe connectivity and 20% had WP (see Table 5.1). In he within parietal lobe connectivity, 40% of the patients had SF, 20% had WP, and 20% had WF for a total of 60% with increased formation. Finally, there were 100% of the patients with RF for the edges, and SF for the GWESP term.

	STERGM Edges, Lobes and GWESP terms						
	Formation and dissolution models						
	P054	P055	P066	P069	P079	P084	P096
Edges	RF	RF	SD	RF	RF	SD	RF
Within Frontal Connectivity	SF	SF	WP	SF	SF	SF	NS
Within Occipital Connectivity	NS	SF	WP	NS	NS	NS	NS
Within Parietal Connectivity	SF	SF	WP	SF	SF	SF	WF
Within Subcortical Connectivity	WP	SF	NS	NS	WF	NS	NS
Within Temporal Connectivity	SF	SF	SF	WP	WF	SF	SF
GWESP	SF	SF	SF	SF	SF	SF	SF

Table 5.1: **Patients in U2C recovery group's coded significance for the edges, within lobes, and GWESP terms.** These are the coded significance for the significant positive or negative PEs for the edges term, nodematch lobe terms, and the GWESP term across both formation and dissolution models. For the edges term, five patients had RF and two patients had SD. There were five patients with SF for the within frontal connectivity and for the within parietal connectivity, and one patient had WF for the within parietal connectivity. Also, one patient had WP for both the within frontal and the within parietal connectivity. All 7 patients had SF for the GWESP term. The LATEX code to create this table was produced by the R package called texreg (Leifeld, 2013).

	STERGM Edges, Lobes and GWESP terms				
	Formation and dissolution models				
	P074	P085	P089	P092	P099
Edges	RF	RF	RF	RF	RF
Within Frontal Connectivity	SF	SF	NS	NS	WP
Within Occipital Connectivity	NS	NS	NS	NS	SF
Within Parietal Connectivity	SF	WP	WF	NS	SF
Within Subcortical Connectivity	NS	NS	NS	NS	WF
Within Temporal Connectivity	SF	WP	SF	WP	WP
GWESP	SF	SF	SF	SF	SF

Table 5.2: **Patients in C2C recovery group's coded significance for the edges, within lobes, and GWESP terms.** These are the coded significance for the significant positive or negative PEs for the edges term, nodematch lobe terms, and the GWESP term across both formation and dissolution models. For the edges term, all five patients had RF. There were three patients with SF for the within frontal connectivity and one patient with WP. For the within parietal connectivity, and two patients had SF, one patient had WF, and one patient had WP. All five patients had SF for the GWESP term. The LATEX code to create this table was produced by the R package called texreg (Leifeld, 2013).

Figure 5.1: **Coded significance for four patients in the U2C recovery group.** All four patients had SF for the within basal ganglia connectivity, and for the within thalamic connectivity. For the within frontoparietal network, two patients had WF and the other two patients WP. One patient had WP for frontoparieto-basal ganglia connectivity.

Figure 5.2: **Coded significance for three patients in the U2C recovery group.** All three patients had WF for the within basal ganglia connectivity, and they had SF for the within thalamic connectivity. For the within frontoparietal network, one patient had WF and one patient WP. Two patients had RF for frontoparieto-basal ganglia connectivity. For the thalamo-basal ganglia connectivity, two patients had WF.

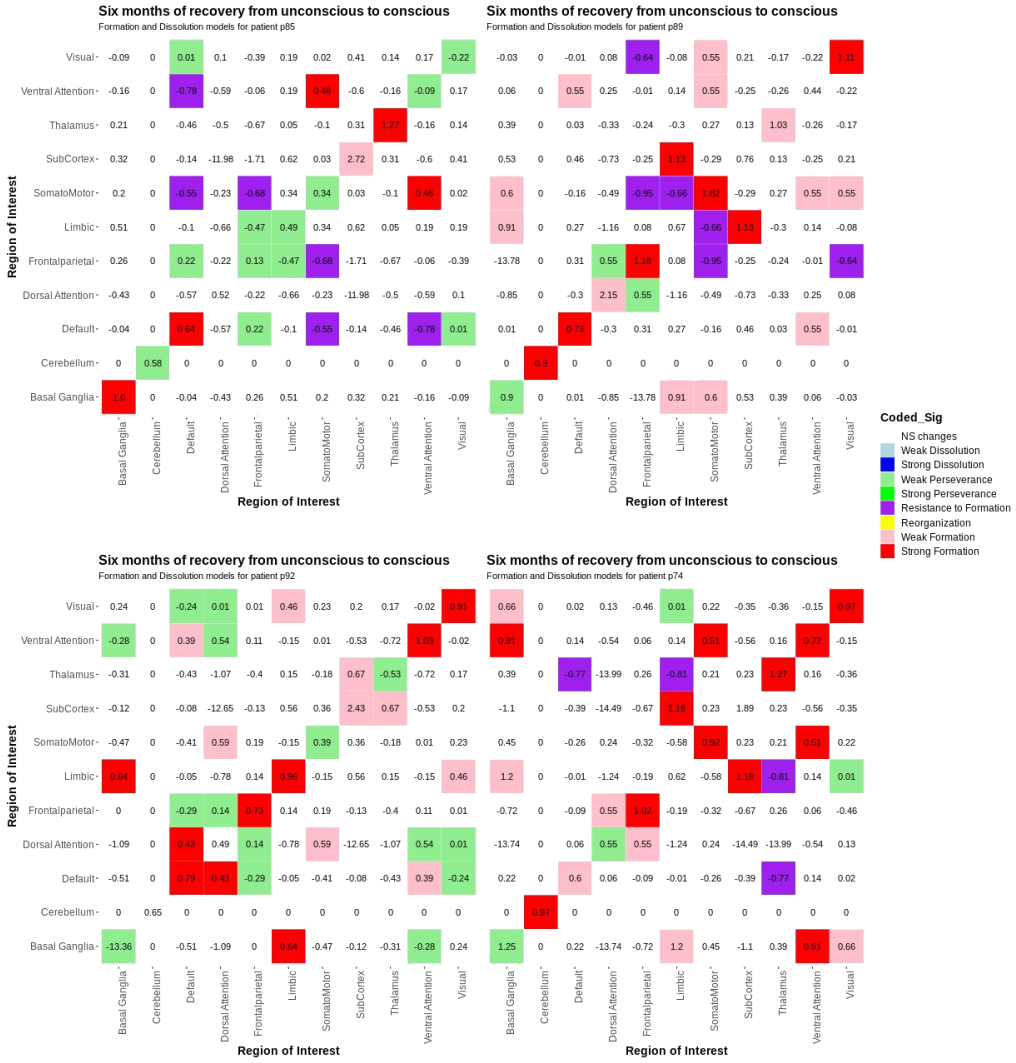

Figure 5.3: **Coded significance for four patients in the C2C recovery group.** For the within basal ganglia connectivity, three patients had WP and one patient had SF. For the within thalamic connectivity. two patients had WF, one had SF, and one had WP. For the within frontoparietal network, three patients had SF and one patient WP.

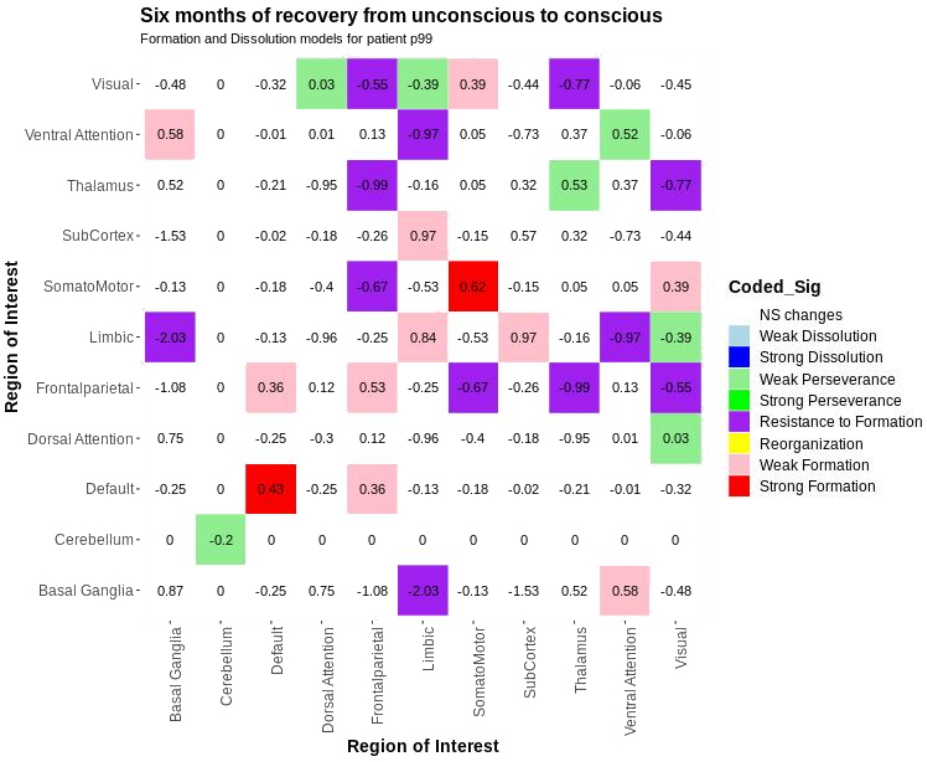

Figure 5.4: **Coded significance for one patient in the C2C recovery group.** This patient had WF for the within frontoparietal network, WP for the within thalamic connectivity, and RF for the thalamo-frontoparietal connectivity.

5.3 Discussion

For the 12 patients, we ran 12 STERGMs to investigate the patterns of functional connectivity while accounting for structural connectivity metrics (i.e., nodal degree, local efficiency, clustering coefficient, and latent clustering) associated with the recovery of consciousness compared to the recovery of complex behavior. Leveraging the ability of STERGM to assess a single group of graphs' formation and dissolution of connectivity we identified 8 types of coded significance (i.e., types of network restructuring) to assess the patterns of differences between our patient recovery groups. Using behavioral assessments to split our patients into two groups (Crone et al., 2018), we were able to identify patients who were VS in the acute stage of TBI and during the chronic stage of TBI recovery (i.e., U2C recovery group with 7 patients), while a second group was conscious during the acute stage of TBI and they remained conscious in the chronic stage of TBI (i.e., C2C recovery group with 5 patients). Both groups of patients recovered complex behavior, but the U2C recovery group had a large recovery of consciousness. Due to the limited number of patients, we did not run statistical analyses for group level effects, instead we summarized the results based on percentages of patients that had formation and dissolution of connectivity for each recovery group.

In the U2C recovery group, there was 100% of patients with formation of basal ganglia connectivity, while the C2C group only had 20% of patients with formation of within basal ganglia connectivity possibly indicating that the formation of within basal ganglia connectivity is a key difference for the recovery of consciousness. Typically, the basal ganglia has been found to play a key roles in arousal for sleep-wake cycles (Lazarus et al., 2012; Qiu et al., 2010) and during anesthesia (Mhuircheartaigh et al., 2010), but there is some evidence that atrophy within the basal ganglia is associated with recovery consciousness (Lutkenhoff et al., 2015). Finally, increased formation of connectivity withing basal ganglia associated with recovery of consciousness can be linked via circuit level effects within cortical-striatopallidal thalamocortical loop systems (Schiff, 2010).

Also in the U2C recovery group, there were 100% of the patients with SF of within thalamic connectivity, while in the C2C group, the patients were split between SF (i.e.,

40%), WF (i.e., 20%), and WP (i.e., 40%). The biggest difference between these groups is in the formation of connectivity (i.e., all patients in the U2C group and only 60% in the C2C group). Previous findings for the level of overall thalamic damage in patients are a key marker of VS (Adams et al., 2000; Lutkenhoff et al., 2013, 2015), and in increase for formation should reduce the overall atrophy, which there is an inverse relationship between thalamic atrophy recovery of complex behavior and consciousness (Lutkenhoff et al., 2013, 2015). This increased formation of within thalamic connectivity also is consistent with the circuit level effects of the cortical-striatopallidal thalamocortical loop systems (Schiff, 2010) on recovery consciousness.

For the C2C recovery group, 80% of the patients had significant formation of connectivity compared to the 42.86% of patients in the U2C recovery group indicating that within the formation frontoparietal network connectivity is more associated with complex behavior. Typically, the frontoparietal network is associated with executive control and adaptive behavior (Cole et al., 2013, 2014; Dixon and Christoff, 2012; Dosenbach et al., 2006; Duncan, 2010; Spreng et al., 2010; Stokes et al., 2013), while there are some findings of reduced functional connectivity in frontroparietal network during anesthesia (Boveroux et al., 2010). Anesthesia induced loss of consciousness has one key difference to disorder of consciousness, there are structural damage in patients with DOC, whereas anesthesia does not have structural damage. These different mechanisms likely result in different routes for losing consciousness.

The within parietal lobe and within frontal lobe connectivity had relatively equal percentage of patients for both the U2C and C2C recovery groups. Although, the U2C patients all had the same pattern for type of connectivity formation and dissolution (i.e., the same patients with SF and WP in both within lobes), while the C2C recovery group did not have this pattern. This synchronized pattern of formation and dissolution was not due to the frontoparietal resting state network having the same synchronized patterns in the types of formation and dissolution, it was specific to the within lobe connectivity. This is likely due to the non-overlapping regions between the frontoparietal network and the frontal and parietal lobes, but could be part of a more general return of intra-lobe connectivity be-

tween the frontal and parietal lobes. The inter-lobe connectivity was not included in our STERGM because of the inclusion of the nodemix for resting state networks. These inter-lobe connectivity in conjunction with the nodemix for resting state connectivity networks was initially attempted, but the models would not converge for any patient, which is likely due to excessive collinearity between the inter-lobe terms and the intra-resting state/inter-resting connectivity and to general degenerancy in the estimated models (Handcock, 2003).

There are two additional explanations based on a general return of metacognitive function or an explanation of circuit level effects described in the mesocircuit hypotheses. First, there is evidence that metacognition is involved in both perceptual processing and memory (Baird et al., 2013; Fleck et al., 2005; Hilgenstock et al., 2014; Morales et al., 2018; Yokoyama et al., 2010). Morales and colleagues 2018 demonstrated that there are domain-general regions for metacognition (e.g., dorsal anterior cingulate cortex, pre-supplementary motor area, and precuneus), and domain-specific regions for perceptual processing (e.g., anterior prefrontal cortex) and memory (e.g., inferior middle and frontal gyri). The synchronized formation and dissolution of within frontal and parietal lobe connectivity could indicate that both the domain-specific and domain-general regions underwent a dynamic reorganization for the support a general return of higher-order representations understood as metacognition. This could be a more general explanation for recovery of consciousness rather for conscious awareness of perceptual processing (Ko and Lau, 2012; Maniscalco and Lau, 2016). These patients are not only regaining metacognition of their perceptual processes, but many other cognitive functions are returning, which would entail metacognitive functions returning for across domain-specific and domain-general regions. These returning metacognitive functions are a possible explanation of the synchronized patterns found in the patients within the U2C recovery group.

A second explanation is that these synchronized patterns are part of a circuit level effect from the formation within thalamic and within basal ganglia associated with recovery of consciousness via the cortical-striatopallidal thalamocortical loop systems (Schiff, 2010). Unfortunately, we did not model the specific thalamo-frontal, thalamo-parietal, fronto-basal ganglia, and parieto-basal ganglia connectivity in our STERGM because we opted to in-

clude the resting state networks with the thalamus and basal ganglia connectivity because the functional connectivity was assessed during a resting state paradigm. If we included those regions in the nodematch term for lobes, it would have not converged due to the same thalamic and basal ganglia regions being modeled in both the nodal covariates.

Overall, both the increased formation for within basal ganglia and thalamic connectivity were consistent with the patients whom recovery differed more for consciousness than complex behavior. For the patients with recovery more associated with complex behavior, the increased formation of frontopaerietal network was the most consistent factor. Taken together, all these findings are evidence of the circuit level descriptions of the recovery of consciousness from the mesocircuit hypothesis (Schiff, 2010). Finally, an overall return of metacognitive functions or the cortical-striatopallidal thalamocortical loop systems could play a key factor in the interesting synchronized patterns of increased formation and dissolution within the parietal and frontal lobes associated with patients recovery differences where more in consciousness than other complex behaviors, but additional investigation is needed to discern between the possible explanations.

5.3.1 Limitations and Future Studies

The limited number of subjects prevent any group level analysis. Additionally, these subjects had their imaging parameters not perfectly matched across subjects nor within subjects. We were not able to account difference imaging parameters using regression (see Chapter 4). The same limitations from study #2 regarding the coarse grained time resolution of the recovery of consciousness apply to this study (see §4.3.1). Also, the limitations on including the structural connectivity metrics from study #1 apply to this study (see §3.5.1).

We will continue to process the data for new patients as they become available. The total number of subjects will need to be at least the size of study #2 before we can attempt the same analysis procedure. The group effects for recovery of consciousness is a necessary component to analyzing the functional data due to the complex interactions of network effects found that could explain the recovery consciousness and complex behavior. Once

group effects are found and replicated, the ability to assess single patients using ERGM and STERGM will be a useful tool to aid in clinical diagnosis without the need of having multiple patients. Furthermore, discovering the formation and dissolution of functional connectivity could be an invaluable tool for guiding future intervention paradigms using neurostimulation procedures because STERGM is used to describe they dynamics of recovery of consciousness.

CHAPTER 6

General Discussions and Concluding Remarks

We have introduced a powerful method in STERGM for discovering the dynamics of network connectivity, which is especially well suited to discover the underlying formation and dissolution of connectivity during recovery of consciousness. Until now, cross-sectional analyses comparing patients to healthy controls (Boly et al., 2011; Crone et al., 2011, 2015; Fernández-Espejo et al., 2012; Kotchoubey et al., 2013; Sitt et al., 2014; Vanhaudenhuyse et al., 2010; Zhou et al., 2011) or between patient groups (e.g., VS compared to MCS; Casali et al., 2013; Casarotto et al., 2016; Crone et al., 2011, 2015; Comolatti et al., 2018; Demertzi et al., 2015; Fernández-Espejo et al., 2011, 2012; Kotchoubey et al., 2013; Laureys et al., 2000a; Rosanova et al., 2012; Sitt et al., 2014; Vanhaudenhuyse et al., 2010; Zhou et al., 2011) have been the methods used to study the types of connectivity associated with recovery of consciousness. Yet, they do not reveal the recovery process of these patients, they are the beginning and end points in a dynamic process. STERGM allows the testing specific hypotheses about the formations and dissolution of edges involved in the network dynamics of recovering consciousness and complex behavior. We found that the formation of both functional and structural connectivity within the thalamus were associated with the recovery of consciousness. These new structural connectivity formations should increase the overall white matter tract integrity (Fernández-Espejo et al., 2011) and the increases in both functional and structural connectivity would produce less overall thalamic atrophy, which is associated with recovery of consciousness (Lutkenhoff et al., 2015). This converging evidence of structural and functional connectivity bolsters the previous findings of the critical role of thalamus in consciousness (Alkire et al., 2000; Guimera et al., 2005; Laureys et al., 2000a; Xie et al., 2011; Zhou et al., 2011). In addition to the thalamus, the SF of functional

connectivity within the basal ganglia was reliably related to the recovered consciousness. Together, these regions are part the mesocircuit (Schiff, 2010) that posits the central thalamus and basal ganglia as possible regions believed to have circuit level effects on both the frontal and parietal lobes. However, we did not find as strong evidence for formation of thalamo-cortical functional and only marginal effects were found for the formation of structural thalamo-frontal connectivity. One possibility is that the formation or perservance of thalamo-cortical connectivity was not necessary to drive these changes (cf., Crone et al., 2018). Instead, structural and functional within the thalamus and basal had restored the overall function of existing connections within the cortical-striatopallidal thalamocortical loop systems. These could result in the synchronized SF of functional connectivity within the frontal and parietal lobes. Another possibility is that there were unobserved mesolevel effects between the structural and functional connectivity. Since we model the generative processes for structural connectivity without accounting for the functional connectivity, we do not know the effect that the functional connectivity had on the structural connectivity. Finally, even in the functional connectivity analysis we do not know the specific effects of the formation of structural connections within the thalamus on the functional connections.

These mesolevel effects are an extension of problem#3 in which the effects of structural connectivity that we accounted for were only achieved through parcelling out the effects of the structural connectivity on the functional connectivity; however, these problems were not fully solved. Structural and functional connectivity are part of a multi-level problem (i.e., there is a structural layer, functional layer within the brain and finally an interaction between these layers). By this, I mean that each have their own generative processes that govern their structure and there are interactions between the levels that drive the brain dynamics. Multilevel ERGMs (Lazega and Snijders, 2016; Wang et al., 2013, 2016) have been developing to capture the the nested structure of networks. A concrete example is collaborative research (Lazega et al., 2008), in which, researchers have advice networks for their research problems and the laboratories have collaboration networks. The researchers advice network would be the micro-level network because they are nested within the laboratories (i.e., macro-level). Each of these levels have their own generative processes associated with the structure, but

there is a third layer (i.e., the meso-level) that affects both levels. In the collaborative research example, the researchers' affiliation with laboratories are the meso-level. This example could be extended to the structural and functional layers of the brain. The functional layer is the micro-level because it is nested within the macro-level structural layer. The meso-level could be the locations of the functional layer within the structural layer or an estimation of joint functional structural connectivity could be the meso-level (e.g., hybrid connICA; Amico et al., 2017). These multi-level ERGMs would allow for a more complete solution to the four problems posed in this thesis because all the levels of functional and structural connectivity could be jointly estimated and properly modeled. This would be a large step in the direction of unraveling the complex interactions between structural and functional connectivity that generate the ability for our complex behavior.

Bibliography

Abdi, H. (2010). Partial least squares regression and projection on latent structure regression (PLS regression). *Wiley Interdisciplinary Reviews: Computational Statistics* 2, 97–106. doi:10.1002/wics.51

Abou-Elseoud, A., Starck, T., Remes, J., Nikkinen, J., Tervonen, O., and Kiviniemi, V. (2010). The effect of model order selection in group PICA. *Human brain mapping* 31, 1207–1216

Adams, J. H., Graham, D., and Jennett, B. (2000). The neuropathology of the vegetative state after an acute brain insult. *Brain* 123, 1327–1338

Alkire, M., Haier, R., and Fallon, J. (2000). Toward a unified theory of narcosis: brain imaging evidence for a thalamocortical switch as the neurophysiologic basis of anesthetic-induced unconsciousness. *Consciousness and cognition* 9, 370–386

Amico, E. and Goñi, J. (2017). Mapping hybrid functional-structural connectivity traits in the human connectome. *arXiv preprint arXiv:1710.02199*

Amico, E., Marinazzo, D., Di Perri, C., Heine, L., Annen, J., Martial, C., et al. (2017). Mapping the functional connectome traits of levels of consciousness. *NeuroImage* 148, 201–211

Aubinet, C., Murphy, L., Bahri, M. A., Larroque, S. K., Cassol, H., Annen, J., et al. (2018). Brain, behavior and cognitive interplay in disorders of consciousness: A multiple case study. *Frontiers in neurology* 9, 665

Avants, B. B., Epstein, C. L., Grossman, M., and Gee, J. C. (2008). Symmetric diffeomorphic image registration with cross-correlation: evaluating automated labeling of elderly and neurodegenerative brain. *Medical image analysis* 12, 26–41

Avants, B. B., Tustison, N. J., Song, G., Cook, P. A., Klein, A., and Gee, J. C. (2011). A

reproducible evaluation of ANTs similarity metric performance in brain image registration. *NeuroImage* 54, 2033–2044

Averbeck, B. B. and Seo, M. (2008). The statistical neuroanatomy of frontal networks in the macaque. *PLoS computational biology* 4, e1000050

Baars, B. J. (1993). *A cognitive theory of consciousness* (Cambridge University Press)

Baars, B. J. (2002). The conscious access hypothesis: origins and recent evidence. *Trends in cognitive sciences* 6, 47–52

Baars, B. J. (2005). Global workspace theory of consciousness: toward a cognitive neuroscience of human experience. *Progress in brain research* 150, 45–53

Baars, B. J., Ramsøy, T. Z., and Laureys, S. (2003). Brain, conscious experience and the observing self. *Trends in neurosciences* 26, 671–675

Baird, B., Smallwood, J., Gorgolewski, K. J., and Margulies, D. S. (2013). Medial and lateral networks in anterior prefrontal cortex support metacognitive ability for memory and perception. *Journal of Neuroscience* 33, 16657–16665

Barttfeld, P., Uhrig, L., Sitt, J. D., Sigman, M., Jarraya, B., and Dehaene, S. (2015). Signature of consciousness in the dynamics of resting-state brain activity. *Proceedings of the National Academy of Sciences* 112, 887–892

Behrens, T., Johansen-Berg, H., Woolrich, M., Smith, S., Wheeler-Kingshott, C., Boulby, P., et al. (2003a). Non-invasive mapping of connections between human thalamus and cortex using diffusion imaging. *Nature neuroscience* 6, 750

Behrens, T. E., Berg, H. J., Jbabdi, S., Rushworth, M. F., and Woolrich, M. W. (2007). Probabilistic diffusion tractography with multiple fibre orientations: What can we gain? *Neuroimage* 34, 144–155

Behrens, T. E., Woolrich, M. W., Jenkinson, M., Johansen-Berg, H., Nunes, R. G., Clare, S., et al. (2003b). Characterization and propagation of uncertainty in diffusion-weighted MR imaging. *Magnetic resonance in medicine* 50, 1077–1088

Bettinardi, R. G., Deco, G., Karlaftis, V. M., Van Hartevelt, T. J., Fernandes, H. M., Kourtzi, Z., et al. (2017). How structure sculpts function: Unveiling the contribution of anatomical connectivity to the brain's spontaneous correlation structure. *Chaos: An Interdisciplinary Journal of Nonlinear Science* 27, 047409

Bhushan, C., Haldar, J. P., Joshi, A. A., and Leahy, R. M. (2012). Correcting susceptibility-induced distortion in diffusion-weighted MRI using constrained nonrigid registration. *Signal and Information Processing Association Annual Summit and Conference (APSIPA), ... Asia-Pacific. Asia-Pacific Signal and Information Processing Association Annual Summit and Conference* 2012

Boly, M., Garrido, M. I., Gosseries, O., Bruno, M.-A., Boveroux, P., Schnakers, C., et al. (2011). Preserved feedforward but impaired top-down processes in the vegetative state. *Science* 332, 858–862

Boly, M., Moran, R., Murphy, M., Boveroux, P., Bruno, M.-A., Noirhomme, Q., et al. (2012). Connectivity changes underlying spectral EEG changes during propofol-induced loss of consciousness. *Journal of Neuroscience* 32, 7082–7090

Boly, M., Tshibanda, L., Vanhaudenhuyse, A., Noirhomme, Q., Schnakers, C., Ledoux, D., et al. (2009). Functional connectivity in the default network during resting state is preserved in a vegetative but not in a brain dead patient. *Human brain mapping* 30, 2393–2400

Boveroux, P., Vanhaudenhuyse, A., Bruno, M.-A., Noirhomme, Q., Lauwick, S., Luxen, A., et al. (2010). Breakdown of within-and between-network resting state functional magnetic resonance imaging connectivity during propofol-induced loss of consciousness. *Anesthesiology: The Journal of the American Society of Anesthesiologists* 113, 1038–1053

Braitenberg, V. and Schüz, A. (1998). Global activity, cell assemblies and synfire chains. In *Cortex: Statistics and Geometry of Neuronal Connectivity* (Springer). 193–204

Braun, U., Plichta, M. M., Esslinger, C., Sauer, C., Haddad, L., Grimm, O., et al. (2012).

Test–retest reliability of resting-state connectivity network characteristics using fMRI and graph theoretical measures. *Neuroimage* 59, 1404–1412

Bruno, M.-A., Fernández-Espejo, D., Lehembre, R., Tshibanda, L., Vanhaudenhuyse, A., Gosseries, O., et al. (2011a). Multimodal neuroimaging in patients with disorders of consciousness showing "functional hemispherectomy". In *Progress in brain research* (Elsevier), vol. 193. 323–333

Bruno, M.-A., Vanhaudenhuyse, A., Thibaut, A., Moonen, G., and Laureys, S. (2011b). From unresponsive wakefulness to minimally conscious plus and functional locked-in syndromes: recent advances in our understanding of disorders of consciousness. *Journal of neurology* 258, 1373–1384

Buckner, R. L. (2010). Human functional connectivity: new tools, unresolved questions. *Proceedings of the National Academy of Sciences* 107, 10769–10770. doi: 10.1073/pnas.1005987107

Bullmore, E. and Sporns, O. (2012). The economy of brain network organization. *Nature Reviews Neuroscience* 13, 336–349

Calhoun, V. D., Adali, T., Giuliani, N. R., Pekar, J. J., Kiehl, K. A., and Pearlson, G. D. (2006). Method for multimodal analysis of independent source differences in schizophrenia: combining gray matter structural and auditory oddball functional data. *Human brain mapping* 27, 47–62. doi:10.1002/hbm.20166

Calhoun, V. D., Liu, J., and Adal, T. (2009). A review of group ICA for fMRI data and ICA for joint inference of imaging, genetic, and ERP data). *Neuroimage* 45, S163–S172. doi:10.1016/j.neuroimage.2008.10.057

Cao, H., Plichta, M. M., Schäfer, A., Haddad, L., Grimm, O., Schneider, M., et al. (2014). Test–retest reliability of fMRI-based graph theoretical properties during working memory, emotion processing, and resting state. *Neuroimage* 84, 888–900

Casali, A. G., Gosseries, O., Rosanova, M., Boly, M., Sarasso, S., Casali, K. R., et al. (2013). A theoretically based index of consciousness independent of sensory processing and behavior. *Science translational medicine* 5, 198ra105–198ra105

Casarotto, S., Comanducci, A., Rosanova, M., Sarasso, S., Fecchio, M., Napolitani, M., et al. (2016). Stratification of unresponsive patients by an independently validated index of brain complexity. *Annals of neurology* 80, 718–729

Chambers, J. M., Hastie, T. J., et al. (1992). *Statistical models in S*, vol. 251 (Wadsworth & Brooks/Cole Advanced Books & Software Pacific Grove, CA)

Chennu, S., Finoia, P., Kamau, E., Allanson, J., Williams, G. B., Monti, M. M., et al. (2014). Spectral signatures of reorganised brain networks in disorders of consciousness. *PLoS computational biology* 10, e1003887

Cohen, A. L., Fair, D. A., Dosenbach, N. U., Miezin, F. M., Dierker, D., Van Essen, D. C., et al. (2008). Defining functional areas in individual human brains using resting functional connectivity MRI. *Neuroimage* 41, 45–57

Cole, M. W., Repovš, G., and Anticevic, A. (2014). The frontoparietal control system: a central role in mental health. *The Neuroscientist* 20, 652–664

Cole, M. W., Reynolds, J. R., Power, J. D., Repovs, G., Anticevic, A., and Braver, T. S. (2013). Multi-task connectivity reveals flexible hubs for adaptive task control. *Nature neuroscience* 16, 1348

Coleman, M., Bekinschtein, T., Monti, M., Owen, A., and Pickard, J. (2009). A multimodal approach to the assessment of patients with disorders of consciousness. *Progress in brain research* 177, 231–248

Comolatti, R., Pigorini, A., Casarotto, S., Fecchio, M., Faria, G., Sarasso, S., et al. (2018). A fast and general method to empirically estimate the complexity of distributed causal interactions in the brain. *bioRxiv* doi:10.1101/445882

Craddock, R. C., James, G. A., Holtzheimer, P. E., Hu, X. P., and Mayberg, H. S. (2012). A whole brain fMRI atlas generated via spatially constrained spectral clustering. *Human brain mapping* 33, 1914–1928

Crick, F. and Koch, C. (2003). A framework for consciousness. *Nature neuroscience* 6, 119–126

Crone, J. S., Bio, B. J., Vespa, P. M., Lutkenhoff, E. S., and Monti, M. M. (2018). Restoration of thalamo-cortical connectivity after brain injury: recovery of consciousness, complex behavior, or passage of time? *Journal of neuroscience research* 96, 671–687. doi: 10.1002/jnr.24115

Crone, J. S., Ladurner, G., Höller, Y., Golaszewski, S., Trinka, E., and Kronbichler, M. (2011). Deactivation of the default mode network as a marker of impaired consciousness: an fmri study. *PloS one* 6, e26373. doi:10.1371/journal.pone.0026373

Crone, J. S., Schurz, M., Höller, Y., Bergmann, J., Monti, M., Schmid, E., et al. (2015). Impaired consciousness is linked to changes in effective connectivity of the posterior cingulate cortex within the default mode network. *Neuroimage* 110, 101–109. doi: 10.1016/j.neuroimage.2015.01.037

Crone, J. S., Soddu, A., Höller, Y., Vanhaudenhuyse, A., Schurz, M., Bergmann, J., et al. (2014). Altered network properties of the fronto-parietal network and the thalamus in impaired consciousness. *NeuroImage: Clinical* 4, 240–248

Dehaene, S. and Changeux, J.-P. (2005). Ongoing spontaneous activity controls access to consciousness: a neuronal model for inattentional blindness. *PLoS biology* 3, e141

Dehaene, S. and Changeux, J.-P. (2011). Experimental and theoretical approaches to conscious processing. *Neuron* 70, 200–227

Dehaene, S., Charles, L., King, J.-R., and Marti, S. (2014). Toward a computational theory of conscious processing. *Current opinion in neurobiology* 25, 76–84. doi: 10.1016/j.conb.2013.12.005

Dehaene, S., Kerszberg, M., and Changeux, J.-P. (1998). A neuronal model of a global workspace in effortful cognitive tasks. *Proceedings of the national Academy of Sciences* 95, 14529–14534

Demertzi, A., Antonopoulos, G., Heine, L., Voss, H. U., Crone, J. S., de Los Angeles, C., et al. (2015). Intrinsic functional connectivity differentiates minimally conscious from unresponsive patients. *Brain* 138, 2619–2631. doi:10.1093/brain/awv169

Díaz-Parra, A., Osborn, Z., Canals, S., Moratal, D., and Sporns, O. (2017). Structural and functional, empirical and modeled connectivity in the cerebral cortex of the rat. *NeuroImage* 159, 170–184

Dixon, M. L. and Christoff, K. (2012). The decision to engage cognitive control is driven by expected reward-value: neural and behavioral evidence. *PloS one* 7, e51637

Dobson, A. J. and Barnett, A. (2008). *An introduction to generalized linear models* (Chapman and Hall/CRC)

Dosenbach, N. U., Visscher, K. M., Palmer, E. D., Miezin, F. M., Wenger, K. K., Kang, H. C., et al. (2006). A core system for the implementation of task sets. *Neuron* 50, 799–812

Duncan, J. (2010). The multiple-demand (md) system of the primate brain: mental programs for intelligent behaviour. *Trends in cognitive sciences* 14, 172–179

Engel, A. K. and Singer, W. (2001). Temporal binding and the neural correlates of sensory awareness. *Trends in cognitive sciences* 5, 16–25

Erdös, P. and Rényi, A. (1959). On random graphs I. *Publicationes Mathematicae (Debrecen)* 6, 290–297

Fernández-Espejo, D., Bekinschtein, T., Monti, M. M., Pickard, J. D., Junque, C., Coleman, M. R., et al. (2011). Diffusion weighted imaging distinguishes the vegetative state from the minimally conscious state. *Neuroimage* 54, 103–112

Fernández-Espejo, D., Soddu, A., Cruse, D., Palacios, E. M., Junque, C., Vanhaudenhuyse, A., et al. (2012). A role for the default mode network in the bases of disorders of consciousness. *Annals of neurology* 72, 335–343

Finger, H., Bönstrup, M., Cheng, B., Messé, A., Hilgetag, C., Thomalla, G., et al. (2016). Modeling of large-scale functional brain networks based on structural connectivity from DTI: comparison with EEG derived phase coupling networks and evaluation of alternative methods along the modeling path. *PLoS computational biology* 12, e1005025

Fleck, M. S., Daselaar, S. M., Dobbins, I. G., and Cabeza, R. (2005). Role of prefrontal and anterior cingulate regions in decision-making processes shared by memory and nonmemory tasks. *Cerebral Cortex* 16, 1623–1630

Fornito, A., Zalesky, A., and Breakspear, M. (2013). Graph analysis of the human connectome: promise, progress, and pitfalls. *Neuroimage* 80, 426–444. doi: 10.1016/j.neuroimage.2013.04.087

Fornito, A., Zalesky, A., and Bullmore, E. (2016). *Fundamentals of brain network analysis* (Academic Press)

Fox, M. D., Corbetta, M., Snyder, A. Z., Vincent, J. L., and Raichle, M. E. (2006). Spontaneous neuronal activity distinguishes human dorsal and ventral attention systems. *Proceedings of the National Academy of Sciences* 103, 10046–10051. doi:10.1073/pnas.0604187103

Fransson, P., Åden, U., Blennow, M., and Lagercrantz, H. (2010). The functional architecture of the infant brain as revealed by resting-state fmri. *Cerebral cortex* 21, 145–154

Freeman, L. C. (1978). Centrality in social networks conceptual clarification. *Social networks* 1, 215–239

Glasser, M. F., Sotiropoulos, S. N., Wilson, J. A., Coalson, T. S., Fischl, B., Andersson, J. L., et al. (2013). The minimal preprocessing pipelines for the human connectome project. *Neuroimage* 80, 105–124

Goodreau, S. M., Kitts, J. A., and Morris, M. (2009). Birds of a feather, or friend of a friend? using exponential random graph models to investigate adolescent social networks. *Demography* 46, 103–125

Guimera, R., Mossa, S., Turtschi, A., and Amaral, L. N. (2005). The worldwide air transportation network: Anomalous centrality, community structure, and cities' global roles. *Proceedings of the National Academy of Sciences* 102, 7794–7799

Haldar, J. P. and Leahy, R. M. (2013). Linear transforms for fourier data on the sphere: Application to high angular resolution diffusion MRI of the brain. *NeuroImage* 71, 233–247

Hallquist, M. N. and Hillary, F. G. (2018). Graph theory approaches to functional network organization in brain disorders: A critique for a brave new small-world. *bioRxiv* , 243741

Handcock, M. S. (2003). *Statistical models for social networks: Inference and degeneracy* (na)

Handcock, M. S., Hunter, D. R., Butts, C. T., Goodreau, S. M., Krivitsky, P. N., and Morris, M. (2017). *ergm: Fit, Simulate and Diagnose Exponential-Family Models for Networks*. R package version 3.8.0

Handcock, M. S., Raftery, A. E., and Tantrum, J. M. (2007). Model-based clustering for social networks. *Journal of the Royal Statistical Society: Series A (Statistics in Society)* 170, 301–354

Hellwig, B. (2000). A quantitative analysis of the local connectivity between pyramidal neurons in layers 2/3 of the rat visual cortex. *Biological cybernetics* 82, 111–121

Hernández, M., Guerrero, G. D., Cecilia, J. M., García, J. M., Inuggi, A., Jbabdi, S., et al. (2013). Accelerating fibre orientation estimation from diffusion weighted magnetic resonance imaging using gpus. *PloS one* 8, e61892

Hilgenstock, R., Weiss, T., and Witte, O. W. (2014). Youd better think twice: post-decision perceptual confidence. *Neuroimage* 99, 323–331

Holland, P. W. and Leinhardt, S. (1981). An exponential family of probability distributions for directed graphs. *Journal of the american statistical association* 76, 33–50

Hunter, D. R. (2007). Curved exponential family models for social networks. *Social networks* 29, 216–230

Hunter, D. R., Handcock, M. S., Butts, C. T., Goodreau, S. M., and Morris, M. (2008). ergm: A package to fit, simulate and diagnose exponential-family models for networks. *Journal of statistical software* 24, nihpa54860

Hyvrinen, A. and Oja, E. (2000). Independent component analysis: algorithms and applications. *Neural networks* 13, 411–430. doi:10.1016/S0893-6080(00)00026-5

Ioannides, A. A. (2007). Dynamic functional connectivity. *Current opinion in neurobiology* 17, 161–170. doi:10.1016/j.conb.2007.03.008

Jenkinson, M., Bannister, P., Brady, M., and Smith, S. (2002). Improved optimization for the robust and accurate linear registration and motion correction of brain images. *Neuroimage* 17, 825–841

Kessler, D., Angstadt, M., Welsh, R. C., and Sripada, C. (2014). Modality-spanning deficits in attention-deficit/hyperactivity disorder in functional networks, gray matter, and white matter. *Journal of Neuroscience* 34, 16555–16566. doi:10.1523/JNEUROSCI.3156-14.2014

Ko, Y. and Lau, H. (2012). A detection theoretic explanation of blindsight suggests a link between conscious perception and metacognition. *Philosophical Transactions of the Royal Society B: Biological Sciences* 367, 1401–1411

Kotchoubey, B., Merz, S., Lang, S., Markl, A., Mller, F., Yu, T., et al. (2013). Global functional connectivity reveals highly significant differences between the vegetative and the minimally conscious state. *Journal of neurology* 260, 975–983. doi:10.1007/s00415-012-6734-9

Krishnan, A., Williams, L. J., McIntosh, A. R., and Abdi, H. (2011). Partial least squares (PLS) methods for neuroimaging: a tutorial and review. *Neuroimage* 56, 455–475. doi: 10.1016/j.neuroimage.2010.07.034

Krivitsky, P. N. and Handcock, M. S. (2008). Fitting position latent cluster models for social networks with latentnet. *Journal of Statistical Software* 24

Krivitsky, P. N. and Handcock, M. S. (2014). A separable model for dynamic networks. *Journal of the Royal Statistical Society* 76, 29–46. doi:10.1111/rssb.12014

Krivitsky, P. N., Handcock, M. S., Raftery, A. E., and Hoff, P. D. (2009). Representing degree distributions, clustering, and homophily in social networks with latent cluster random effects models. *Social networks* 31, 204–213

Ku, S.-W., Lee, U., Noh, G.-J., Jun, I.-G., and Mashour, G. A. (2011). Preferential inhibition of frontal-to-parietal feedback connectivity is a neurophysiologic correlate of general anesthesia in surgical patients. *PloS one* 6, e25155. doi:10.1371/journal.pone.0025155

Lamme, V. A. (2006). Towards a true neural stance on consciousness. *Trends in cognitive sciences* 10, 494–501. doi:10.1016/j.tics.2006.09.001

Lamme, V. A. (2010). How neuroscience will change our view on consciousness. *Cognitive Neuroscience* 1, 204–220. doi:10.1080/17588921003731586

Lamme, V. A. and Roelfsema, P. R. (2000). The distinct modes of vision offered by feedforward and recurrent processing. *Trends in neurosciences* 23, 571–579. doi:10.1016/S0166-2236(00)01657-X

Lashkari, D., Vul, E., Kanwisher, N., and Golland, P. (2010). Discovering structure in the space of fMRI selectivity profiles. *Neuroimage* 50, 1085–1098. doi: 10.1016/j.neuroimage.2009.12.106

Lau, H. (2011). Theoretical motivations for investigating the neural correlates of consciousness. *Wiley Interdisciplinary Reviews: Cognitive Science* 2, 1–7

Lau, H. and Rosenthal, D. (2011). Empirical support for higher-order theories of conscious awareness. *Trends in cognitive sciences* 15, 365–373. doi:10.1016/j.tics.2011.05.009

Lau, H. C. (2007). A higher order bayesian decision theory of consciousness. *Progress in brain research* 168, 35–48. doi:10.1016/S0079-6123(07)68004-2

Lau, H. C. and Passingham, R. E. (2006). Relative blindsight in normal observers and the neural correlate of visual consciousness. *Proceedings of the National Academy of Sciences* 103, 18763–18768

Laureys, S. (2005). The neural correlate of (un) awareness: lessons from the vegetative state. *Trends in cognitive sciences* 9, 556–559

Laureys, S., Faymonville, M. E., Degueldre, C., Fiore, G. D., Damas, P., Lambermont, B., et al. (2000a). Auditory processing in the vegetative state. *Brain: a journal of neurology* 123 (Pt 8), 1589–1601

Laureys, S., Faymonville, M. E., Luxen, A., Lamy, M., Franck, G., and Maquet, P. (2000b). Restoration of thalamocortical connectivity after recovery from persistent vegetative state. *Lancet (London, England)* 355, 1790–1791

Lazarus, M., Huang, Z.-L., Lu, J., Urade, Y., and Chen, J.-F. (2012). How do the basal ganglia regulate sleep–wake behavior? *Trends in neurosciences* 35, 723–732

Lazega, E., Jourda, M.-T., Mounier, L., and Stofer, R. (2008). Catching up with big fish in the big pond? multi-level network analysis through linked design. *Social Networks* 30, 159–176

[Dataset] Lazega, E. and Snijders, T. (2016). Multilevel network analysis for the social sciences

Lee, U., Kim, S., Noh, G.-J., Choi, B.-M., Hwang, E., and Mashour, G. A. (2009). The directionality and functional organization of frontoparietal connectivity during consciousness and anesthesia in humans. *Consciousness and cognition* 18, 1069–1078. doi: 10.1016/j.concog.2009.04.004

Leifeld, P. (2013). texreg: Conversion of statistical model output inrtolatexand html tables. *Journal of Statistical Software* 55. doi:10.18637/jss.v055.i08

Lucek, P. R. and Ott, J. (1997). Neural network analysis of complex traits. *Genetic epidemiology* 14, 1101–1106. doi:10.1002/(SICI)1098-2272(1997)14:6¡1101::AID-GEPI90¿3.0.CO;2-K

Luke, D. A. and Harris, J. K. (2007). Network analysis in public health: history, methods, and applications. *Annual review of public health* 28, 69–93. doi:10.1146/annurev.publhealth.28.021406.144132

Lutkenhoff, E. S., Chiang, J., Tshibanda, L., Kamau, E., Kirsch, M., Pickard, J. D., et al. (2015). Thalamic and extrathalamic mechanisms of consciousness after severe brain injury. *Annals of neurology* 78, 68–76. doi:10.1002/ana.24423

Lutkenhoff, E. S., McArthur, D. L., Hua, X., Thompson, P. M., Vespa, P. M., and Monti, M. M. (2013). Thalamic atrophy in antero-medial and dorsal nuclei correlates with six-month outcome after severe brain injury. *NeuroImage: Clinical* 3, 396–404

Lutkenhoff, E. S., Rosenberg, M., Chiang, J., Zhang, K., Pickard, J. D., Owen, A. M., et al. (2014). Optimized brain extraction for pathological brains (optiBET). *PloS one* 9, e115551. doi:10.1371/journal.pone.0115551

Maniscalco, B. and Lau, H. (2016). The signal processing architecture underlying subjective reports of sensory awareness. *Neuroscience of Consciousness* 2016

Martuzzi, R., Ramani, R., Qiu, M., Rajeevan, N., and Constable, R. T. (2010). Functional connectivity and alterations in baseline brain state in humans. *Neuroimage* 49, 823–834

McCullagh, P. (2018). *Generalized linear models* (Routledge)

McIntosh, A. R. and Lobaugh, N. J. (2004). Partial least squares analysis of neuroimaging data: applications and advances. *Neuroimage* 23, S250–S263. doi:10.1016/j.neuroimage.2004.07.020

McIntosh, A. R. and Mii, B. (2013). Multivariate statistical analyses for neuroimaging data. *Annual review of psychology* 64, 499–525. doi:10.1146/annurev-psych-113011-143804

McPherson, M., Smith-Lovin, L., and Cook, J. M. (2001). Birds of a feather: Homophily in social networks. *Annual review of sociology* 27, 415–444

McQuillan, J. M. (1977). Graph theory applied to optimal connectivity in computer networks. *SIGCOMM Computer Communications Review* 7, 13–41. doi: 10.1145/1024857.1024860

Mess, A., Rudrauf, D., Giron, A., and Marrelec, G. (2015). Predicting functional connectivity from structural connectivity via computational models using mri: an extensive comparison study. *NeuroImage* 111, 65–75. doi:10.1016/j.neuroimage.2015.02.001

Mhuircheartaigh, R. N., Rosenorn-Lanng, D., Wise, R., Jbabdi, S., Rogers, R., and Tracey, I. (2010). Cortical and subcortical connectivity changes during decreasing levels of consciousness in humans: a functional magnetic resonance imaging study using propofol. *Journal of Neuroscience* 30, 9095–9102

Micheloyannis, S., Vourkas, M., Tsirka, V., Karakonstantaki, E., Kanatsouli, K., and Stam, C. J. (2009). The influence of ageing on complex brain networks: a graph theoretical analysis. *Human brain mapping* 30, 200–208. doi:10.1002/hbm.20492

Milham, M. P., Fair, D., Mennes, M., Mostofsky, S. H., et al. (2012). The ADHD-200 consortium: a model to advance the translational potential of neuroimaging in clinical neuroscience. *Frontiers in systems neuroscience* 6, 62

Mii, B., Betzel, R. F., De Reus, M. A., Van Den Heuvel, M. P., Berman, M. G., McIntosh, A. R., et al. (2016). Network-level structure-function relationships in human neocortex. *Cerebral Cortex* 26, 3285–3296. doi:10.1093/cercor/bhw089

Monti, M. M., Laureys, S., and Owen, A. M. (2010). The vegetative state. *BMJ (Clinical Research ed.)* 341, c3765

Monti, M. M., Lutkenhoff, E. S., Rubinov, M., Boveroux, P., Vanhaudenhuyse, A., Gosseries, O., et al. (2013). Dynamic change of global and local information processing in propofol-induced loss and recovery of consciousness. *PLoS computational biology* 9, e1003271. doi:10.1371/journal.pcbi.1003271

Morales, J., Lau, H., and Fleming, S. M. (2018). Domain-general and domain-specific patterns of activity supporting metacognition in human prefrontal cortex. *Journal of Neuroscience* 38, 3534–3546

Murphy, K., Birn, R. M., Handwerker, D. A., Jones, T. B., and Bandettini, P. A. (2009). The impact of global signal regression on resting state correlations: are anti-correlated networks introduced? *Neuroimage* 44, 893–905

Nagaraj, N. and Virmani, M. (2017). Is informationfundamental for a scientific theory of consciousness? In *Self, Culture and Consciousness* (Springer). 357–378

Narayan, M., Allen, G. I., and Tomson, S. (2015). Two sample inference for populations of graphical models with applications to functional connectivity. *arXiv preprint arXiv:1502.03853*

Newcombe, V. F. J., Williams, G. B., Scoffings, D., Cross, J., Carpenter, T. A., Pickard, J. D., et al. (2010). Aetiological differences in neuroanatomy of the vegetative state: insights from diffusion tensor imaging and functional implications. *Journal of neurology, neurosurgery, and psychiatry* 81, 552–561. doi:10.1136/jnnp.2009.196246

Nielsen, J. A., Zielinski, B. A., Fletcher, P. T., Alexander, A. L., Lange, N., Bigler, E. D., et al. (2013). Multisite functional connectivity MRI classification of autism: Abide results. *Frontiers in human neuroscience* 7, 599. doi:10.3389/fnhum.2013.00599

Oguz, I., Farzinfar, M., Matsui, J., Budin, F., Liu, Z., Gerig, G., et al. (2014). DTIPrep: quality control of diffusion-weighted images. *Frontiers in neuroinformatics* 8. doi:10.3389/fninf.2014.00004

Oizumi, M., Albantakis, L., and Tononi, G. (2014). From the phenomenology to the mechanisms of consciousness: integrated information theory 3.0. *PLoS computational biology* 10, e1003588. doi:10.1371/journal.pcbi.1003588

Pandit, A. S., Expert, P., Lambiotte, R., Bonnelle, V., Leech, R., Turkheimer, F. E., et al. (2013). Traumatic brain injury impairs small-world topology. *Neurology* 80, 1826–1833. doi:10.1212/WNL.0b013e3182929f38

Power, J. D., Barnes, K. A., Snyder, A. Z., Schlaggar, B. L., and Petersen, S. E. (2012). Spurious but systematic correlations in functional connectivity MRI networks arise from subject motion. *NeuroImage* 59, 2142–2154. doi:10.1016/j.neuroimage.2011.10.018

Qiu, M.-H., Vetrivelan, R., Fuller, P. M., and Lu, J. (2010). Basal ganglia control of sleep–wake behavior and cortical activation. *European Journal of Neuroscience* 31, 499–507

Raichle, M. E., MacLeod, A. M., Snyder, A. Z., Powers, W. J., Gusnard, D. A., and Shulman, G. L. (2001). A default mode of brain function. *Proceedings of the National Academy of Sciences of the United States of America* 98, 676–682. doi:10.1073/pnas.98.2.676

Ray, K. L., McKay, D. R., Fox, P. M., Riedel, M. C., Uecker, A. M., Beckmann, C. F., et al. (2013). Ica model order selection of task co-activation networks. *Frontiers in neuroscience* 7, 237. doi:10.3389/fnins.2013.00237

Robins, G., Pattison, P., Kalish, Y., and Lusher, D. (2007). An introduction to exponential random graph (p^*) models for social networks. *Social Networks* 29, 173–191. doi:10.1016/j.socnet.2006.08.002

Rosanova, M., Gosseries, O., Casarotto, S., Boly, M., Casali, A. G., Bruno, M.-A., et al. (2012). Recovery of cortical effective connectivity and recovery of consciousness in vegetative patients. *Brain: a journal of neurology* 135, 1308–1320. doi:10.1093/brain/awr340

Rounis, E., Maniscalco, B., Rothwell, J. C., Passingham, R. E., and Lau, H. (2010). Theta-burst transcranial magnetic stimulation to the prefrontal cortex impairs metacognitive visual awareness. *Cognitive neuroscience* 1, 165–175. doi:10.1080/17588921003632529

Rubinov, M. and Sporns, O. (2010). Complex network measures of brain connectivity: uses and interpretations. *NeuroImage* 52, 1059–1069. doi:10.1016/j.neuroimage.2009.10.003

Rubinov, M. and Sporns, O. (2011). Weight-conserving characterization of complex functional brain networks. *NeuroImage* 56, 2068–2079. doi:10.1016/j.neuroimage.2011.03.069

Saad, Z., Gotts, S. J., Murphy, K., Chen, G., Jo, H. J., Martin, A., et al. (2012). Trouble at rest: how correlation patterns and group differences become distorted after global signal regression. *Brain connectivity* 2, 25–32. doi:10.1089/brain.2012.0080

Sanz-Arigita, E. J., Schoonheim, M. M., Damoiseaux, J. S., Rombouts, S. A. R. B., Maris, E., Barkhof, F., et al. (2010). Loss of 'small-world' networks in alzheimer's disease: graph analysis of fMRI resting-state functional connectivity. *PloS one* 5, e13788. doi: 10.1371/journal.pone.0013788

Schiff, N. D. (2010). Recovery of consciousness after brain injury: a mesocircuit hypothesis. *Trends in neurosciences* 33, 1–9. doi:10.1016/j.tins.2009.11.002

Schröter, M. S., Spoormaker, V. I., Schorer, A., Wohlschläger, A., Czisch, M., Kochs, E. F., et al. (2012). Spatiotemporal reconfiguration of large-scale brain functional networks during propofol-induced loss of consciousness. *Journal of Neuroscience* 32, 12832–12840

Schrouff, J., Perlbarg, V., Boly, M., Marrelec, G., Boveroux, P., Vanhaudenhuyse, A., et al. (2011). Brain functional integration decreases during propofol-induced loss of consciousness. *NeuroImage* 57, 198–205. doi:10.1016/j.neuroimage.2011.04.020

Shadi, K., Bakhshi, S., Gutman, D. A., Mayberg, H. S., and Dovrolis, C. (2016). A symmetry-based method to infer structural brain networks from probabilistic tractography data. *Frontiers in neuroinformatics* 10, 46. doi:10.3389/fninf.2016.00046

Shattuck, D. W., Sandor-Leahy, S. R., Schaper, K. A., Rottenberg, D. A., and Leahy, R. M. (2001). Magnetic resonance image tissue classification using a partial volume model. *NeuroImage* 13, 856–876. doi:10.1006/nimg.2000.0730

Simpson, S. L., Hayasaka, S., and Laurienti, P. J. (2011). Exponential random graph modeling for complex brain networks. *PloS one* 6, e20039. doi:10.1371/journal.pone.0020039

Simpson, S. L., Lyday, R. G., Hayasaka, S., Marsh, A. P., and Laurienti, P. J. (2013). A permutation testing framework to compare groups of brain networks. *Frontiers in computational neuroscience* 7, 171. doi:10.3389/fncom.2013.00171

Simpson, S. L., Moussa, M. N., and Laurienti, P. J. (2012). An exponential random graph modeling approach to creating group-based representative whole-brain connectivity networks. *NeuroImage* 60, 1117–1126. doi:10.1016/j.neuroimage.2012.01.071

Sitt, J. D., King, J.-R., El Karoui, I., Rohaut, B., Faugeras, F., Gramfort, A., et al. (2014). Large scale screening of neural signatures of consciousness in patients in a vegetative or minimally conscious state. *Brain: a journal of neurology* 137, 2258–2270. doi: 10.1093/brain/awu141

Sitt, J. D., King, J.-R., Naccache, L., and Dehaene, S. (2013). Ripples of consciousness. *Trends in cognitive sciences* 17, 552–554. doi:10.1016/j.tics.2013.09.003

Smith, S. M. (2002). Fast robust automated brain extraction. *Human brain mapping* 17, 143–155. doi:10.1002/hbm.10062

Sporns, O. and Ktter, R. (2004). Motifs in brain networks. *PLoS biology* 2, e369. doi: 10.1371/journal.pbio.0020369

Spreng, R. N., Stevens, W. D., Chamberlain, J. P., Gilmore, A. W., and Schacter, D. L. (2010). Default network activity, coupled with the frontoparietal control network, supports goal-directed cognition. *Neuroimage* 53, 303–317

Stamatakis, E. A., Adapa, R. M., Absalom, A. R., and Menon, D. K. (2010). Changes in resting neural connectivity during propofol sedation. *PloS one* 5, e14224. doi: 10.1371/journal.pone.0014224

Stokes, M. G., Kusunoki, M., Sigala, N., Nili, H., Gaffan, D., and Duncan, J. (2013). Dynamic coding for cognitive control in prefrontal cortex. *Neuron* 78, 364–375

Sui, J., Pearlson, G., Caprihan, A., Adali, T., Kiehl, K. A., Liu, J., et al. (2011). Discriminating schizophrenia and bipolar disorder by fusing fMRI and DTI in a multimodal CCA+ joint ICA model. *Neuroimage* 57, 97–106. doi:10.1016/j.neuroimage.2011.05.055

Tallon-Baudry, C. (2009). The roles of gamma-band oscillatory synchrony in human visual cognition. *Frontiers in bioscience (Landmark edition)* 14, 321–332

Tan, X., Zhou, Z., Gao, J., Meng, F., Yu, Y., Zhang, J., et al. (2019). Structural connectome alterations in patients with disorders of consciousness revealed by 7-tesla magnetic resonance imaging. *NeuroImage: Clinical* 22, 101702

Tange, O. (2011). Gnu parallel-the command-line power tool. *The USENIX Magazine* 36, 42–47

Teasdale, G. and Jennett, B. (1974). Assessment of coma and impaired consciousness: a practical scale. *The Lancet* 304, 81–84

Tegmark, M. (2016). Improved measures of integrated information. *PLoS computational biology* 12, e1005123

Thengone, D. J., Voss, H. U., Fridman, E. A., and Schiff, N. D. (2016). Local changes in network structure contribute to late communication recovery after severe brain injury. *Science translational medicine* 8, 368re5–368re5. doi:10.1126/scitranslmed.aaf6113

Tollard, E., Galanaud, D., Perlbarg, V., Sanchez-Pena, P., Le Fur, Y., Abdennour, L., et al. (2009). Experience of diffusion tensor imaging and 1H spectroscopy for outcome prediction in severe traumatic brain injury: Preliminary results. *Critical care medicine* 37, 1448–1455. doi:10.1097/CCM.0b013e31819cf050

Tononi, G. (2008). Consciousness as integrated information: a provisional manifesto. *The Biological bulletin* 215, 216–242. doi:10.2307/25470707

Tononi, G., Boly, M., Massimini, M., and Koch, C. (2016). Integrated information theory: from consciousness to its physical substrate. *Nature Reviews Neuroscience* 17, 450. doi:10.1038/nrn.2016.44

Tononi, G. and Koch, C. (2015). Consciousness: here, there and everywhere? *Phil. Trans. R. Soc. B* 370, 20140167. doi:10.1098/rstb.2014.0167

Van Essen, D. C., Smith, S. M., Barch, D. M., Behrens, T. E., Yacoub, E., Ugurbil, K., et al. (2013). The wu-minn human connectome project: an overview. *Neuroimage* 80, 62–79

van Wijk, B. C. M., Stam, C. J., and Daffertshofer, A. (2010). Comparing brain networks of different size and connectivity density using graph theory. *PloS one* 5, e13701. doi: 10.1371/journal.pone.0013701

Vanhaudenhuyse, A., Noirhomme, Q., Tshibanda, L. J.-F., Bruno, M.-A., Boveroux, P., Schnakers, C., et al. (2010). Default network connectivity reflects the level of consciousness in non-communicative brain-damaged patients. *Brain: a journal of neurology* 133, 161–171. doi:10.1093/brain/awp313

Venables, W. N. and Ripley, B. D. (2013). *Modern applied statistics with S-PLUS* (Springer Science & Business Media)

Vincent, J. L., Kahn, I., Snyder, A. Z., Raichle, M. E., and Buckner, R. L. (2008). Evidence for a frontoparietal control system revealed by intrinsic functional connectivity. *Journal of neurophysiology* 100, 3328–3342. doi:10.1152/jn.90355.2008

Voss, H. U., Uluç, A. M., Dyke, J. P., Watts, R., Kobylarz, E. J., McCandliss, B. D., et al. (2006). Possible axonal regrowth in late recovery from the minimally conscious state. *The Journal of clinical investigation* 116, 2005–2011. doi:10.1172/JCI27021

Wang, P., Robins, G., Pattison, P., and Lazega, E. (2013). Exponential random graph models for multilevel networks. *Social Networks* 35, 96–115

Wang, P., Robins, G., Pattison, P., and Lazega, E. (2016). Social selection models for multilevel networks. *Social Networks* 44, 346–362

Wang, Y., Ghumare, E., Vandenberghe, R., and Dupont, P. (2017). Comparison of different generalizations of clustering coefficient and local efficiency for weighted undirected graphs. *Neural computation* 29, 313–331

Watts, D. J. and Strogatz, S. H. (1998). Collective dynamics of small-worldnetworks. *nature* 393, 440

Wilson, C. (2010). Aetiological differences in neuroanatomy of the vegetative state: insights from diffusion tensor imaging and functional implications. *Journal of neurology, neurosurgery, and psychiatry* 81, 475–476. doi:10.1136/jnnp.2010.205815

Wilson, J. L., Pettigrew, L. E., and Teasdale, G. M. (1998). Structured interviews for the Glasgow Outcome Scale and the extended Glasgow Outcome Scale: guidelines for their use. *Journal of neurotrauma* 15, 573–585

Wu, T., Wang, L., Chen, Y., Zhao, C., Li, K., and Chan, P. (2009). Changes of functional connectivity of the motor network in the resting state in parkinson's disease. *Neuroscience letters* 460, 6–10. doi:10.1016/j.neulet.2009.05.046

Xie, G., Deschamps, A., Backman, S., Fiset, P., Chartrand, D., Dagher, A., et al. (2011). Critical involvement of the thalamus and precuneus during restoration of consciousness with physostigmine in humans during propofol anaesthesia: a positron emission tomography study. *British journal of anaesthesia* 106, 548–557

Yeo, B. T. T., Krienen, F. M., Sepulcre, J., Sabuncu, M. R., Lashkari, D., Hollinshead, M., et al. (2011). The organization of the human cerebral cortex estimated by intrinsic functional connectivity. *Journal of neurophysiology* 106, 1125–1165. doi:10.1152/jn.00338.2011

Yokoyama, O., Miura, N., Watanabe, J., Takemoto, A., Uchida, S., Sugiura, M., et al. (2010). Right frontopolar cortex activity correlates with reliability of retrospective rating of confidence in short-term recognition memory performance. *Neuroscience research* 68, 199–206

Zalesky, A., Fornito, A., and Bullmore, E. (2012). On the use of correlation as a measure of network connectivity. *NeuroImage* 60, 2096–2106. doi:10.1016/j.neuroimage.2012.02.001

Zheng, Z. S., Reggente, N., Lutkenhoff, E., Owen, A. M., and Monti, M. M. (2017). Disen-

tangling disorders of consciousness: Insights from diffusion tensor imaging and machine learning. *Human brain mapping* 38, 431–443. doi:10.1002/hbm.23370

Zhou, J., Liu, X., Song, W., Yang, Y., Zhao, Z., Ling, F., et al. (2011). Specific and nonspecific thalamocortical functional connectivity in normal and vegetative states. *Consciousness and cognition* 20, 257–268. doi:10.1016/j.concog.2010.08.003